DYNAMICAL SYSTEMS OF THE BCM LEARNING RULE:

EMERGENT PROPERTIES AND APPLICATION TO CLUSTERING

by

Lawrence C. Udeigwe

M.A. Mathematics, University of Pittsburgh, 2008

M.S. Applied Mathematics, University of Delaware, 2006

B.S. Mathematics, Duquesne University, 2004

B.A. Computer Science, Duquesne University, 2004

Submitted to the Graduate Faculty of

the School of Information Science in partial fulfillment

of the requirements for the degree of

Doctor of Philosophy

University of Pittsburgh

2014

UNIVERSITY OF PITTSBURGH

SCHOOL OF INFORMATION SCIENCE

This dissertation was presented

by

Lawrence C. Udeigwe

It was defended on

July 18th 2014

and approved by

Paul W. Munro, Associate Professor, School of Information Sciences

G. Bard Ermentrout, Professor, Department of Mathematics

Stephen C. Hirtle, Professor, School of Information Sciences

Hassan Karimi, Professor, School of Information Sciences

Jonathan Rubin, Professor, Department of Mathematics

Dissertation Advisors: Paul W. Munro, Associate Professor, School of Information Sciences,

G. Bard Ermentrout, Professor, Department of Mathematics

DYNAMICAL SYSTEMS OF THE
BCM LEARNING RULE:
EMERGENT PROPERTIES AND APPLICATION TO CLUSTERING

Lawrence C. Udeigwe , PhD
University of Pittsburgh, 2014

The BCM learning rule has been used extensively to model how neurons in the brain cortex respond to stimulus. One reason for the popularity of the BCM learning rule is that, unlike its predecessors which use static thresholds to modulate neuronal activity, the BCM learning rule incorporates a dynamic threshold that serves as a homeostasis mechanism, thereby providing a larger regime of stability.

This dissertation explores the properties of the BCM learning rule – as a dynamical system– in different time-scale parametric regimes. The main observation is that, under certain stimulus conditions, when homeostasis is at least as fast as synapse, the dynamical system undergoes bifurcations and may trade stability for oscillations, torus dynamics, and chaos. Analytically, it is shown that the conditions for stability are a function of the homeostasis time-scale parameter and the angle between the stimuli coming into the neuron.

When the learning rule achieves stability, the BCM neuron becomes selective. This means that it exhibits high-response activities to certain stimuli and very low-response activities to others. With data points as stimuli, this dissertation shows how this property

of the BCM learning rule can be used to perform data clustering analysis. The advantages and limitations of this approach are discussed, in comparison to a few other clustering algorithms.

TABLE OF CONTENTS

1.0 INTRODUCTION 1

1.1 OBJECTIVE 2

1.2 OVERVIEW OF RELATED TOPICS 3

1.2.1 Neurons and synapses 3

1.2.2 Sensory neurons 4

1.2.3 Dynamical systems 5

1.2.4 Clustering 5

1.3 RELATED WORK 6

1.4 OUTLINE OF DISSERTATION 8

2.0 THEORETICAL BACKGROUND 9

2.1 STIMULUS PATTERN 9

2.2 NEURON MODEL 10

2.3 THE BCM LEARNING RULE 11

3.0 EMERGENT DYNAMICAL PROPERTIES OF A SINGLE BCM NEURON 14

3.1 METHODS 14

3.1.1 Stochastic experiment 15

3.1.2 Mean-field model 18

3.2 OSCILLATORY PROPERTIES 20

3.2.1 Preliminary analysis . . . 20
3.2.2 Stimulus parametrization . . . 25
3.2.3 Phase plane analysis . . . 29
3.2.4 Bifurcation analysis . . . 34
3.2.5 Selectivity analysis . . . 37
3.3 STABILITY THEOREMS . . . 39
3.4 SUMMARY . . . 42
4.0 EMERGENT DYNAMICAL PROPERTIES OF COUPLED BCM NEURONS . . . 43
4.1 METHODS . . . 43
4.1.1 Mutually inhibiting neurons . . . 43
4.1.2 Two mutually inhibiting BCM neurons . . . 48
4.1.3 Stochastic experiment . . . 52
4.1.4 Mean-field model . . . 53
4.2 OSCILLATORY, TOROIDAL, AND CHAOTIC PROPERTIES . . . 57
4.3 SUMMARY . . . 66
5.0 CLUSTERING PROPERTY OF BCM NEURON . . . 68
5.1 PRELIMINARY ANALYSIS . . . 68
5.2 METHODS . . . 72
5.2.1 Variables . . . 72
5.2.2 Algorithm pseudocode . . . 73
5.2.3 Algorithm complexity . . . 76
5.2.3.1 Algorithm 1 . . . 76
5.2.3.2 The BCM clustering algorithm (Algorithm 2) . . . 77
5.3 PERFORMANCE . . . 77
5.3.1 Performance on data sets . . . 77

5.3.2 Performance comparison 82
5.3.3 Computational complexity and run time comparison 86
5.4 SUMMARY 87
6.0 DISCUSSION 89
6.1 CONTRIBUTIONS OF DISSERTATION 89
6.2 FUTURE WORK 91
7.0 Bibliography 92

LIST OF TABLES

5.1 Average number of iterations needed for convergence (over 10 runs), as a function of the angle between two stimulus vectors. $\tau_w = 100$, $\tau_\theta = 10$ 76

5.2 Mean Rand indices (over 100 runs) for different clustering algorithms 85

5.3 Mean DB indices (over 100 runs) for different clustering algorithms 86

5.4 Mean CPU time, in seconds, (over 100 runs) for different clustering algorithms . 87

LIST OF FIGURES

2.1 19 retina cells. The gray bar is an oriented stimulus. Cells that lie on the bar intersection are considered to have a high excitation value (1), while the other have a low excitation values (0). Diagram by P.W. Munro [45] 10

2.2 Response to an N-dimensional stimulus $\mathbf{x}$ coming with a set of synaptic weight $\mathbf{w}$ 11

2.3 A non-linear function ϕ of the post-synaptic neuronal activity, v, and a threshold θ, of the activity 12

3.1 When $\tau_\theta/\tau_w = 0.1$, response converges to a steady state and neuron selects stimulus $\mathbf{x}^{(2)}$ 15

3.2 When $\tau_\theta/\tau_w = 1.1$, responses oscillate but neuron still selects stimulus $\mathbf{x}^{(2)}$ . . . 16

3.3 When $\tau_\theta/\tau_w = 1.7$, neuron is no longer selective 17

3.4 $\rho = 0.5$, $\mathbf{x}^{(1)} = (1,0)$, $\mathbf{x}^{(2)} = (0,1)$ (a) $\tau_\theta/\tau_w = 0.1$ (b) $\tau_\theta/\tau_w = 1.1$ 21

3.5 $\rho = 0.5$, $\mathbf{x}^{(1)} = (1,0)$, $\mathbf{x}^{(2)} = (0.5,0.5)$ (a) $\tau_\theta/\tau_w = 0.1$ (b) $\tau_\theta/\tau_w = 1.7$ 22

3.6 $\rho = 0.7$, $\mathbf{x}^{(1)} = (1,0)$, $\mathbf{x}^{(2)} = (1,1)$ (a) $\tau_\theta/\tau_w = 0.1$ (b) $\tau_\theta/\tau_w = 1.1$ 23

3.7 $\rho = 0.5$, $\mathbf{x}^{(1)} = (0.7071,0.7071)$, $\mathbf{x}^{(2)} = (-0.7071,0.7071)$ (a) $\tau_\theta/\tau_w = 0.1$ (b) $\tau_\theta/\tau_w = 1.1$ 24

3.8 (a) Stimulus patterns when $\alpha > 0$ (b) Stimulus patterns when $\alpha < 0$ 28

3.9 Nullcline of (a) equation 3.13 (weight space) (b) equation 3.14 (response space) when $\alpha = 0.128$, θ is steady 30

3.10 Trajectory of (a) equation 3.13 (weight space) (b) equation 3.14 (response space) when $\alpha = 0.128$, $\tau_\theta/\tau_w = 0.1$ 31
3.11 Trajectory of (a) equation 3.13 (weight space) (b) equation 3.14 (response space) when $\alpha = 0.128$, $\tau_\theta/\tau_w = 1.1$ 32
3.12 Oscillatory steady state of equation (a) 3.13 (weight space) (b) 3.14 (response space) when $\alpha = 0.128$ and $\tau_\theta/\tau_w = 1.1$ 33
3.13 Bifurcation diagram (as α varies) of equation 3.13 when $\tau_\theta/\tau_w = 1.1$ 35
3.14 α bifurcation values for different values of τ_θ/τ_w 36
3.15 Relative selectivity vs τ_θ/τ_w. $\alpha = 0.128$ 38
4.1 Three mutually coupled neurons inhibiting one another 44
4.2 When $\tau_\theta/\tau_w = 0.1$, neuronal responses converge to a stable steady state and each neuron selects a different stimulus pattern 49
4.3 When $\tau_\theta/\tau_w = 1.1$, neuronal responses tend to an oscillatory steady state 50
4.4 When $\tau_\theta/\tau_w = 1.7$, neuronal responses tend to an oscillatory non-selective steady state 51
4.5 Bifurcation Diagram when starting from the symmetric fixed point. $\alpha = 0.4$, $\gamma = 0.25$ 58
4.6 symmetric fixed point bifurcates to phase shifted oscillations. $\tau_\theta/\tau_w = 1.64$, $\alpha = 0.4$, $\gamma = 0.25$ 59
4.7 Bifurcation Diagram when starting from the asymmetric fixed point. $\alpha = 0.4$, $\gamma = 0.25$ 60
4.8 Synchronous oscillations when $\tau_\theta/\tau_w = 1.742$, $\alpha = 0.4$, $\gamma = 0.25$ 61
4.9 Asynchronous oscillations when $\tau_\theta/\tau_w = 1.84$, $\alpha = 0.4$, $\gamma = 0.25$ 62
4.10 Period of oscillation doubles when $\tau_\theta/\tau_w = 1.95$, $\alpha = 0.4$, $\gamma = 0.25$ 63
4.11 Torus when $\tau_\theta/\tau_w = 1.965$, $\alpha = 0.4$, $\gamma = 0.25$ 64
4.12 Torus poincare map when $\tau_\theta/\tau_w = 1.965$ ($w_{a1} = 1$ section) , $\alpha = 0.4$, $\gamma = 0.25$. 65
4.13 Chaotic behavior when $\tau_\theta/\tau_w = 2$ ($w_{a1} = 1$ section), $\alpha = 0.4$, $\gamma = 0.25$ 66

5.1 C_1, C_2, and C_3 for (a) $b = 0.2$ (b) $b = 0.4$ and $\varepsilon = 0.3$ 69
5.2 Distributions of rand indices for 100 simulations of each value of b. In each case $\varepsilon = 0.3$ 70
5.3 High RI performance of BCM clustering algorithm on a data set with three linearly separable clusters 78
5.4 High RI performance of BCM clustering algorithm on a data set with four linearly separable clusters 79
5.5 A typical performance of BCM clustering algorithm on a data set with linearly non-separable clusters 80
5.6 (a) Iris data set (b) Iris data set clustered using the BCM clustering algorithm. . . 81

1.0 INTRODUCTION

Information processing in the nervous system involves interactions between neurons and in some cases, interactions between a neuron and stimuli from external environment. Most neural and cognitive functionalities of any organism highly depend on the strengthening or weakening – and even pruning – of these interactions. Learning, for example, is closely associated with the interaction of cortical neurons and external stimuli. These facts have led to philosophical questions such as: Does the strengthening and weakening of cell-stimulus interaction facilitate learning? Does the modification rate of interaction strength correlate with the rate of learning? And, when learning slows down (say at an older age), does it imply that this modification rate is near zero?

Questions about learning, like the ones above, have engendered many neuroscience research projects. Furthermore many theoretical models have been devised in response to related empirical results. Some of these models have been appropriately termed *learning rules*, as they attempt to theoretically suggest answers to the above questions. One of these theories is the BCM learning rule [7], named for Elie Bienenstock, Leon Cooper, and Paul Munro, which models the aforementioned strength modification in the primary visual cortex, and its dependence on input stimuli. Evidences of neuronal adherence to the BCM learning rule have been found in other areas of the brain, including other sensory cortices [23] [47] and the hippocampus [36], [40], [5].

1.1 OBJECTIVE

Mathematically speaking, the BCM learning rule is a system of differential equations involving the synaptic weights, the stimulus coming into the neuron, the activity response v of the neuron to the stimulus, and the threshold for the activity. Unlike its predecessors, which use static thresholds to modulate neuronal activity, the BCM learning rule allows the threshold to be dynamic. This dynamic threshold provides stability to the learning rule, and from a biological perspective, provides homeostasis to the system.

The objective of this dissertation is two-fold:

1. **To explore the stability properties of the BCM learning rule:** The dynamic nature of the threshold guarantees stability only in certain regime of homeostasis time scale. This dissertation treats the BCM learning rule as a dynamical system and explores the stability properties as a function of the relationship between homeostasis time scale and the stimuli set.
2. **To develop and analyze a clustering algorithm based on the BCM learning rule:** Once its dynamics is at a stable steady state, the BCM neuron is selective. This means that it exhibits high-response activities to relatively small set of stimuli and exhibits very low-response activities to others. With data points as stimuli, this property of the BCM learning rule can be used to perform cluster analysis. In this dissertation, a clustering algorithm based on this BCM property is developed, analyzed and compared with other clustering algorithms.

1.2 OVERVIEW OF RELATED TOPICS

This section presents an overview of the major background topics related to this dissertation, and may be skipped by readers who are already familiar with these topics.

1.2.1 Neurons and synapses

Neurons are the basic units of the nervous system. Collectively, neurons form complex neural networks which are responsible for a range of information processing tasks including memory, perception, cognition, and action. Communications between neurons take place via the transmission of electrical and chemical signals. The structures that allow this process are known as *synapses*. This term was coined by Sherrington [59] in 1906 to indicate a junction between two neurons. The neuron membrane maintains a resting electrical potential of about -60 mV. Each synapse transduces the incident signal to a slight disturbance in the resting potential across the membrane. If the membrane is sufficiently depolarized (driven above about -45mV), a pulse is transmitted by the neuron. The pulse frequency increases with membrane depolarization to a maximum, while the amplitude remains constant. The frequency-coded signal is sent to many other neurons. This signal then either inhibits or excites other neurons at synaptic sites by hyperpolarizing or depolarizing (respectively) other membranes.

Synapses are directly linked to the ability of the brain to develop and adapt. Although, this characteristic of the brain is well agreed upon in the neuroscience community, researchers, at one time, believed that the human brain grew and changed in response to new experiences as a child, but that the process slowed and the brain even became immutable in adulthood. Research has shown that the brain remains adaptive well into old age. Changes in environment and behavior can lead to modifications in cortical maps, neural pathways

and synapses in the brain [9]. Modifications of these sort, which are collectively known as *neural plasticity*, can also be brought about by changes resulting from bodily injuries [52].

Of importance in this dissertation are synaptic modifications known as *synaptic plasticity*, in which the strength of a synapse gets stronger or weaker in response to increases or decreases in the activity of the neuron involved. Although it is agreed that synaptic plasticity continues into adulthood, researchers have also argued that the strength and rate of synaptic plasticity varies across individuals and declines through age-span. Pascal-Leone et al [51] argue that this variation is defined by genetic, biological, and environmental factors and that neuro-developmental and neuro-degenerative disorders such as autism spectrum disorder or Alzheimer's disease are products of outlier behavior in synaptic plasticity.

1.2.2 Sensory neurons

In mammals, the *cerebral cortex* is the outermost layered structure of the brain. In terms of functions, the cerebral cortex can be divided in three broad collections of areas: sensory areas, motor areas, and association areas. The *sensory areas* are responsible for receiving and processing information from the senses. For instance the primary visual cortex, primary auditory cortex and primary somatosensory cortex are among the sensory areas and serve the senses of vision, audition, and touch respectively[39]. Sensory neurons are activated by physical modalities such as visible light, sound, heat, physical contact, etc., or by chemical signals (for example in the case of smell or taste).

It is well corroborated that when trained in the right environment, sensory neurons respond to a certain class of stimuli but not others. Experiments by Hubel and Wiesel for instance, revealed that neurons of the visual cortex of cats may respond preferentially to stimulus orientation[27]. Their studies also show that these neurons detect edges regardless of where they are placed in the receptive field of the neuron, and can preferentially

detect motion in certain directions [27] [28] [26]. While all sensory neurons are selective, their preference and degree of selectivity vary[46]. Nevertheless, neurons that respond to similar sensory stimuli tend to be in close proximity [11] [14] [49].

1.2.3 Dynamical systems

A *dynamical system* is a mathematical concept that describes the state space of a set of related variables. At any given time, the state of each variable is a real or complex number, and the state of the dynamical system is a vector comprising the states of all the variables; this vector represent a point in the appropriate state space. Small changes in the state of the system create small changes in this vector. The evolution rule of the dynamical system is a fixed rule that describes what future states follow from a current state.

Differential equations are dynamical systems. The BCM learning rule, for instance, describes the evolution of the synaptic variables with time. The beginning state of the dynamical system is referred to as the *initial condition*, and the *trajectory* of the system may terminate at a final state, called the *steady state* or *fixed point*. The steady state is said to be *stable*, if after the system arrives at the steady state, a small perturbation in the system leads back to a neighborhood of the state, otherwise, it is said to be *unstable*. In the case of the differential equations, the steady state may be obtained analytically by setting the right hand side of the equation to zero and solving for the variables.

In [53], L. Perko gives a good treatment to the kind of dynamical systems seen in this dissertation.

1.2.4 Clustering

In data mining, the term clustering refers to the task of grouping samples in a data set in such a way that samples in the same group are more similar to one another than samples in

different groups. In other words, the goal of a clustering algorithm is to form clusters that are as dissimilar from one another as possible. There are several classes of clustering algorithms – some of these algorithms will be discussed later in chapter 5 – and the measure of similarity that each class uses is sometimes the only thing that makes it unique. Clustering has had applications in fields like marketing, medicine, and psychology [44], just to mention a few. In marketing, for example, a clustering algorithm can be used to find groups of customers with similar behavior, given a large database of customer data containing their past buying records [22] [63]. There are researchers whose works are targeted on improving clustering techniques specific to medical data [38] and these algorithms have become very useful in making inferences in medicine. For instance, with clustering algorithms, patients with thyroid gland diseases can be classified as normal, hyperthyroid function and hypothyroid function [1].

1.3 RELATED WORK

Over the years, experimentalists have approached the study of neural functions using the *stimulus-response* (SR) methodology. Thus, a neuron is viewed as a black box accepting multidimensional stimulus input and generating a single-valued response; and a neural network accepts input for a population of neurons and yields, as output, observable properties such as the average firing rate and architecture of the network. Notable pioneering work in the fields of neuroscience and psychology, which helped establish the SR methodology, include those of Sherrington [59] and Skinner [62]. Their findings helped build a foundation for Hubel and Wiesel's [27] [28] experiment for obtaining electrophysiological data from orientation-specific neurons in the visual cortex. This and other experiments helped create a fertile ground for mathematical models involving neural plasticity and neuronal

selectivity.

One of the most cited theories in the field of neuropsychology is the Hebbian theory of synaptic modification [24], [25]. Donald Hebb in 1949 proposed that when neuron A repeatedly participates in firing neuron B, the strength of the influence of A onto B increases. This implies that changes in synaptic strengths in a neural network is a function of the pre- and post-synaptic neural activities. A few decades later, Nass and Cooper [48] developed a Hebbian synaptic modification theory for the synapses of the visual cortex, which was later extended to a threshold dependent setup by Cooper at al [13]. In this setup, the sign of a weight modification is based on whether the post-synaptic response is below or above a static threshold. A response above the threshold is meant to strengthen the active synapse, and a response below the threshold should lead to a weakening of the active synapse.

One of the most accurate models of synaptic plasticity to date is the BCM learning rule [7], with which Bienenstock et al (by incorporating a dynamic threshold that is a function of the average post-synaptic activity over time), captured the development of stimulus selectivity in the primary visual cortex of higher vertebrates. In corroborating the BCM theory, Shouval et al [4] and Intrator and Cooper[41] showed that a BCM network develops orientation selectivity and ocular dominance in natural scene environment. [60] Although the BCM rule was developed to model selectivity of visual cortical neurons, it has been successfully applied to other classes of neuron. For instance, it has been used to explain experience-dependent plasticity in the mature somatosensory cortex. Furthermore the BCM rule has been reformulated and adapted to suit various interaction environments of neural networks, including laterally interacting neurons [10] [12] and stimuli generalizing neurons [46].

Based on the BCM learning rule, a few data mining applications of neuronal selectivity have emerged. Intrator et al showed that a BCM neural network can perform projection

pursuit [33], [16] , [34], i.e it can find projections in which a data set departs from statistical normality. This is an important finding that highlights the feature detecting property of a BCM neural model. As a result, the BCM neural network has been successfully applied to some specific pattern recognition tasks. For example Bachman et al [3] incorporated the BCM learning rule in their algorithm for classifying radar data. Intrator et al developed an algorithm for recognizing 3D objects from 2D view by combining existing statistical feature extraction models with the BCM model [32] [35]. In [54], Poljovka and Benuskova presents a preliminary simulation on how the BCM learning rule has the potential to identify alpha numeric letters.

1.4 OUTLINE OF DISSERTATION

Chapter 2 gives a summary of the theoretical background to this dissertation . In chapter 3, both numerical an analytical results on the BCM dynamics of one neuron are presented. The results start with a general two-stimulus perspective and then focuses on a class of equal magnitude, parameterized stimulus set. Chapter 4 presents a similar result for two mutually inhibiting neurons. Chapter 5 presents an algorithm and numerical results on the clustering properties of a BCM neuron. Chapter 6 is a conclusive discussion on the contributions of this dissertation, and how the work presented can be extended in the future.

2.0 THEORETICAL BACKGROUND

The influence, upon a neuron, of other neurons or external stimuli is quantified as *synaptic weights*. These synaptic weights along with other variables generally determine the electrophysiological properties of a neural network. Thus, most mathematical models of neuronal activity are based on this notion.

2.1 STIMULUS PATTERN

A stimulus pattern comprises N afferent signals $\{x_i\}_{i=1}^{N}$, therefore each stimulus pattern is expressed as an $N-$dimensional vector $\mathbf{x}$. An example of how such a vector is generated for stimulus coming through the retina is described by Munro [45] using figure 2.1. The figure comprises 19 retina cells and an oriented stimulus (gray bar). The intersection of the bar and the retina determines the excitation intensity of the cells: cells that lie in the intersection are considered to have high excitation intensity and are assigned high values in the stimulus vector, while the others are assigned low values. In this particular example, a high excitation intensity is 1 and a low excitation intensity is 0, giving rise to the stimulus pattern $\mathbf{x} = (1,0,0,0,1,0,0,0,0,1,0,0,0,0,1,0,0,0,1)$.

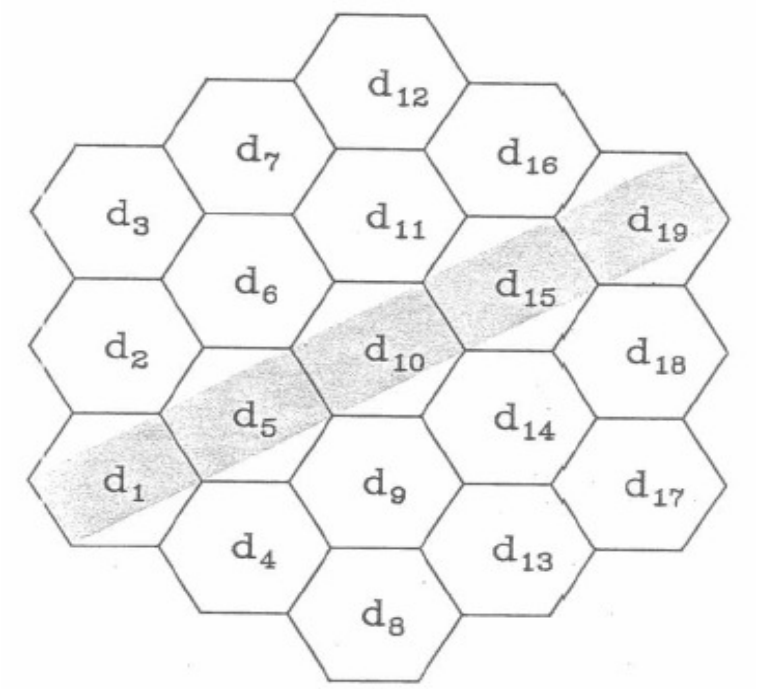

$$\mathbf{x} = (1,0,0,0,1,0,0,0,0,1,0,0,0,0,1,0,0,0,1)$$

Figure 2.1: 19 retina cells. The gray bar is an oriented stimulus. Cells that lie on the bar intersection are considered to have a high excitation value (1), while the other have a low excitation values (0). Diagram by P.W. Munro [45]

2.2 NEURON MODEL

At any instant, a neuron generates a dynamic scalar response to a time-varying stimulus pattern and the response properties evolve with experience. This response is an idealized spatiotemporal integration expressed as an instantaneous linear sum v of N inputs weighted

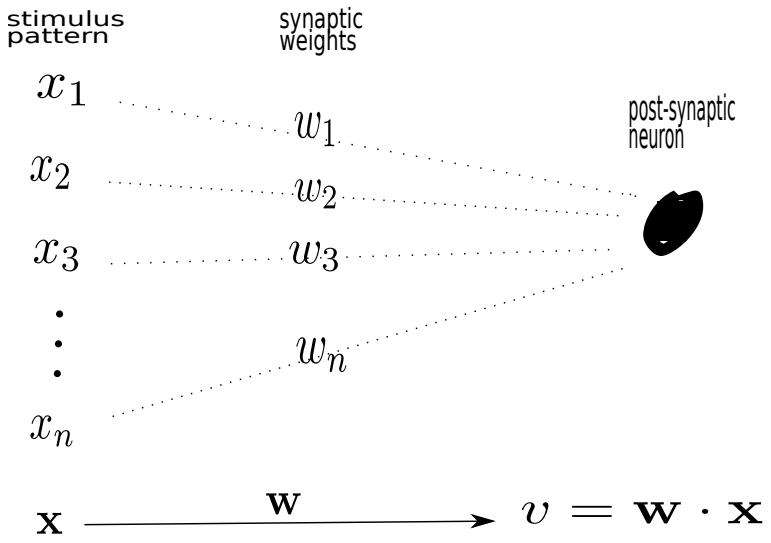

Figure 2.2: Response to an N-dimensional stimulus **x** coming with a set of synaptic weight **w**

by a corresponding set of N synaptic efficacies $\{w_i\}_{i=1}^{N}$. Thus

$$\begin{aligned} v &= \mathbf{w} \cdot \mathbf{x} \\ &= w_1 x_1 + w_2 x_2 + \ldots + w_N x_N \end{aligned} \tag{2.1}$$

A neuron whose response is modeled this way is referred to as a linear neuron

2.3 THE BCM LEARNING RULE

The concept of synaptic weight modification is fundamental to synaptic plasticity and neuronal selectivity. The BCM learning rule models changes in synaptic weights (and thus neuronal response) to a set of stimuli. The underlying theory expresses the changes

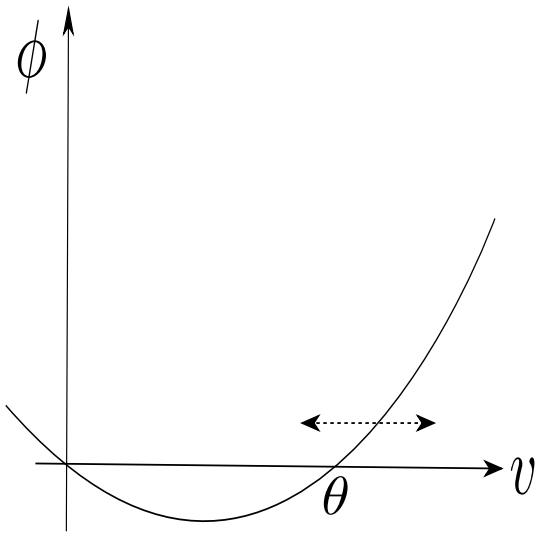

Figure 2.3: A non-linear function ϕ of the post-synaptic neuronal activity, v, and a threshold θ, of the activity

in synaptic weights as a product of the input stimulus pattern vector, $\mathbf{x}$, and a function, ϕ. Here, ϕ is a non-linear function of the post-synaptic neuronal activity, v, and a dynamic threshold, θ. (see figure 2.3).

If at any time the neuron receives a stimulus pattern $\mathbf{x}$ from a stimulus pattern set, say $\{\mathbf{x}^{(1)}, \mathbf{x}^{(2)}, \ldots, \mathbf{x}^{(n)}\}$, the BCM rule expresses the dynamics of the weight vector, $\mathbf{w}$, as

$$\begin{aligned} \frac{d\mathbf{w}}{dt} &= \phi(v;\theta)\mathbf{x} \\ \theta &= E^p[v] \end{aligned} \tag{2.2}$$

where

θ is sometimes referred to as the "sliding threshold" because, as can be seen from equation 2.2 , it changes with time, and this change depends on v, the sum of the weighted

input to the neuron. ϕ has the following property: for low values of the post-synaptic activity ($v < \theta$), ϕ is negative; for $v > \theta$, ϕ is positive. In the results presented by Bienenstock et al [7], $\phi(v) = v(v-\theta)$ is used, $E[v]$ is a running temporal average of v and the learning rule is stable for $p > 1$. Later formulations of the learning rule (for instance by Intrator and Copper [33]) have shown that a temporal average can be used in lieu of a spatial average, and that with $p = 2$, $E[v^p]$ is an excellent approximation of $E^p[v]$. Thus a differential form of the learning rule is

$$\begin{aligned} \tau_w \frac{d\mathbf{w}}{dt} &= v\mathbf{x}(v-\theta) \\ \tau_\theta \frac{\theta}{dt} &= (v^2-\theta) \end{aligned} \tag{2.3}$$

where τ_w and τ_θ are time scale factors. In simulated environments, these parameters can be used to monitor how fast the system is changing with respect to time.

The neuron whose synapses are modified using the BCM learning rule is referred to as a BCM neuron.

3.0 EMERGENT DYNAMICAL PROPERTIES OF A SINGLE BCM NEURON

In this chapter, the dynamics of a single BCM neuron are studied. Section 3.1 presents a preliminary experiment on the dynamics of the BCM learning rule, and a mean-field formulation of the learning rule. Oscillatory steady states are observed in certain parametric regimes. This oscillatory dynamical property of the BCM neuron is analyzed in section 3.2. Section 3.3 presents theorems that summarize the conditions for stability and oscillatory instability. The numerical results presented in this chapter are obtained using XPPAUT [17] except where noted.

3.1 METHODS

Consider a single linear neuron that receives a stimulus pattern $\mathbf{x} = (x_1, \ldots, x_n)$ with synaptic weights $\mathbf{w} = (w_1, \ldots, w_n)$. Recall that the BCM learning rule for this neuron is given by

$$\begin{aligned} \tau_w \frac{d\mathbf{w}}{dt} &= v\mathbf{x}(v-\theta) \\ \tau_\theta \frac{d\theta}{dt} &= v^2 - \theta \end{aligned} \tag{3.1}$$

where $v = \mathbf{w} \cdot \mathbf{x}$ is the neuronal response to the stimulus pattern, and θ is a dynamic threshold for the response. For $n = 2$, the neuronal response is $v = w_1 x_1 + w_2 x_2$. Thus the BCM

learning rule for this neuron becomes:

$$\begin{aligned}
\tau_w \dot{w}_1 &= {w_1}^2 {x_1}^3 + 2 w_1 w_2 {x_1}^2 x_2 + {w_2}^2 x_2^2 x_1 - ({w_1 x_1}^2 + w_2 x_1 x_2)\theta \\
\tau_w \dot{w}_2 &= {w_2}^2 {x_2}^3 + 2 w_1 w_2 x_2^2 x_1 + {w_1}^2 {x_1}^2 x_2 - ({w_2 x_2}^2 + w_1 x_1 x_2)\theta \\
\tau_\theta \dot{\theta} &= {w_1}^2 {x_1}^2 + 2 w_1 w_2 x_1 x_2 + {w_2}^2 {x_2}^2 - \theta
\end{aligned} \tag{3.2}$$

where the dot operator denotes derivative with respect to time. That is $\dot{f} = \frac{df}{dt}$.

3.1.1 Stochastic experiment

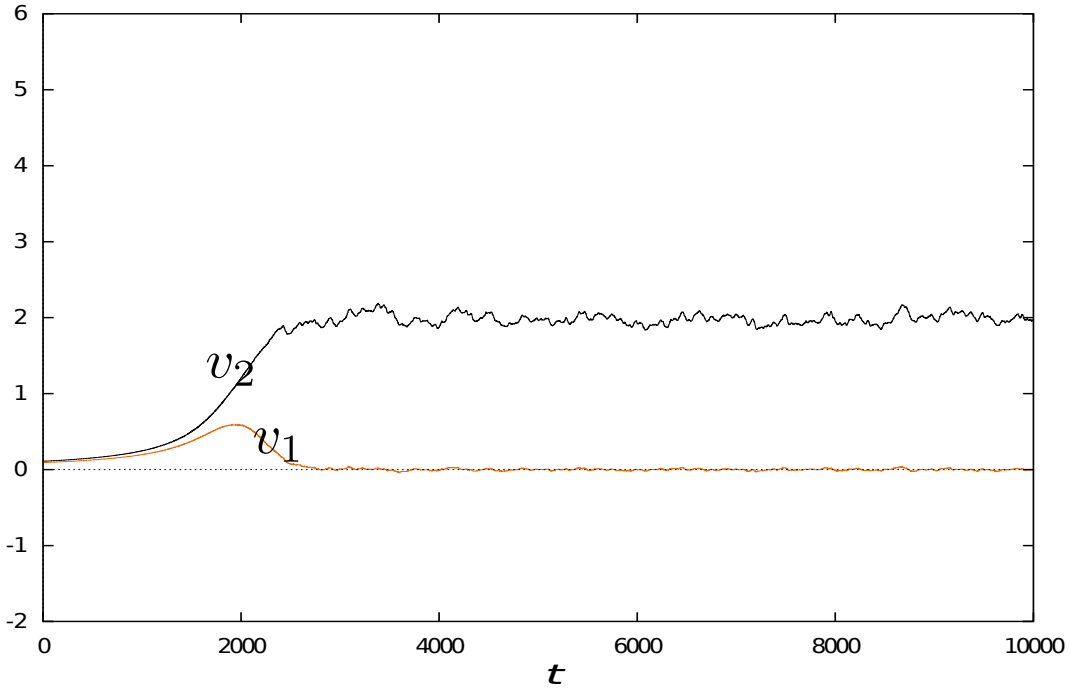

Figure 3.1: When $\tau_\theta / \tau_w = 0.1$, response converges to a steady state and neuron selects stimulus $\mathbf{x}^{(2)}$

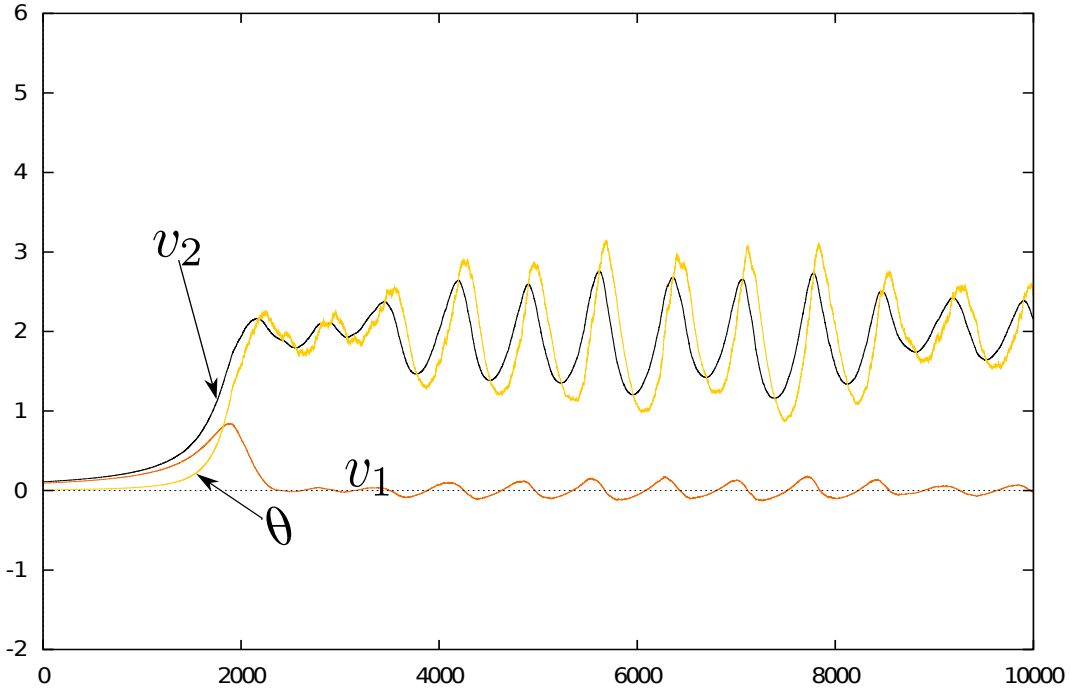

Figure 3.2: When $\tau_\theta/\tau_w = 1.1$, responses oscillate but neuron still selects stimulus $\mathbf{x}^{(2)}$

A good starting point in studying the dynamical properties of the BCM neuron is to explore the steady states of v for different time scale factors of θ. This is equivalent to varying the ratio τ_θ/τ_w in equation 3.2.

Consider a BCM neuron that receives a stimulus input $\mathbf{x}$ stochastically from the set $\{\mathbf{x}^{(1)}, \mathbf{x}^{(2)}\}$ with equal probabilities. That is, $Pr[\mathbf{x}(t) = \mathbf{x}^{(1)}] = Pr[\mathbf{x}(t) = \mathbf{x}^{(2)}] = \frac{1}{2}$. Figures 3.1, 3.2, and 3.3 plot the neuronal response v as a function of time. In each case, the initial conditions of w_1, w_2 and θ lie in the interval $(0, 0.3)$. $v_1 = \mathbf{w} \cdot \mathbf{x}^{(1)}$ is the response of the neuron to the stimulus $\mathbf{x}^{(1)} = (0.9239, 0.3827)$ and $v_2 = \mathbf{w} \cdot \mathbf{x}^{(2)}$ is the response of the neuron to the stimulus $\mathbf{x}^{(2)} = (0.3827, 0.9239)$. In each simulation, the presentation of

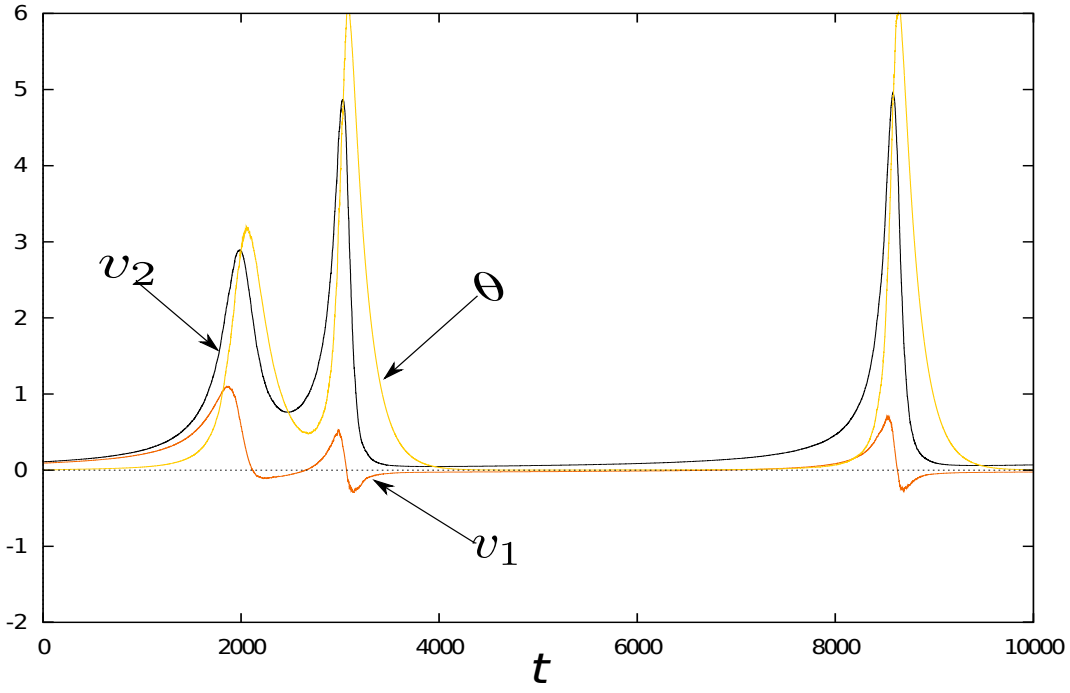

Figure 3.3: When $\tau_\theta/\tau_w = 1.7$, neuron is no longer selective

stimulus patterns is a Poisson process with rate $\lambda = 5$ presentations per second.

When $\tau_\theta/\tau_w = 0.1$, figure 3.1 shows a stable selective steady state of the neuron. At this state, $v_1 = 2$ while $v_1 = 0$, implying that the neuron selects $\mathbf{x}^{(2)}$. This scenario is equivalent to one of the selective steady states demonstrated by Bienenstock et al in [7].

When the synaptic weights $\mathbf{w}$ change just as fast as (or a little faster than) the threshold, θ, the dynamics of the BCM neuron take on a different kind of behavior. In figure 3.2, $\tau_\theta/\tau_w = 1.1$. As can be seen, there is a stark difference between this figure and figure 3.1. Here, the steady state of the system loses stability and an oscillation emerges. At the steady state, the range of the oscillation of v_2 and that of v_1 are $(1.2, 2.7)$ and $(-0.1, 0.1)$

respectively. The neuron is still selective since there is a large enough empty intersection between these ranges of oscillation. Notice that the value of θ is always approximately equal to that of the response to the selected stimulus, which in this case, is v_2.

Setting the time scale factor of θ to be roughly twice that of the rate of change of $\mathbf{w}$ reveals a different kind of oscillation than the one seen in figure 3.2. In figure 3.3 where $\tau_\theta/\tau_w = 1.7$, the oscillation has very sharp maxima and flat minima and can be described as an alternating combination of spikes and rest states. As can be seen, the neuron is hardly selective, except within a very small neighborhood of the maxima.

3.1.2 Mean-field model

The dynamics of the BCM neuron (equation 3.2) are stochastic in nature, since at each time step, the neuron randomly receives one out of two stimulus patterns. One way to gain more insight into the nature of these dynamics is to study a mean-field deterministic approximation of the learning rule. Consider a BCM neuron that receives a stimulus input $\mathbf{x}$, stochastically from the set $\{\mathbf{x}^{(1)} = (x_{11}, x_{12}), \mathbf{x}^{(2)} = (x_{21}, x_{22})\}$ such that $Pr[\mathbf{x}(t) = \mathbf{x}^{(1)}] = \rho$ and $Pr[\mathbf{x}(t) = \mathbf{x}^{(2)}] = 1 - \rho$. Thus, a mean-field version of equation 3.2 is

$$\begin{aligned}
\tau_w \dot{w}_1 &= \rho[{w_1}^2 {x_{11}}^3 + 2w_1 w_2 {x_{11}}^2 x_{12} + {w_2}^2 {x_{12}}^2 x_{11} - ({w_1} {x_{11}}^2 + w_2 x_{11} x_{12})\theta] \\
&+ (1-\rho)[{w_1}^2 {x_{21}}^3 + 2w_1 w_2 {x_{21}}^2 x_{22} + {w_2}^2 {x_{22}}^2 x_{21} - ({w_1} {x_{21}}^2 + w_2 x_{21} x_{22})\theta] \\
\tau_w \dot{w}_2 &= \rho[{w_2}^2 {x_{12}}^3 + 2w_1 w_2 {x_{12}}^2 x_{11} + {w_1}^2 {x_{11}}^2 x_{12} - ({w_2} {x_{12}}^2 + w_1 x_{11} x_{12})\theta] \\
&+ (1-\rho)[{w_2}^2 {x_{22}}^3 + 2w_1 w_2 {x_{22}}^2 x_{21} + {w_1}^2 {x_{21}}^2 x_{22} - ({w_2} {x_{22}}^2 + w_1 x_{21} x_{22})\theta] \\
\tau_\theta \dot{\theta} &= \rho[{w_1}^2 {x_{11}}^2 + 2w_1 w_2 x_{11} x_{12} + {w_2}^2 {x_{12}}^2 - \theta] \\
&+ (1-\rho)[{w_1}^2 {x_{21}}^2 + 2w_1 w_2 x_{21} x_{22} + {w_2}^2 {x_{22}}^2 - \theta]
\end{aligned} \tag{3.3}$$

This simplifies to

$$\begin{aligned}
\tau_\theta \dot{\theta} &= {w_1}^2 r_1 + 2 w_1 w_2 s + {w_2}^2 r_2 - \theta \\
\tau_w \dot{w}_1 &= {w_1}^2 p_1 + 2 w_1 w_2 q_1 + {w_2}^2 q_2 - (w_1 r_1 + w_2 s)\theta \\
\tau_w \dot{w}_2 &= {w_2}^2 p_2 + 2 w_1 w_2 q_2 + {w_1}^2 q_1 - (w_2 r_2 + w_1 s)\theta
\end{aligned} \tag{3.4}$$

where

$$\begin{aligned}
r_1 &= \rho {x_{11}}^2 + (1-\rho){x_{21}}^2 \\
r_2 &= \rho {x_{12}}^2 + (1-\rho){x_{22}}^2 \\
s &= \rho x_{11} x_{12} + (1-\rho) x_{21} x_{22} \\
p_1 &= \rho {x_{11}}^3 + (1-\rho){x_{21}}^3 \\
p_2 &= \rho {x_{12}}^3 + (1-\rho){x_{22}}^3 \\
q_1 &= \rho {x_{11}}^2 x_{12} + (1-\rho){x_{21}}^2 x_{22} \\
q_1 &= \rho x_{11} {x_{12}}^2 + (1-\rho) x_{21} {x_{22}}^2
\end{aligned} \tag{3.5}$$

Now let the responses to the two stimuli be $v_1 = \mathbf{w} \cdot \mathbf{x}^{(1)}$ and $v_2 = \mathbf{w} \cdot \mathbf{x}^{(2)}$. With this, changes in the responses can be written as

$$\begin{aligned}
\dot{v}_1 &= x_{11}\dot{w}_1 + x_{12}\dot{w}_2 \\
\dot{v}_2 &= x_{21}\dot{w}_1 + x_{22}\dot{w}_2
\end{aligned} \tag{3.6}$$

Recall that $\dot{w}_i = x_{ji} v (v - \theta)$ where $i, j \in \{1,2\}$. So, if $Pr[\mathbf{x}(t) = \mathbf{x}^{(1)}] = \rho$ and $Pr[\mathbf{x}(t) = \mathbf{x}^{(2)}] = 1 - \rho$, then the mean-field equation derived above can be written in terms of the responses as

$$\begin{aligned}
\tau_\theta \dot{\theta} &= [\rho {v_1}^2 + (1-\rho){v_2}^2 - \theta] \\
\tau_w \dot{v}_1 &= [\rho \mathbf{x}^{(1)} \cdot \mathbf{x}^{(1)} v_1 (v_1 - \theta) + (1-\rho)\mathbf{x}^{(1)} \cdot \mathbf{x}^{(2)} v_2 (v_2 - \theta)] \\
\tau_w \dot{v}_2 &= [\rho \mathbf{x}^{(1)} \cdot \mathbf{x}^{(2)} v_1 (v_1 - \theta) + (1-\rho)\mathbf{x}^{(2)} \cdot \mathbf{x}^{(2)} v_2 (v_2 - \theta)]
\end{aligned} \tag{3.7}$$

Since each of ρ, $\mathbf{x}^{(1)}$, and $\mathbf{x}^{(2)}$ is non-zero, setting the right-hand side of equation 3.7 results in

$$\begin{aligned} \theta &= \rho {v_1}^2 + (1-\rho){v_2}^2 \\ 0 &= v_1(v_1 - \theta) \\ 0 &= v_2(v_2 - \theta) \end{aligned}$$

which simplifies to

$$\begin{aligned} v_1(v_1 - (\rho {v_1}^2 + (1-\rho){v_2}^2)) &= 0 \\ v_2(v_2 - (\rho {v_1}^2 + (1-\rho){v_2}^2)) &= 0 \end{aligned} \tag{3.8}$$

and gives the fixed points

$$(v_1, v_2, \theta) = \left\{ (0,0,0), \left(\frac{1}{\rho}, 0, \frac{1}{\rho}\right), \left(0, \frac{1}{1-\rho}, \frac{1}{1-\rho}\right), (1,1,1) \right\} \tag{3.9}$$

Bienenstock et al discussed the stability of these fixed points as they pertain to the original formulation [7]. Castellani et al [10] and Intrator and Cooper [33] gave a similar treatment to the objective formulation. They showed that the fixed points $\left(\frac{1}{\rho}, 0, \frac{1}{\rho}\right)$ and $\left(0, \frac{1}{1-\rho}, \frac{1}{1-\rho}\right)$ are stable and selective, while $(0,0,0)$ and $(1,1,1)$ are neither stable nor selective. In the next two sections, it will be shown that the stability of $\left(\frac{1}{\rho}, 0, \frac{1}{\rho}\right)$ and $\left(0, \frac{1}{1-\rho}, \frac{1}{1-\rho}\right)$ depends on the angle between the stimuli and the ratio of τ_θ to τ_w.

3.2 OSCILLATORY PROPERTIES

3.2.1 Preliminary analysis

As seen in the preceding section, the fixed points to the mean-field BCM equation are invariant (with regards to stimuli and synaptic weights) and depend on the probabilities with which the stimuli are presented. The stability of the selective fixed points, however, depends on the time-scale parameters and the angular relationship between the stimuli.

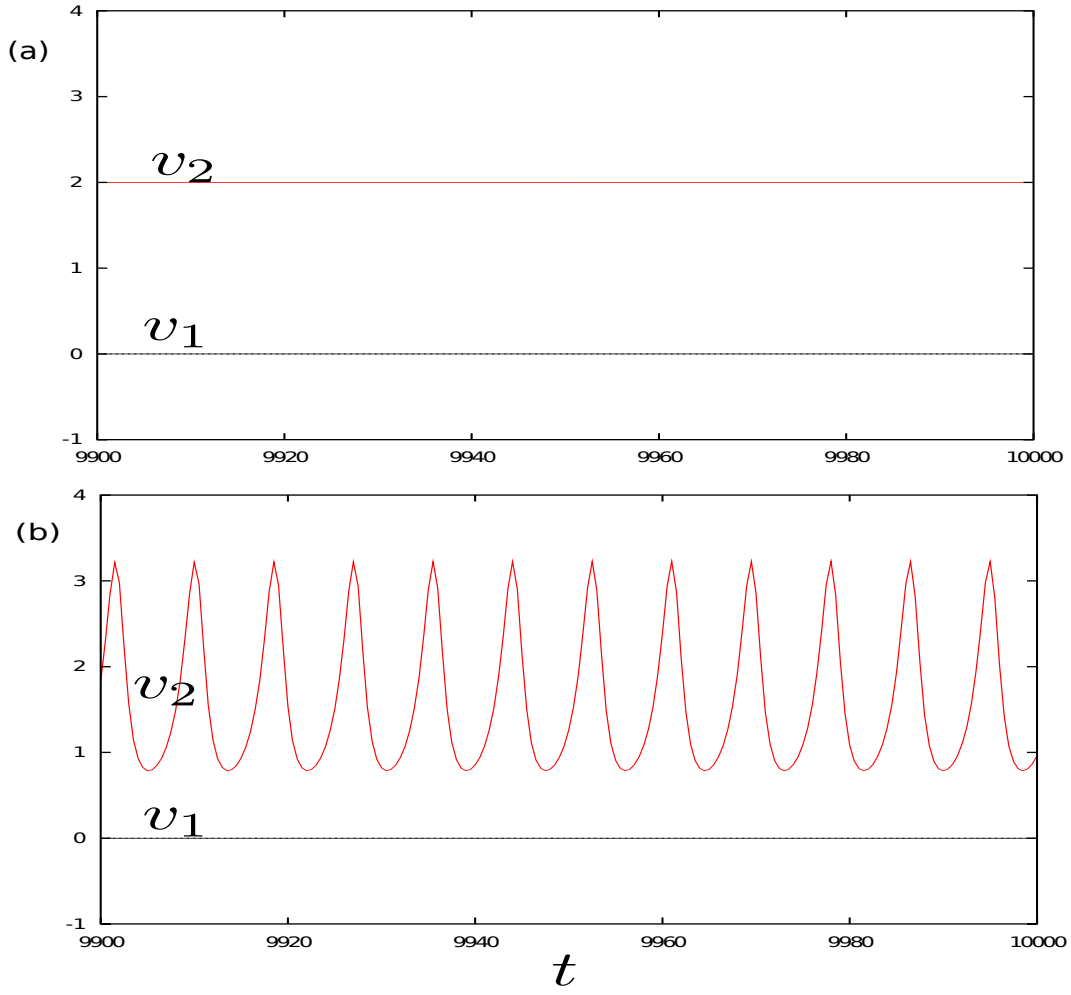

Figure 3.4: $\rho = 0.5$, $\mathbf{x}^{(1)} = (1,0)$, $\mathbf{x}^{(2)} = (0,1)$ (a) $\tau_\theta/\tau_w = 0.1$ (b) $\tau_\theta/\tau_w = 1.1$

To get a preliminary understanding of this property of the system, consider the following simulations of equation 3.4; each with different stimulus set characteristics. The initial conditions of w_1, w_2, and θ all lie in the interval $(0, 0.3)$.

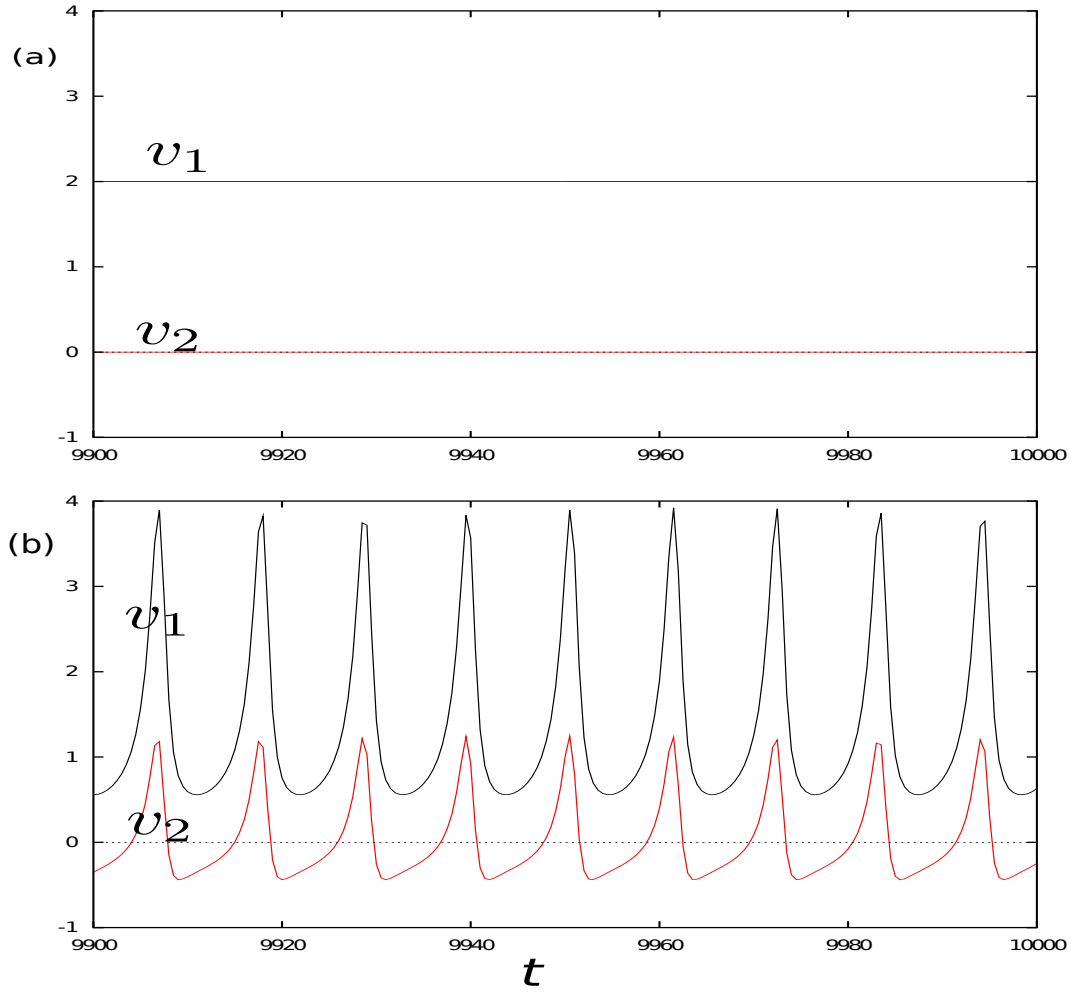

Figure 3.5: $\rho = 0.5$, $\mathbf{x}^{(1)} = (1,0)$, $\mathbf{x}^{(2)} = (0.5,0.5)$ (a) $\tau_\theta/\tau_w = 0.1$ (b) $\tau_\theta/\tau_w = 1.7$

1. **simulation 0: Perpendicular, equal magnitudes, equal probabilities**

   Let $\rho = 0.5$, $\mathbf{x}^{(1)} = (1,0)$, $\mathbf{x}^{(2)} = (0,1)$. In this case, the two stimuli have equal magnitudes, are perpendicular to each other, and are presented with equal probabilities. Figure 3.4 is the evolution of v_1 and v_2 in the last 100 time-steps. 3.4(a) shows a stable

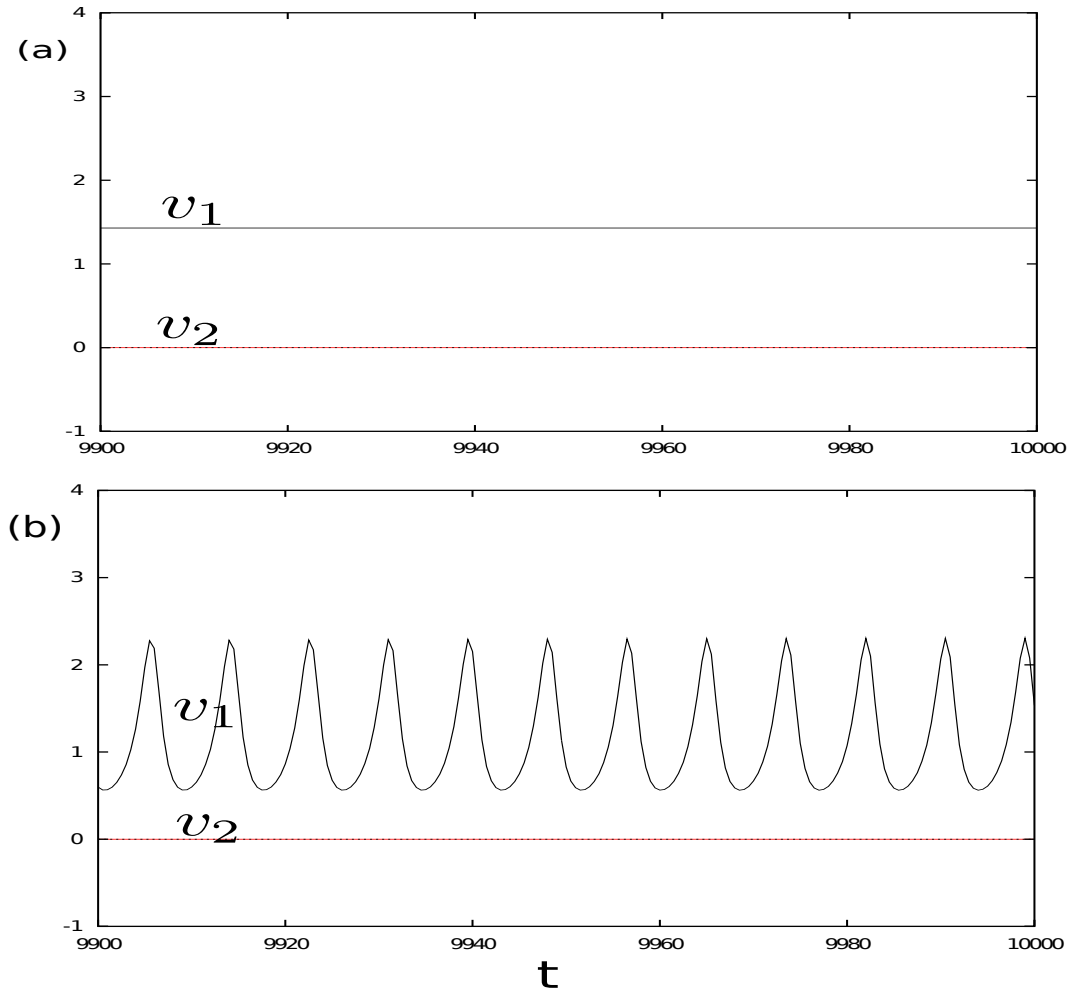

Figure 3.6: $\rho = 0.7$, $\mathbf{x}^{(1)} = (1,0)$, $\mathbf{x}^{(2)} = (1,1)$ (a) $\tau_\theta/\tau_w = 0.1$ (b) $\tau_\theta/\tau_w = 1.1$

steady state of $(0,2,2)$ for $\tau_\theta/\tau_w = 0.1$, and 3.4(b) shows an oscillatory steady state for $\tau_\theta/\tau_w = 1.1$.

2. **simulation 1: Non-perpendicular, unequal magnitudes, equal probabilities**

   Let $\rho = 0.5$, $\mathbf{x}^{(1)} = (1,0)$, $\mathbf{x}^{(2)} = (0.5,0.5)$. In this case, the two stimuli have unequal

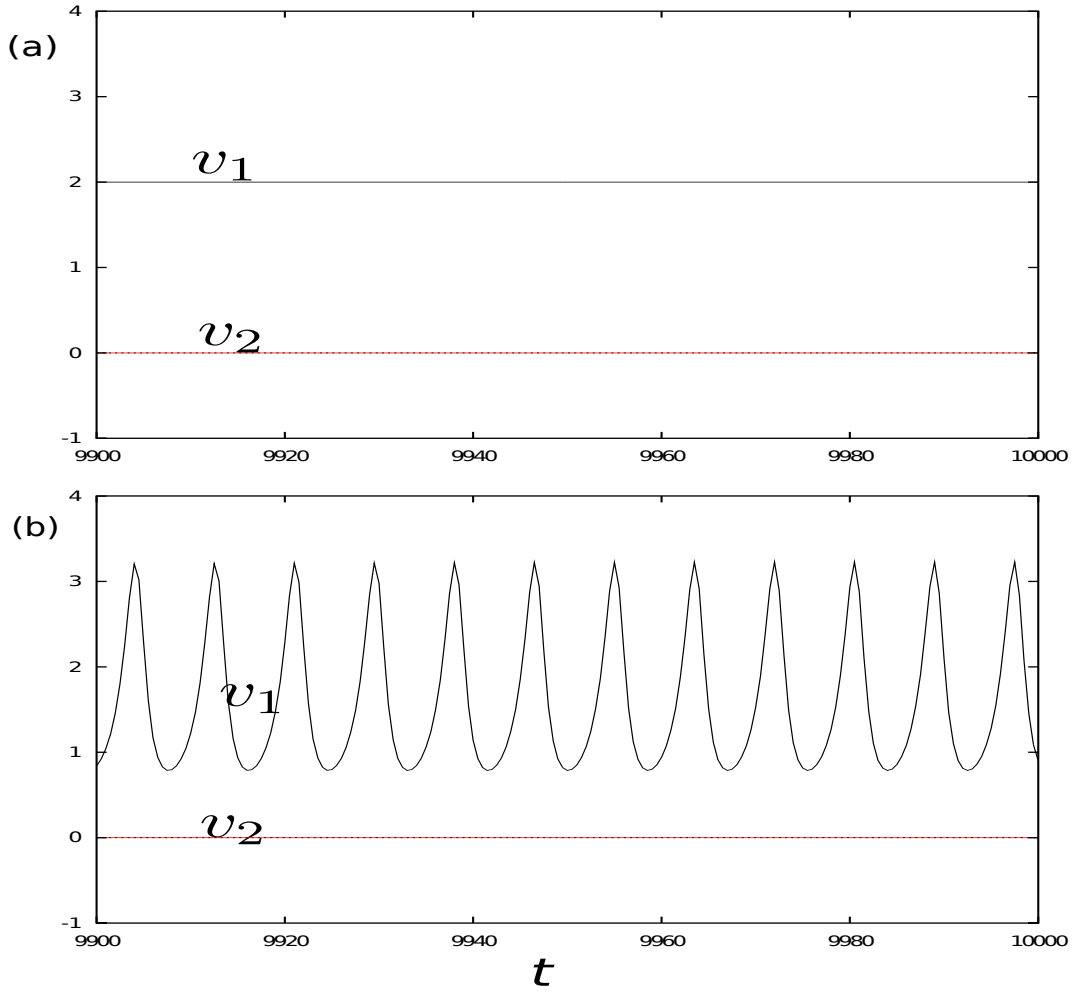

Figure 3.7: $\rho = 0.5$, $\mathbf{x}^{(1)} = (0.7071, 0.7071)$, $\mathbf{x}^{(2)} = (-0.7071, 0.7071)$ (a) $\tau_\theta/\tau_w = 0.1$ (b) $\tau_\theta/\tau_w = 1.1$

magnitudes, are not perpendicular to each other but still are presented with equal probabilities. Figure 3.5(a) shows a stable steady state of $(2,0,2)$ for $\tau_\theta/\tau_w = 0.1$, and 3.5(b) shows an oscillatory steady state for $\tau_\theta/\tau_w = 1.7$.

3. **simulation 2: Perpendicular, equal magnitudes, unequal probabilities**

   Let $\rho = 0.7$, $\mathbf{x}^{(1)} = (1,0)$, $\mathbf{x}^{(2)} = (0,1)$. The only difference between this case and simulation 0 is that the stimuli are now presented with unequal probabilities. Figure 3.5(a) shows a stable steady state of $(1.43,0,1.43)$ for $\tau_\theta/\tau_w = 0.1$ and 3.5(b) shows an oscillatory steady state for $\tau_\theta/\tau_w = 1.1$.

4. **simulation 3: Rotated stimuli**

   Let $\rho = 0.5$, $\mathbf{x}^{(1)} = (0.7071,0.7071)$, $\mathbf{x}^{(2)} = (-0.7071,0.7071)$. The only difference between this case and simulation 0 is that the stimuli are rotated $\pi/4$ rad in the anti-clockwise direction. The result is similar to the result of simulation 0. Figure 3.5(a) shows a stable steady state of $(2,0,2)$ for $\tau_\theta/\tau_w = 0.1$ and 3.5(b) shows an oscillatory steady state for $\tau_\theta/\tau_w = 1.1$.

Notice that the selected stimulus varies according to the characteristics of the stimulus set, as these affect accessibility of the system to the different fixed points. Notice also that in simulations 0, 2, and 3, only the higher responses oscillate. This is possibly because of the perpendicularity of the stimuli in these cases. It is quite possible that as τ_θ/τ_w increases, the two responses will each oscillate.

3.2.2 Stimulus parametrization

The following proposition is useful in describing the class of stimulus patterns used in the remaining results presented in this chapter.

Proposition 3.1. *For any two angles β_1 and β_2, there exists an angle α such that a uniform rotation converts the set of unit vectors $\{\mathbf{x^{(1)}} = (\cos\beta_1, \sin\beta_1),\ \mathbf{x^{(2)}} = (\cos\beta_2, \sin\beta_2)\}$ to $\{\mathbf{x^{(1)}} = (\cos\alpha, \sin\alpha),\ \mathbf{x^{(2)}} = (\sin\alpha, \cos\alpha)\}$*

Proof. It suffices to find the required rotation angle. If this angle is h, then α is such

rotating $\mathbf{x^{(1)}}$ by h gives

$$\cos\alpha = \cos(\beta_1 + h), \quad \sin\alpha = \sin(\beta_1 + h) \tag{3.10}$$

and rotating $\mathbf{x^{(2)}}$ by h gives

$$\sin\alpha = \cos(\beta_2 + h), \quad \cos\alpha = \sin(\beta_2 + h) \tag{3.11}$$

Now, recall that for any y, $\sin y = \cos(\pi/2 - y)$. So setting $\cos\alpha$ of equation 3.10 equal to the $\cos\alpha$ of equation 3.11 gives

$$\beta_1 + h = \pi/2 - (\beta_2 + h)$$

Thus the required rotation angle is

$$h = \frac{\pi}{4} - \frac{(\beta_1 + \beta_2)}{2}$$

and the required parametric angle for the two vectors is

$$\alpha = \frac{(\beta_1 - \beta_2)}{2} + \frac{\pi}{4}$$

□

In order to achieve a deeper exploration of the oscillatory instability observed so far, it is important to be able to express the stimuli as a function of as few parameters as possible. Consider the stimulus pattern set $\mathring{A} = \{\mathbf{x}^{(1)}, \mathbf{x}^{(2)}\}$ of unit vectors where

$$\begin{aligned} \mathbf{x}^{(1)} &= (x_{11}, x_{12}) &&= (\cos\alpha, \sin\alpha) \\ \mathbf{x}^{(2)} &= (x_{21}, x_{22}) &&= (\sin\alpha, \cos\alpha) \end{aligned} \tag{3.12}$$

The set $\mathring{A}$ is linearly independent and such an α exists as a consequence of proposition 3.1. Figure 3.8(a) shows the relationship between the two stimuli when $\alpha > 0$ and figure 3.8(b) shows their relationship when $\alpha < 0$. In each case, the angle between $\mathbf{x}^{(1)}$ and $\mathbf{x}^{(2)}$ is $\pi/2 - 2\alpha$. According to a theorem in [7], a BCM neuron is most selective when the set of stimulus patterns is linearly independent. When $\alpha = \pi/4$, the two stimuli are the same. When $\alpha = -\pi/4$, the angle between the two stimuli is π, implying that they are opposite of each other, and thus linearly dependent. Therefore it is important to restrict α to $-\pi/4 < \alpha < \pi/4$.

Consider a BCM neuron receiving stimulus input $\mathbf{x}$ from $\mathring{A}$ such that $Pr[\mathbf{x}(t) = \mathbf{x}^{(1)}] = Pr[\mathbf{x}(t) = \mathbf{x}^{(2)}] = \frac{1}{2}$. With this stimulus set, the mean field models (equations 3.3 and 3.4 and 3.7) can be written as

$$\begin{aligned} \tau_\theta \dot{\theta} &= {w_1}^2 r + 2 w_1 w_2 s + {w_2}^2 r - \theta \\ \tau_w \dot{w_1} &= {w_1}^2 p + 2 w_1 w_2 q + {w_2}^2 q - (w_1 r + w_2 s)\theta \\ \tau_w \dot{w_2} &= {w_2}^2 p + 2 w_1 w_2 q + {w_1}^2 q - (w_2 r + w_1 s)\theta \end{aligned} \tag{3.13}$$

where

$$\begin{aligned} r = r_1 = r_2 &= \tfrac{1}{2} \\ s &= \sin\alpha\cos\alpha \\ p = p_1 = p_2 &= \tfrac{1}{2}(\cos^3\alpha + \sin^3\alpha) \\ q = q_1 = q_2 &= \tfrac{1}{2}(\sin\alpha\cos\alpha)(\sin\alpha + \cos\alpha) \end{aligned}$$

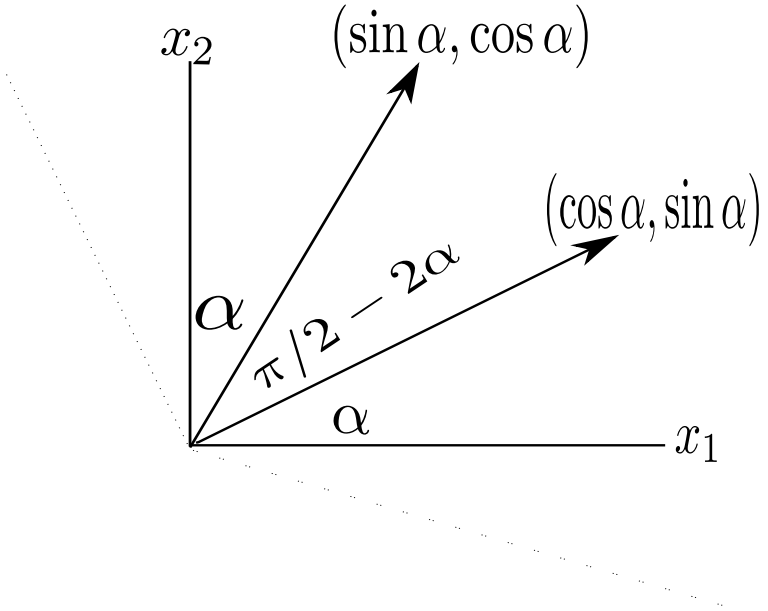

(a)

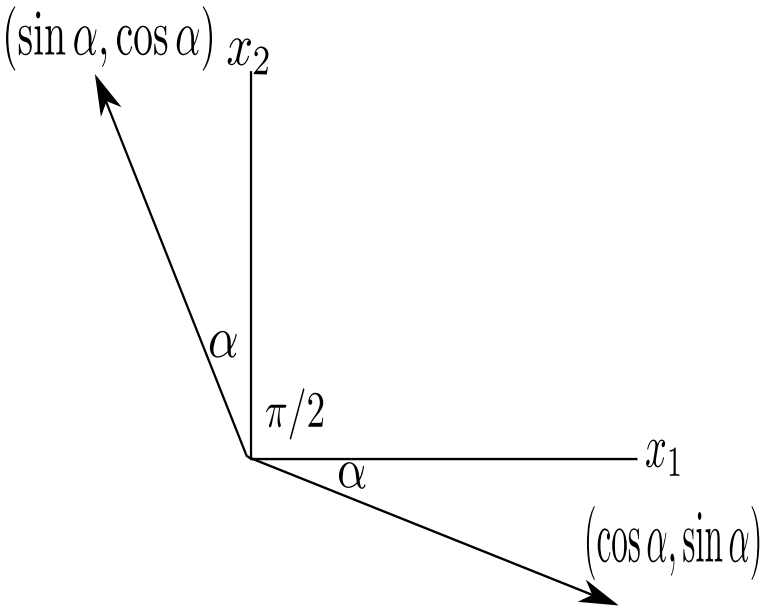

(b)

Figure 3.8: (a) Stimulus patterns when $\alpha > 0$ (b) Stimulus patterns when $\alpha < 0$

and

$$\begin{aligned} \tau_\theta \dot{\theta} &= [\tfrac{1}{2}({v_1}^2 + {v_2}^2) - \theta] \\ \tau_w \dot{v}_1 &= \tfrac{1}{2}[v_1(v_1 - \theta) + \cos\beta v_2(v_2 - \theta)] \\ \tau_w \dot{v}_2 &= \tfrac{1}{2}[\cos\beta v_1(v_1 - \theta) + v_2(v_2 - \theta)] \end{aligned} \tag{3.14}$$

where β is the angle between $\mathbf{x}^{(1)}$ and $\mathbf{x}^{(2)}$. Derivations done in section 3.1.2 show that equation 3.14 has the stable fixed points

$$(v_1, v_2, \theta) = \{(2,0,2), (0,2,2)\}$$

and the unstable fixed points

$$(v_1, v_2, \theta) = \{(0,0,0), (1,1,1)\}$$

3.2.3 Phase plane analysis

With θ set to steady state, for $\alpha = 0.128$, figure 3.9(a) is a $w_1 - vs - w_2$ nullcline of equation 3.13 and figure 3.9(b) is a $v_1 - vs - v_2$ nullcline of equation 3.14. The points of intersection labelled **s** are the stable fixed points of the system while the points labelled **u** are the unstable fixed points.

In sections 3.1.1 and 3.2.1, it was observed that the dynamics of a single BCM neuron along with its selectivity depend on the ratio of the time scale factors τ_θ and τ_w (see equation 3.2). For instance, for $\alpha = 0.28$, when $\tau_\theta/\tau_w = 0.1$ the neuronal responses converge to stable steady state where the neuron is selective. Meanwhile when $\tau_\theta/\tau_w = 1.7$, the responses tend to an oscillatory state where the neuron is hardly selective. In this section, these dynamics are studied further using the mean-field model (equation 3.13). Attention is also paid to the parameter α in order to get more information about how the dynamics in question change with the angular relationship between the stimulus patterns.

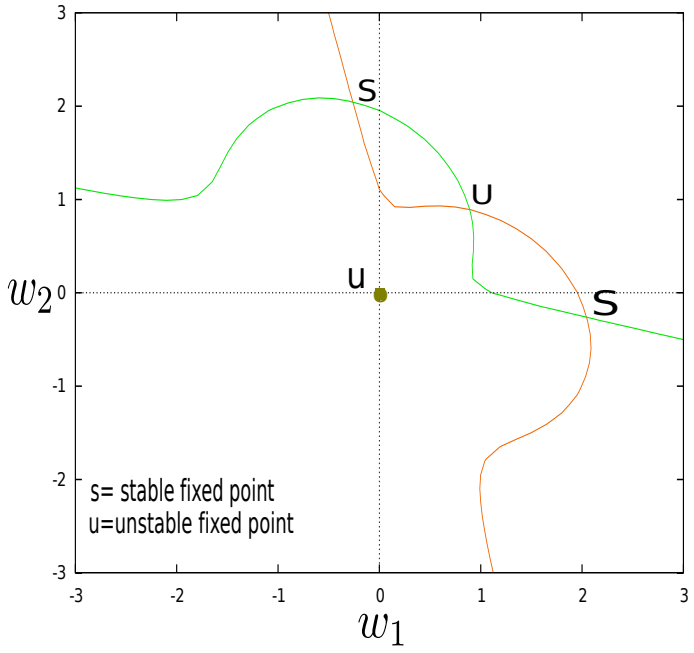

(a)

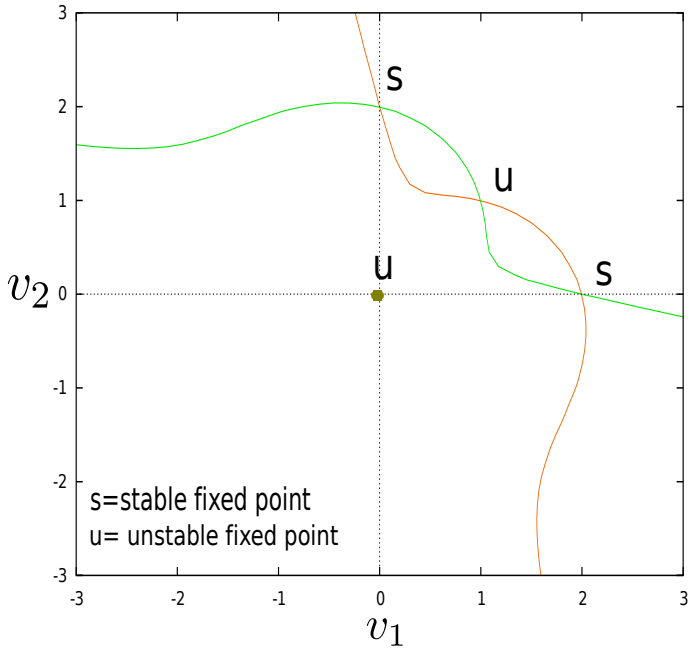

(b)

Figure 3.9: Nullcline of (a) equation 3.13 (weight space) (b) equation 3.14 (response space) when $\alpha = 0.128$, θ is steady

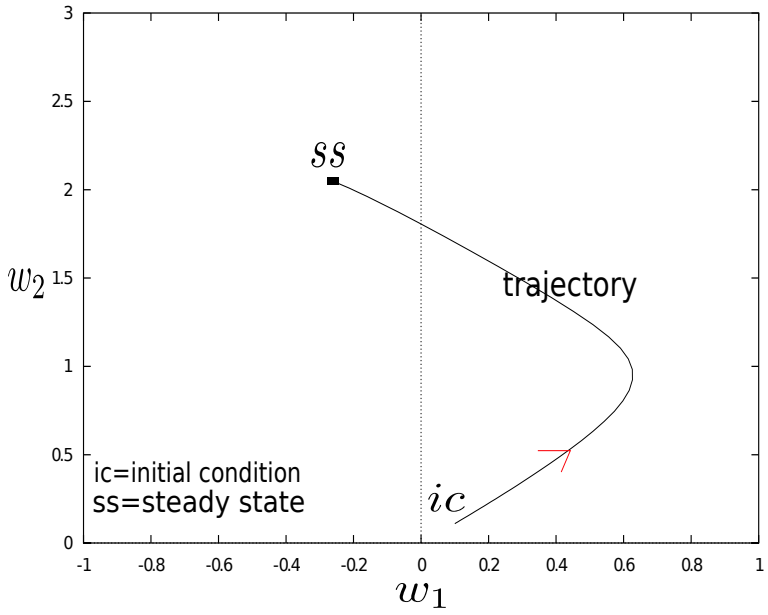

(a)

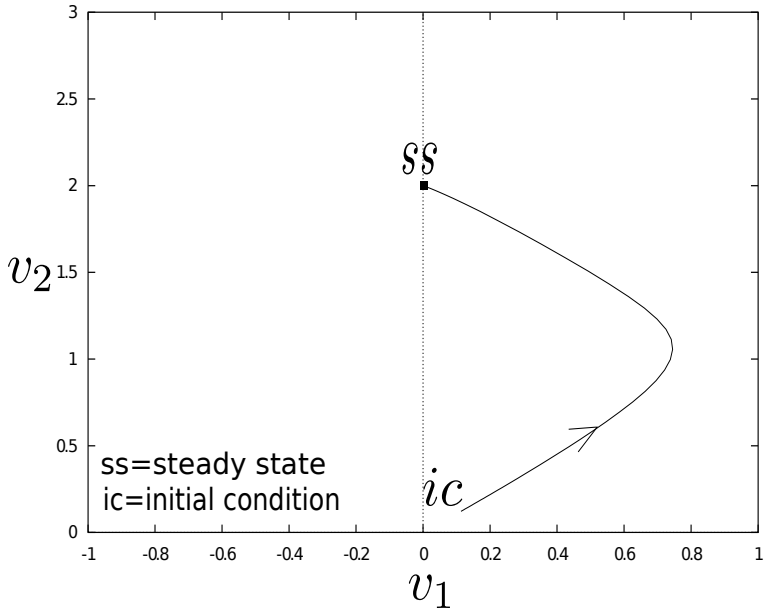

(b)

Figure 3.10: Trajectory of (a) equation 3.13 (weight space) (b) equation 3.14 (response space) when $\alpha = 0.128$, $\tau_\theta/\tau_w = 0.1$

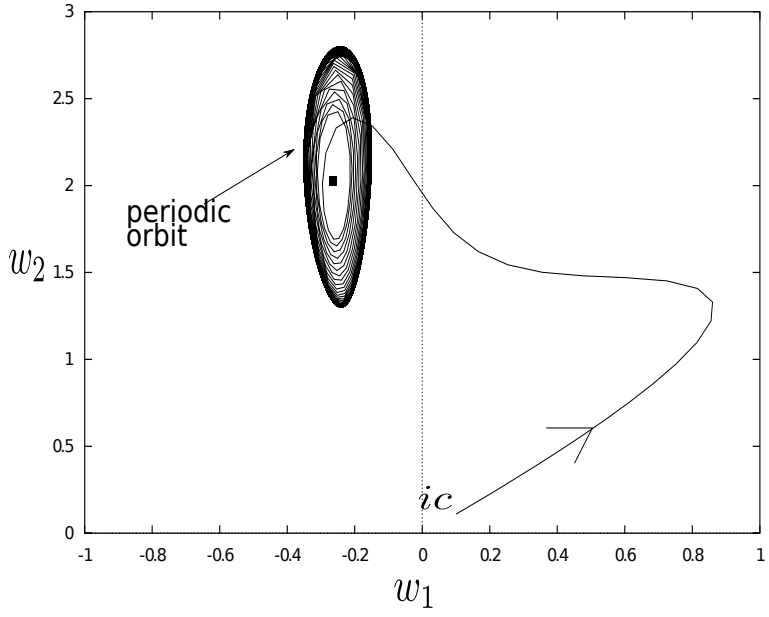

(a)

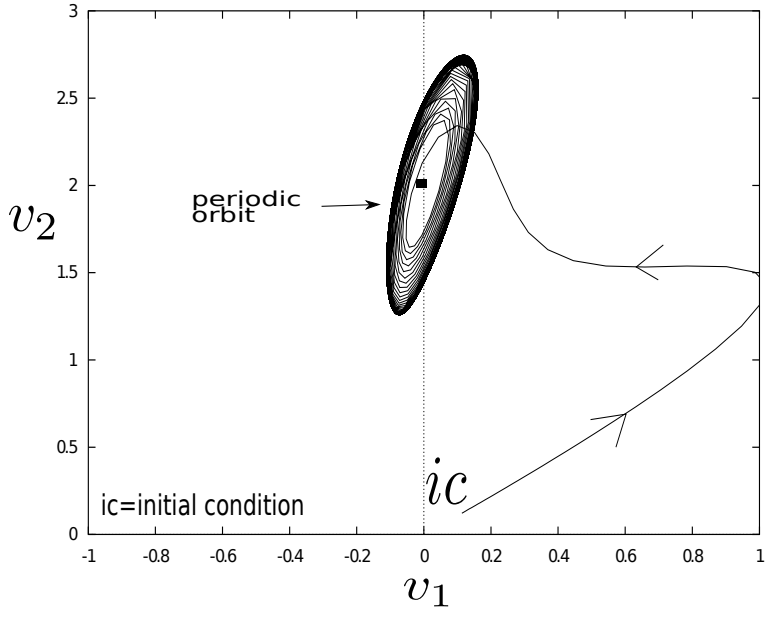

(b)

Figure 3.11: Trajectory of (a) equation 3.13 (weight space) (b) equation 3.14 (response space) when $\alpha = 0.128$, $\tau_\theta/\tau_w = 1.1$

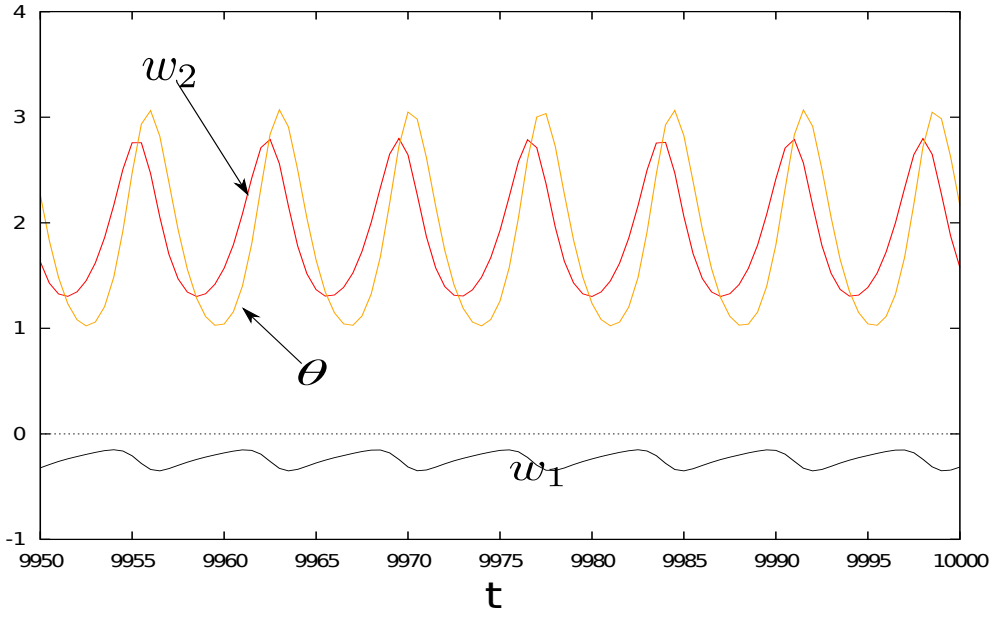

(a)

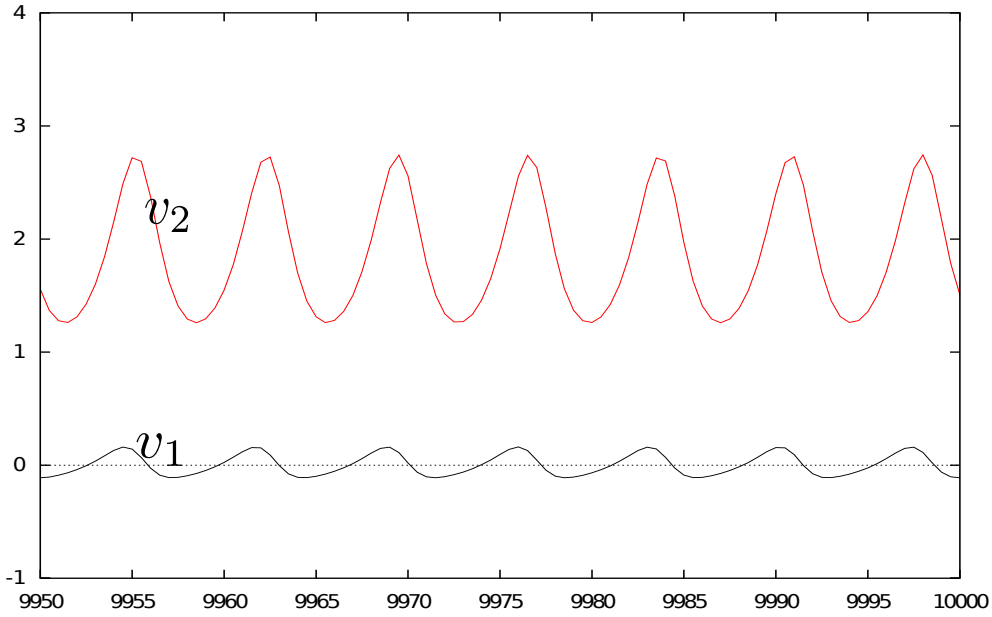

(b)

Figure 3.12: Oscillatory steady state of equation (a) 3.13 (weight space) (b) 3.14 (response space) when $\alpha = 0.128$ and $\tau_\theta/\tau_w = 1.1$

Figure 3.10(a) shows the w_1-w_2 trajectory of a solution to equation 3.13 when $\alpha = 0.128$ and $\tau_\theta/\tau_w = 0.1$. The initial condition is $(\theta, w_1, w_2) = (0, 0.1, 0.11)$. The system converges to the stable steady state $(\theta, w_1, w_2) = (-.03, 2.07, 2)$. The stable nature of this steady state should not come as a surprise since the same τ_θ/τ_w value gave a selective stable steady state (see figure 3.1) when the simulation was stochastic with equation 3.2. A corresponding v_1-v_2 trajectory for equation 3.14 is shown in figure 3.10(b). As expected, the trajectory converges to one of the fixed points listed in section 3.1.2; which in this case is $(0, 2, 2)$.

Figure 3.11 shows the trajectory of a solution to the same equation when $\tau_\theta/\tau_w = 1.1$ with the same α and initial condition. As can be seen, the trajectory converges to a periodic orbit with center $\approx (-.03, 2.07, 2)$. A similar v_1-v_2 trajectory for equation 3.14 is shown in figure 3.11(b) and as expected, the periodic orbit has center $(0, 2, 2)$. Figure 3.12(a) shows the oscillations of w_1 and w_2 corresponding to this periodic orbit. θ, along with the neuronal responses (see figure 3.12(b)), display similar oscillations. Again this should not come as a surprise since a similar behavior was observed in the stochastic model (figure 3.2) for the same value of τ_θ/τ_w.

3.2.4 Bifurcation analysis

What values of α lead to an oscillatory steady state? For $\tau_\theta/\tau_w = 1.1$, the answer to this question can be summarized with figure 3.13, a bifurcation diagram of $w_1 - vs - \alpha$, $w_2 - vs - \alpha$, $\theta - vs - \alpha$, $v_1 - vs - \alpha$, and $v_2 - vs - \alpha$. The red lines are stable steady state values while the green points are the maximum and minimum values of oscillation. For example, when $\alpha = 0.4$, the steady state is $(\theta, w_1, w_2) = (2, -0.5, 2.2)$, meanwhile, when $\alpha = 0$, the system converges to a state where θ oscillates with an amplitude of 3.3 (since it has the maximum value of oscillation is 3.8 and the minimum value is 0.5), w_2 with an amplitude

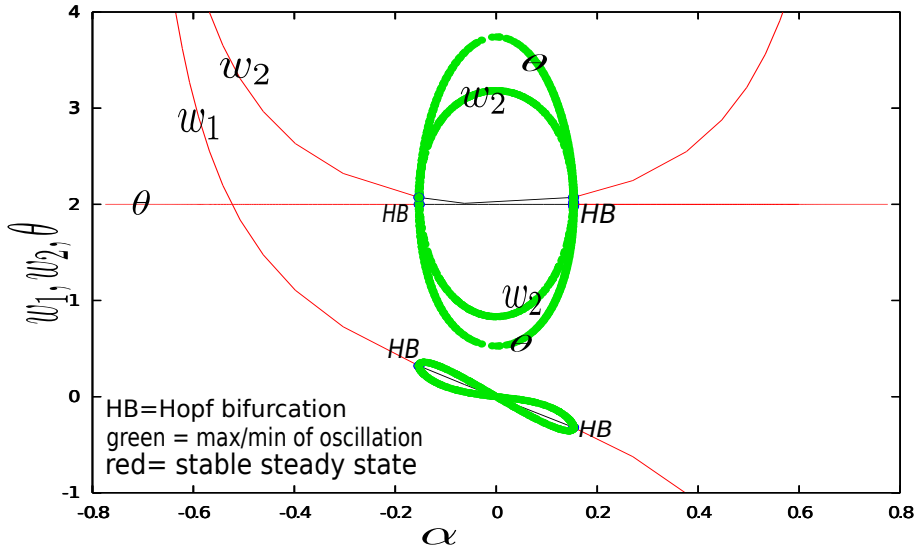

(a)

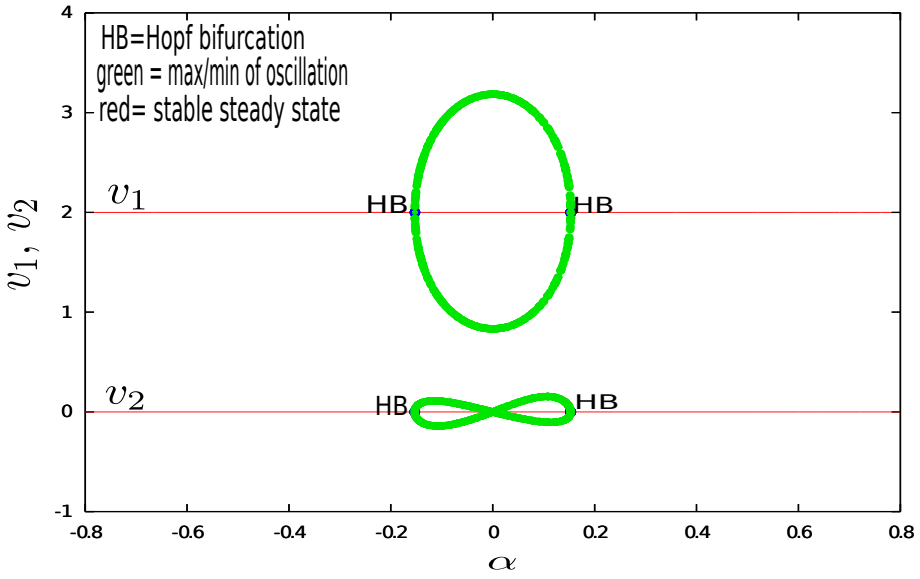

(b)

Figure 3.13: Bifurcation diagram (as α varies) of equation 3.13 when $\tau_\theta/\tau_w = 1.1$

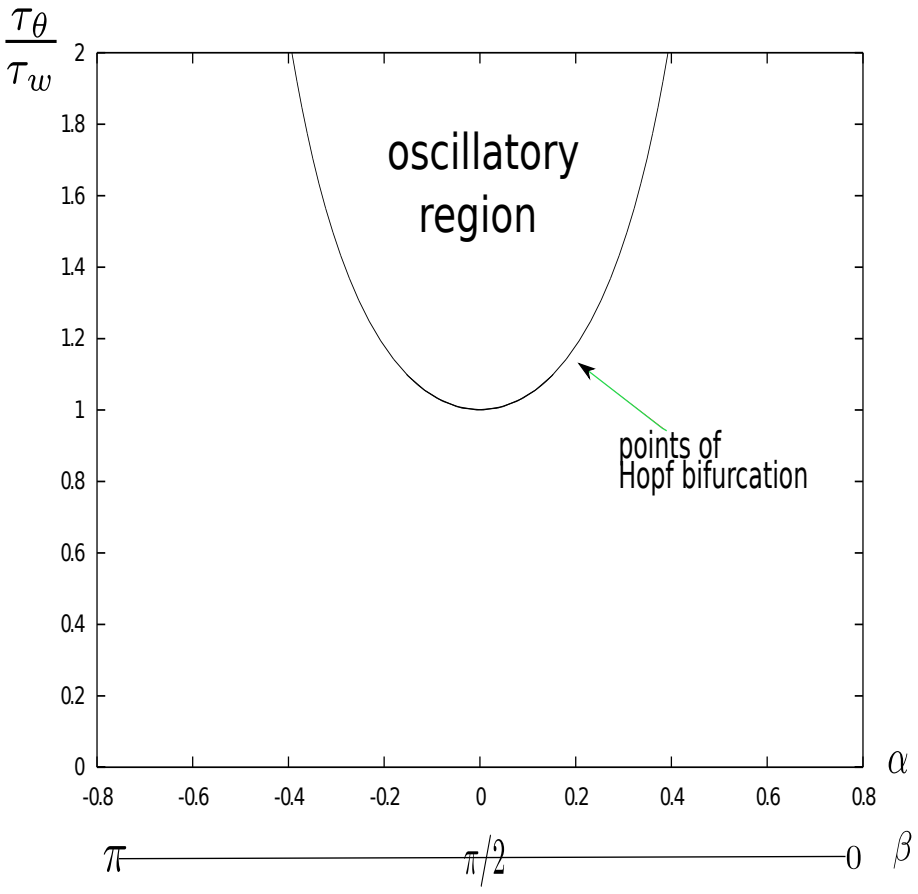

Figure 3.14: α bifurcation values for different values of τ_θ/τ_w

of 2.7 and w_1 with an amplitude of 0. At $\alpha = -0.153$ the system undergoes a Hopf bifurcation and as a result, the steady losses stability and becomes oscillatory. Another Hopft Bifurcation occurs at $\alpha = 0.153$ when the steady states cease to be oscillatory and return to stability.

Not every τ_θ/τ_w value exhibits bifurcation when α is varied. Figure 3.14 shows the α

bifurcation values for $0 < \tau_\theta/\tau_w < 2$. When $\tau_\theta/\tau_w = 1.1$, the Hopf bifurcation values of $\alpha = -0.153$ and $\alpha = 0.153$ can clearly be seen. If β is the angle between the two stimuli (i.e $\beta = \pi/2 - 2\alpha$), then we can conclude that, starting at $\beta = \pi/2$, the larger β gets, the higher the τ_θ Hopf bifurcation point. Also, starting at $\beta = \pi/2$, the smaller β gets, the higher the τ_θ Hopf bifurcation point. A major qualitative information to be deduced from this figure is that all $(\alpha, \tau_\theta/\tau_w)$ pairs above the curve leads to an oscillatory steady state while the pairs above the curve lead to stable steady states.

3.2.5 Selectivity analysis

For a single neuron $\mathscr{N}$ presented with a set of stimuli $\mathring{A}$, Bienenstock et al [7] defines the selectivity of $\mathscr{N}$ as a function of the area under the tuning curve of the neuronal reponses to the stimuli in $\mathring{A}$. This definition, however, assumes that the BCM learning rule of $\mathscr{N}$ converges to a stable steady state. To analyze the selectivity of a neuron as τ_θ/τ_w varies, one needs a measure of selectivity that addresses an oscillatory steady state.

Definition 3.1. (Relative selectivity) *Let $\mathscr{N}$ be a linear BCM neuron that receives stimulus patterns from the set $\mathring{A} = \{\mathbf{x}^{(1)} = (x_{11}, x_{12}), \mathbf{x}^{(2)} = (x_{21}, x_{22})\}$ with synaptic weights $\mathbf{w} = (w_1, w_2)$. For a given (τ_θ, τ_w) pair, let t_o be the point in time at which the dynamics of $\mathscr{N}$ achieve a stable steady state or an oscillatory steady state. Finally, let*

- $v_1(t) = w_1(t)x_{11} + w_2(t)x_{12}$
- $v_2(t) = w_1(t)x_{21} + w_2(t)x_{22}$
- $d(\tau_\theta, \tau_w) = min_{t \geq t_o} |v_1(t) - v_2(t)|$

The **relative selectivity, RS** *of $\mathscr{N}$ is defined as*

$$RS_{\mathscr{N}}(\tau_\theta, \tau_w) = \frac{d(\tau_\theta, \tau_w)}{\max\limits_{\frac{\tau_1}{\tau_2} \in (0,\infty)} d(\tau_1, \tau_2)}$$

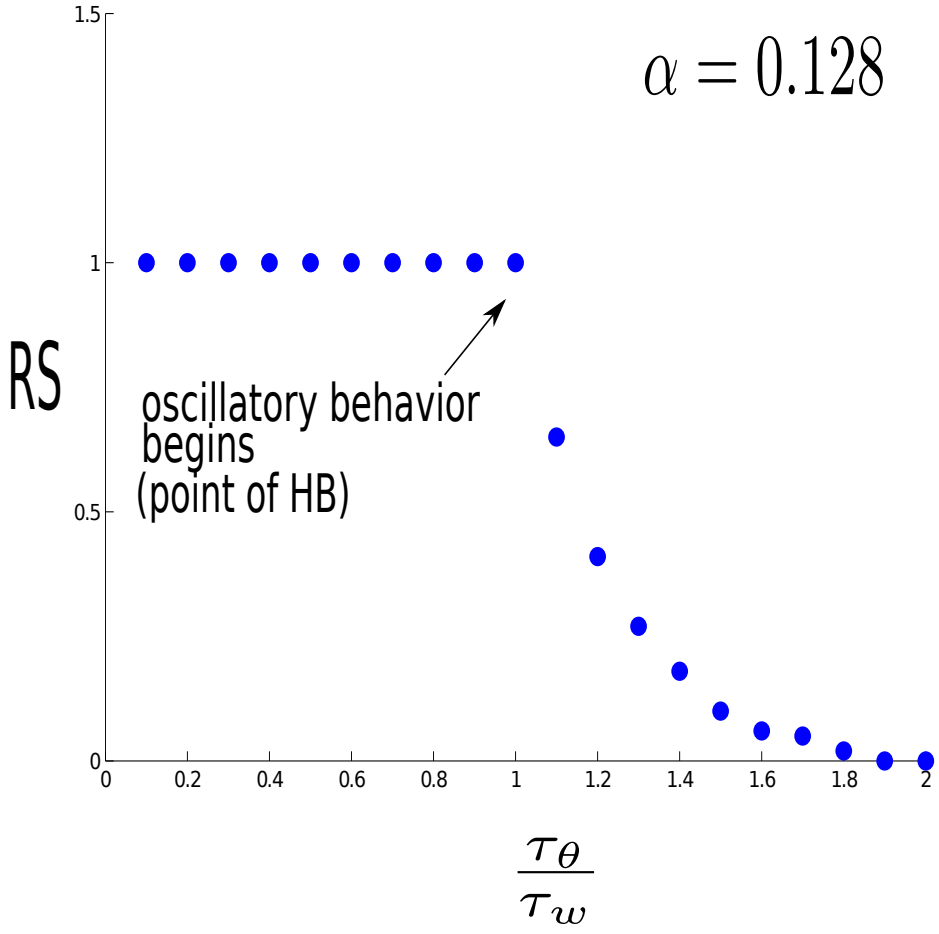

Figure 3.15: Relative selectivity vs τ_θ/τ_w. $\alpha = 0.128$

Note that $0 \leq RS \leq 1$, since it is defined as a fraction of the maximum selectivity. For this reason it tends to have the same maximum value and shape for all values of $\alpha \in (-\pi/4, \pi/4)$. As can be seen in figure 3.15, RS stays pretty much at it maximum between $\tau_\theta/\tau_w = 0$ and the value of τ_θ/τ_w that gives rise to a supercritical Hopf bifurcation

(1.05 for $\alpha = 0.128$), after which RS decays to 0. This curve is in agreement with the two-parameter curve of supercritical Hopf bifurcation points shown in figure 3.14. The regime where $RS < 1$ corresponds to the regime of oscillations shown in figure 3.14.

3.3 STABILITY THEOREMS

Theorem 3.1. *Assume that the linear neuron $\mathcal{N}$ receives the unit vector stimulus pattern* $\mathbf{x}$ *from the set* $\{\mathbf{x^{(1)}}, \mathbf{x^{(2)}}\}$ *with* $Pr[\mathbf{x}(t) = \mathbf{x^{(1)}}] = Pr[\mathbf{x}(t) = \mathbf{x^{(2)}}] = \frac{1}{2}$. *Let β be the angle between* $\mathbf{x^{(1)}}$ *and* $\mathbf{x^{(2)}}$, *let* $\mathbf{w}$ *be the synaptic weights with which $\mathcal{N}$ receives* $\mathbf{x}$, *and let* $v_1 = \mathbf{w} \cdot \mathbf{x^{(1)}}$ *and* $v_2 = \mathbf{w} \cdot \mathbf{x^{(2)}}$ *be the respective responses of $\mathcal{N}$ to* $\mathbf{x^{(1)}}$ *and* $\mathbf{x^{(2)}}$. *Then the fixed points* $(v_1, v_2, \theta) = \{(2,0,2), (0,2,2)\}$ *of the BCM dynamics (given in equation 3.7) of $\mathcal{N}$ are stable if and only if* $0 < \tau_\theta / \tau_w < 1/sin^2\beta$

Proof. In terms of v_1 and v_2, the BCM dynamics of $\mathcal{N}$ is given by

$$\begin{aligned} \tau_\theta \dot{\theta} &= [\tfrac{1}{2}({v_1}^2 + {v_2}^2) - \theta] \\ \tau_w \dot{v_1} &= \tfrac{1}{2}[v_1(v_1 - \theta) + \cos\beta\, v_2(v_2 - \theta)] \\ \tau_w \dot{v_2} &= \tfrac{1}{2}[\cos\beta\, v_1(v_1 - \theta) + v_2(v_2 - \theta)] \end{aligned}$$

(see section 3.1.2)

Let $\tau = \tau_\theta / \tau_w$ and without loss of generality, let $\tau_w = 1$.

Also let $f_\theta = \dot{\theta}$, $f_1 = \dot{v}_1$ and $f_2 = \dot{v}_2$. Compute the partial derivates of f_θ as follows:

$$\begin{aligned}
\frac{\partial f_\theta}{\partial \theta} &= -1/\tau \\
\frac{\partial f_\theta}{\partial v_1} &= v_1/\tau \\
\frac{\partial f_\theta}{\partial v_2} &= v_2/\tau
\end{aligned}$$

Compute the partial derivates of f_1 as follows:

$$\begin{aligned}
\frac{\partial f_1}{\partial \theta} &= -\tfrac{1}{2}(v_1 + \cos\beta\, v_2) \\
\frac{\partial f_1}{\partial v_1} &= v_1 - \tfrac{1}{2}\theta \\
\frac{\partial f_1}{\partial v_2} &= \cos\beta(v_2 - \tfrac{1}{2}\theta)
\end{aligned}$$

Compute the partial derivates of f_2 as follows:

$$\begin{aligned}
\frac{\partial f_2}{\partial \theta} &= -\tfrac{1}{2}(v_2 + \cos\beta\, v_1) \\
\frac{\partial f_2}{\partial v_1} &= \cos\beta(v_1 - \tfrac{1}{2}\theta) \\
\frac{\partial f_2}{\partial v_2} &= v_2 - \tfrac{1}{2}\theta
\end{aligned}$$

Linearizing around the fixed point $(2,0,2)$ gives the Jacobian

$$J = \begin{pmatrix} -1/\tau & 2/\tau & 0 \\ -1 & 1 & -\cos\beta \\ -\cos\beta & \cos\beta & -1 \end{pmatrix}$$

If λ is the eigenvalue of J, then

$$\begin{aligned} det(\lambda I - J) &= (\lambda + \tfrac{1}{\tau})((\lambda - 1)(\lambda + 1) + \cos^2\beta) + \tfrac{2}{\tau}(\lambda + 1 - \cos^2\beta) \\ &= (\lambda + \tfrac{1}{\tau})(\lambda^2 - \sin^2\beta) + \tfrac{2}{\tau}(\lambda + \sin^2\beta) \\ &= \lambda^3 + \tfrac{1}{\tau}\lambda^2 + (\tfrac{2}{\tau} - \sin^2\beta)\lambda + \tfrac{1}{\tau}\sin^2\beta \end{aligned} \tag{3.15}$$

Linearizing around the fixed point $(0,2,2)$ gives the same expression for the determinant of $\lambda I - J$.

The Routh Hurwitz criteria [64] can be employed to determine stability. According to these criteria, the roots of the polynomial $P(x) = x^3 + ax^2 + bx + c$ all have negative real parts if and only if $a > 0$, $c > 0$ and $ab - c > 0$ [21] . This means that right hand side of equation 3.15 have roots with negative real parts if

$$\frac{1}{\tau}(\frac{2}{\tau} - \sin^2\beta) - \frac{1}{\tau}\sin^2\beta > 0 \tag{3.16}$$

or

$$\tau < 1/sin^2\beta \tag{3.17}$$

which implies the fixed points are stable if $0 < \tau_\theta/\tau_w < 1/sin^2\beta$. □

Theorem 3.2. *Assume the same stimulus set, synaptic weight, and response hypotheses for neuron $\mathcal{N}$ in theorem 3.1. If $\tau_\theta/\tau_w \geq 1/sin^2\beta$, then the fixed points $(v_1, v_2, \theta) = \{(2,0,2),(0,2,2)\}$, of the BCM dynamics of $\mathcal{N}$, remain unstable in a the interior of emergent limit cycles.*

Proof. Refer to the proof of theorem 3.1.

W. Liu [42] proved (by use of the Routh Hurwitz criteria) that one can conclude the existence of a Hopf bifurcation when inequality 3.16 becomes an equality. Thus, for $\tau = \tau_\theta/\tau_w \geq 1/sin^2\beta$, there is a branching of limit cycles from the fixed points $(v_1, v_2, \theta) = \{(2,0,2),(0,2,2)\}$ □

3.4 SUMMARY

The dynamic threshold, θ, of the BCM learning rule (equation 3.2), is a homeostatic mechanism that serves to provide stability to the system. As demonstrated by Bienenstock et al, the dynamics of a single BCM neuron converge to a stable steady state when homeostasis changes much faster than synaptic weights $\mathbf{w}$. In the present chapter, a mean-field analysis shows that slowing down homeostasis past a given parametric value leads to an unstable steady state. In other words, the system undergoes a bifurcation at a certain value of the ratio τ_θ/τ_w (ratio of time scale factor of homeostasis to that of synaptic weights) and this gives rise to an oscillatory steady state. The bifurcation value depends on the angular relationship between the stimulus patterns. In addition, this bifurcation value also bifurcates the selectivity behavior of the neuron, as the selectivity of the neuron starts to decay to zero at this value.

4.0 EMERGENT DYNAMICAL PROPERTIES OF COUPLED BCM NEURONS

In this chapter, the dynamics of mutually inhibiting coupled BCM neurons are studied. The methods of the study are presented in section 4.1 . In particular, a stability condition for a network of mutually inhibiting linear neurons is developed in 4.1.1. This condition is useful in setting up the system of equations for two mutually inhibiting BCM neurons (4.1.2) and its stochastic experimentation (4.1.3). In 4.1.4 a mean-field model for the BCM learning rule of two mutually inhibiting neurons is derived. Oscillatory, toroidal and chaotic dynamics are observed in certain parametric regimes. These dynamical properties of the system are analyzed in section 4.2. The numerical results presented in this chapter are obtained using XPPAUT [17] except where noted.

4.1 METHODS

4.1.1 Mutually inhibiting neurons

To implement a network of coupled BCM neurons receiving stimulus patterns from a common set, it is important to incorporate a mechanism for competitive selectivity within the network. A mechanism of this sort, found in visual processes [19] (and also in tactile [37], auditory [50], and olfactory processing [66]) is called lateral inhibition. During

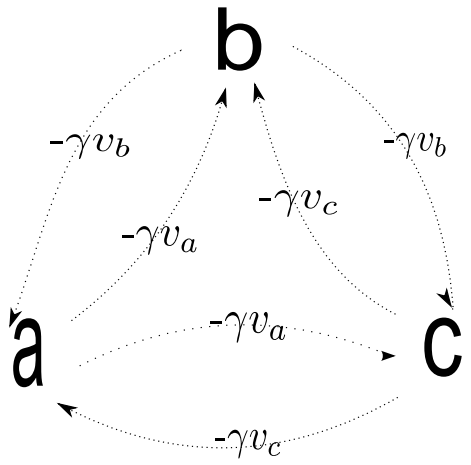

Figure 4.1: Three mutually coupled neurons inhibiting one another

lateral inhibition, an excited neuron reduces the activity of its neighbors by disabling the spreading of action potentials to neighboring neurons in the lateral direction. This creates a contrast in stimulation that allows increased sensory perception.

Consider a network of N mutually inhibiting neurons. At any time, let $\{v_i\}_{i=1}^N$ be the net activities of the neurons. Let $\{s_i\}_{i=1}^N$ be the partial activities induced by a stimulus pattern $\mathbf{x}$ i.e $s_i = \mathbf{w_i} \cdot \mathbf{x}$ where $\mathbf{w_i}$ is the synaptic weight vector for neuron i. At any given time, the activity, v_i of the linear neuron i (where $i \in \{1,2,\ldots N\}$) follows the differential equation:

$$\frac{dv_i}{dt} = -v_i + I_i \tag{4.1}$$

where I_i is the external input to the neuron [18]. Since neuron i is inhibited by its neighbors (see figure 4.1 for illustration)

$$I_i = s_i - \gamma \sum_{j \neq i} v_j \tag{4.2}$$

where γ is the inhibition parameter, measuring the amount of inhibition that i gets. Substituting equation 4.2 into 4.1 gives

$$\frac{dv_i}{dt} = -v_i + s_i - \gamma \sum_{j \neq i} v_j \tag{4.3}$$

At a steady state, equation 4.3 becomes

$$s_i = v_i + \gamma \sum_{j \neq i} v_j \tag{4.4}$$

Thus, the overall activity of the network can be expressed as

$$\mathbf{s} = G\mathbf{v} \tag{4.5}$$

or

$$\mathbf{v} = G^{-1}\mathbf{s} \tag{4.6}$$

where

$$G = \begin{bmatrix} 1 & \gamma & \gamma & \dots & \gamma \\ \gamma & 1 & \gamma & \dots & \gamma \\ \gamma & \gamma & 1 & \dots & \gamma \\ \vdots & \vdots & \vdots & \ddots & \vdots \\ \gamma & \gamma & \gamma & \dots & 1 \end{bmatrix} \tag{4.7}$$

A condition for stability within this network is summarized in the following proposition

Proposition 4.1. *At any time, let* $\{v_i\}_{i=1}^N$ *be the net activities of N coupled mutually inhibiting linear neurons. Let* $\{s_i\}_{i=1}^N$ *be the partial activities induced by a stimulus pattern* $\mathbf{x}$ *i.e* $s_i = \mathbf{w_i} \cdot \mathbf{x}$ *where* $\mathbf{w_i}$ *is the synaptic weight vector for neuron i. Let* γ *be the inhibition parameter. For* $0 < \gamma < 1$*, the stable steady state activity of the neurons can be expressed as* $\mathbf{v} = G^{-1}\mathbf{s}$ *where G is as defined in equation 4.7,* $\mathbf{v} = (v_1, v_2, \dots v_N)$ *and* $\mathbf{s} = (s_1, s_2, \dots, s_N)$

Proof. To prove this proposition, one must show the following:

1. the invertibility of G for $0 < \gamma < 1$
2. the stability of the network for $0 < \gamma < 1$

Invertibility of G for $0 < \gamma < 1$:

Let $V = \sum_{j=1}^{N} v_j$. Then one can write equation 4.4 as

$$v_i = s_i - \gamma V + \gamma v_i \tag{4.8}$$

or

$$v_i = \frac{s_i - \gamma V}{1 - \gamma} \tag{4.9}$$

thus

$$\begin{aligned} V &= \textstyle\sum_{j=1}^{N} \frac{s_j - \gamma V}{1-\gamma} \\ &= \textstyle\frac{1}{1-\gamma}(\sum_{j=1}^{N} s_j - \gamma \sum_{j=1}^{N} V) \\ &= \textstyle\frac{1}{1-\gamma}(\sum_{j=1}^{N} s_j - \gamma N V) \end{aligned} \tag{4.10}$$

implying

$$(1 + \gamma(N-1))V = \sum_{j=1}^{N} s_j \tag{4.11}$$

or

$$V = \frac{\sum_{j=1}^{N} s_j}{1 + \gamma(N-1)} \tag{4.12}$$

Substituting V into equation 4.9 we get

$$v_i = \frac{1}{1-\gamma} s_i - \frac{\gamma}{(1-\gamma)(1+\gamma(N-1))} \sum_{j=1}^{N} s_j \tag{4.13}$$

The left-hand side of equation 4.13 is undefined when $\gamma = 1$ or $\gamma = -\frac{1}{N-1}$. Thus G is invertible when $0 < \gamma < 1$.

Stability of the network for $0 < \gamma < 1$:

For $i \in \{1, 2, \ldots, N\}$ let $f_i = \frac{dv_i}{dt}$. To linearize around the steady state solution of equation 4.3 take the partial derivatives of each f_i to obtain the Jacobian

$$M = \begin{bmatrix} -1 & -\gamma & -\gamma & \ldots & -\gamma \\ -\gamma & -1 & -\gamma & \ldots & -\gamma \\ -\gamma & -\gamma & -1 & \ldots & -\gamma \\ \vdots & \vdots & \vdots & \ddots & \vdots \\ -\gamma & -\gamma & -\gamma & \ldots & -1 \end{bmatrix}$$

Notice that $(1, 1, \ldots, 1)^T$ is an eigenvector of M with corresponding eigenvalue $-(1+N\gamma)$. This eigenvalue is negative when $\gamma > -1/N$.

Also notice that M can be written as

$$M = -\gamma \mathbb{1} + (\gamma - 1)\mathbb{I}$$

where $\mathbb{1}$ is the $N - by - N$ matrix of all 1's and $\mathbb{I}$ is the $N - by - N$ identity matrix. Note that $nullity(\mathbb{1}) = 1$, since $dim(\mathbb{1}) = N$ and $rank(\mathbb{1}) = 1$.

$null(\mathbb{1})$ is in the eigenspace of M because if $\mathscr{U} \in null(\mathbb{1})$ then

$$\begin{aligned} M\mathscr{U} &= -\gamma \mathbb{1}\mathscr{U} + (\gamma - 1)\mathbb{I}\mathscr{U} \\ &= (\gamma - 1)\mathscr{U} \end{aligned}$$

Thus $\mathscr{U}$ is an eigenvector of M corresponding to the eigenvalue $\gamma - 1$. This eigenvalue is negative when $0 < \gamma < 1$. which proves the theorem.

□

4.1.2 Two mutually inhibiting BCM neurons

Consider two neurons **a** and **b** who mutually inhibit each other and, at any instant, receive the same stimulus pattern **x**, with synaptic weight vectors $\mathbf{w_a}$ (for neuron **a**) and $\mathbf{w_b}$ (for neuron **b**). Let their responses to **x** be s_a and s_b, and their net responses (after accounting for inhibition) be v_a and v_b. Finally, let the dynamic threshold to v_a and v_b be θ_a and θ_b respectively. The BCM learning rule of these two neurons is given by

$$\begin{aligned} \tau_w \dot{\mathbf{w}}_a &= \mathbf{x} v_a (v_a - \theta_a) \\ \tau_\theta \dot{\theta}_a &= {v_a}^2 - \theta_a \\ \tau_w \dot{\mathbf{w}}_b &= \mathbf{x} v_b (v_b - \theta_b) \\ \tau_\theta \dot{\theta}_b &= {v_b}^2 - \theta_b \end{aligned} \tag{4.14}$$

where $s_a = \mathbf{w_a} \cdot \mathbf{x}$ and $s_b = \mathbf{w_b} \cdot \mathbf{x}$ and as a result of theorem 4.1 (with $0 < \gamma < 1$)

$$\begin{bmatrix} v_a \\ v_b \end{bmatrix} = \begin{bmatrix} 1 & \gamma \\ \gamma & 1 \end{bmatrix}^{-1} \begin{bmatrix} s_a \\ s_b \end{bmatrix} \tag{4.15}$$

or

$$\begin{aligned} v_a &= \tfrac{1}{1-\gamma^2} s_a - \tfrac{\gamma}{1-\gamma^2} s_b \\ v_b &= \tfrac{-\gamma}{1-\gamma^2} s_a + \tfrac{1}{1-\gamma^2} s_b \end{aligned} \tag{4.16}$$

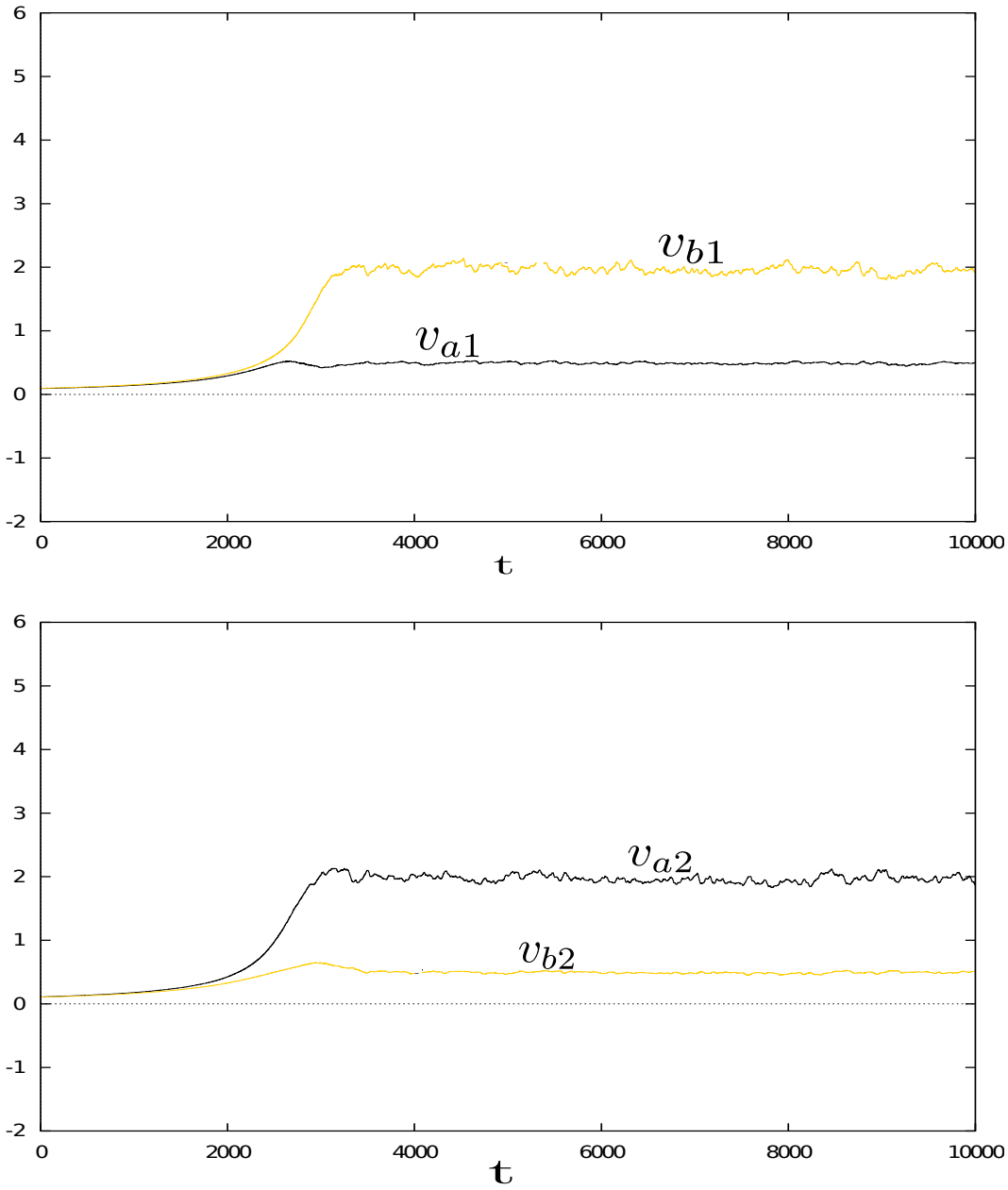

Figure 4.2: When $\tau_\theta/\tau_w = 0.1$, neuronal responses converge to a stable steady state and each neuron selects a different stimulus pattern

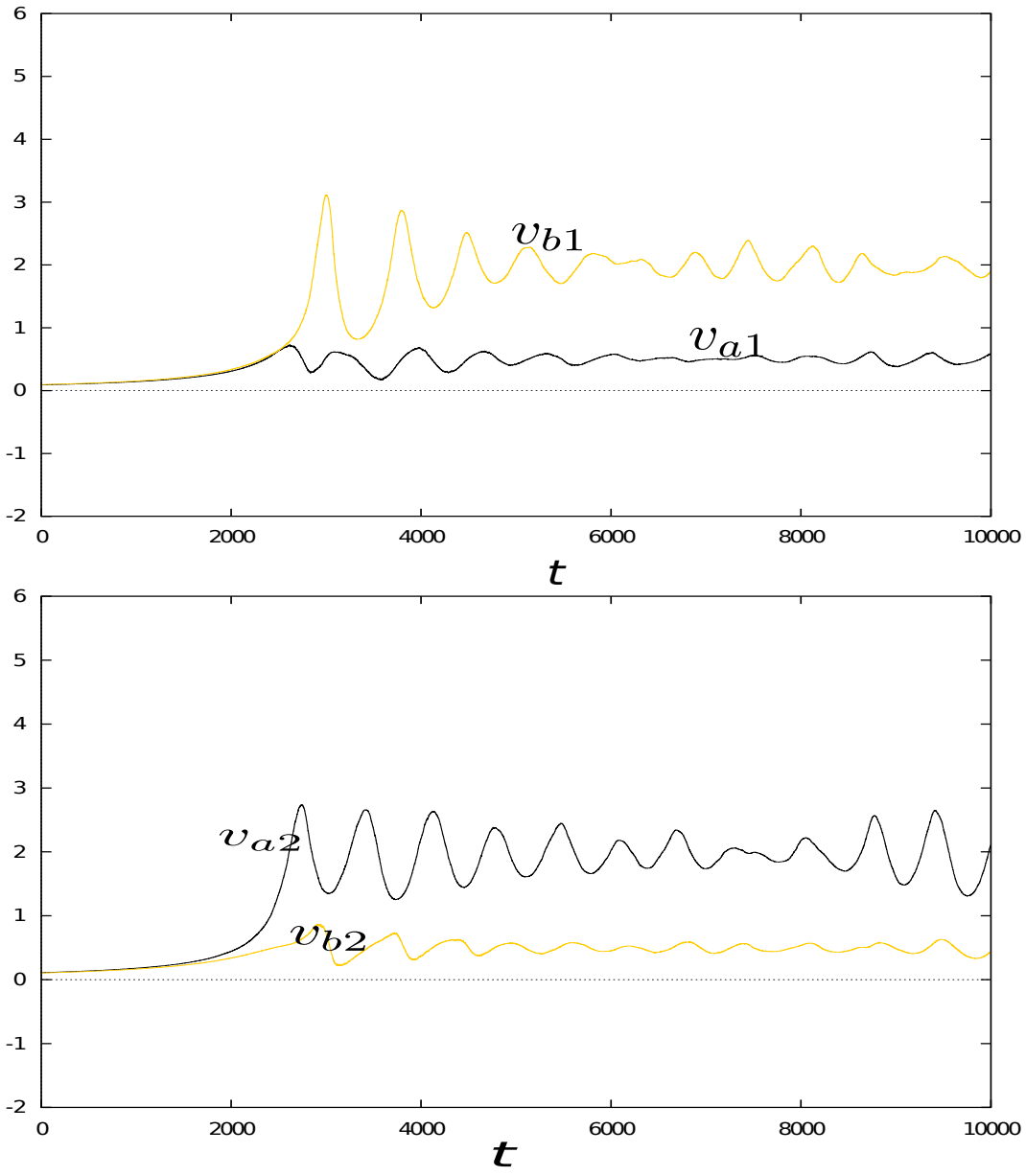

Figure 4.3: When $\tau_\theta/\tau_w = 1.1$, neuronal responses tend to an oscillatory steady state

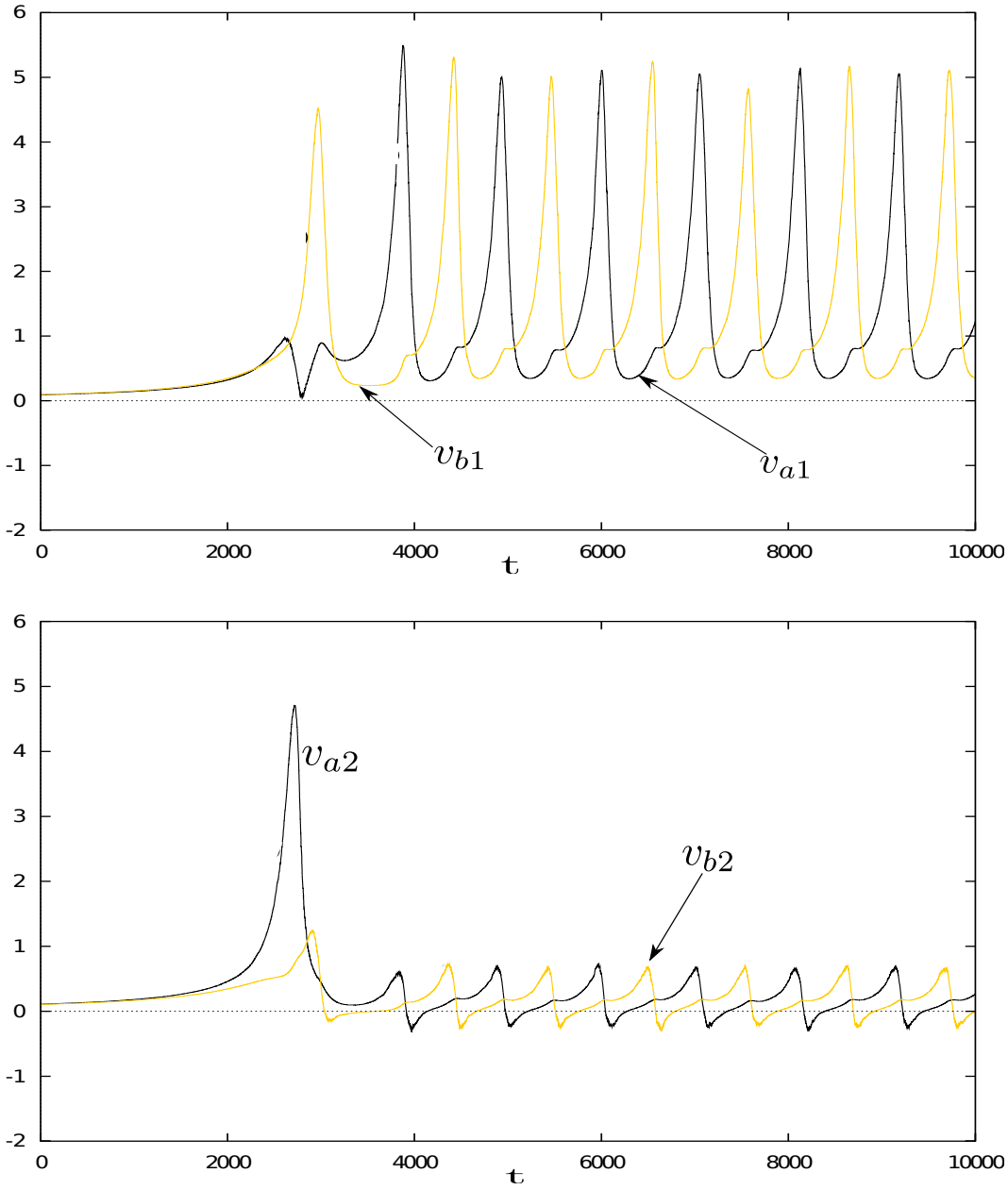

Figure 4.4: When $\tau_\theta/\tau_w = 1.7$, neuronal responses tend to an oscillatory non-selective steady state

4.1.3 Stochastic experiment

Now assume that the two neurons receive stimulus patterns from the set $\mathring{A} = \{(\cos\alpha, \sin\alpha), (\sin\alpha, \cos\alpha)\}$ described in section 3.2.2. That is, at any time, both neurons receive the common stimulus pattern $\mathbf{x}$, where $Pr[\mathbf{x} = (\cos\alpha, \sin\alpha)] = Pr[\mathbf{x} = (\sin\alpha, \cos\alpha)] = \frac{1}{2}$. Just like in the case of the single BCM neuron, a great deal can be learned about the dynamics of the coupled BCM neurons by observing what happens to the responses v_a and v_b as τ_θ/τ_w varies. Varying this ratio reveals several properties of equation 4.14 that mirror those found in the case of a single neuron.

For $\alpha = 0.128$ and $\gamma = 0.24$, figures 4.2, 4.3, and 4.4 plot the responses of the neurons over time. In each case the initial conditions for $\mathbf{w_a}$, $\mathbf{w_b}$, θ_a and θ_b all lie in the interval $(0, 0.3)$. $v_{a1} = \mathbf{w_a} \cdot x^{(1)}$ and $v_{a2} = \mathbf{w_a} \cdot x^{(2)}$ are the respective responses of neuron $\mathbf{a}$ to $(\cos\alpha, \sin\alpha)$ and $(\sin\alpha, \cos\alpha)$ while $v_{b1} = \mathbf{w_b} \cdot x^{(1)}$ and $v_{b2} = \mathbf{w_b} \cdot x^{(2)}$ are the respective responses of neuron $\mathbf{b}$ to $(\cos\alpha, \sin\alpha)$ and $(\sin\alpha, \cos\alpha)$. In each simulation, the presentation of stimulus patterns is treated as a Poisson process with rate $\lambda = 5$ presentations per second.

When $\tau_\theta/\tau_w = 0.1$ the two-neuron system (equation 4.14) converges to a stable steady state and the two neurons are selective; each of them selecting a different stimulus pattern. Just like in the single neuron case, increasing τ_θ/τ_w affects the stability of the system. In figure 4.3, $\tau_\theta/\tau_w = 1.1$ and the responses tend to an oscillatory state even though each neuron still selects a different stimulus. When $\tau_\theta/\tau_w = 1.7$, as seen in figure 4.4, the neurons cease to be selective.

4.1.4 Mean-field model

Consider the general two-dimensional stimulus pattern $\mathbf{x} = (x_1, x_2)$. If the two neurons, **a** and **b**, receive this stimulus with the synaptic weight vectors $\mathbf{w_a} = (w_{a1}, w_{a2})$ and $\mathbf{w_b} = (w_{b1}, w_{b2})$, then according to equation 4.16

$$\begin{aligned} v_a &= c_{a1}x_1 + c_{a2}x_2 \\ v_b &= c_{b1}x_1 + c_{b2}x_2 \end{aligned} \tag{4.17}$$

where, with $\xi = 1/(1-\gamma^2)$ and $\eta = -\gamma/(1-\gamma^2)$

$$\begin{aligned} c_{a1} &= \xi w_{a1} + \eta w_{b1} \\ c_{a2} &= \xi w_{a2} + \eta w_{b2} \\ c_{b1} &= \xi w_{b1} + \eta w_{a1} \\ c_{b2} &= \xi w_{b2} + \eta w_{a2} \end{aligned} \tag{4.18}$$

Assume that $\mathbf{x}$ is from the set $\{\mathbf{x}^{(1)} = (x_{11}, x_{12}), \mathbf{x}^{(2)} = (x_{21}, x_{22})\}$ such that $Pr[\mathbf{x}(t) = \mathbf{x}^{(1)}] = \rho$ and $Pr[\mathbf{x}(t) = \mathbf{x}^{(2)}] = 1 - \rho$. Then a derivation identical to that of equation 3.4 gives the following mean-field version of the BCM learning rule for two mutually inhibiting neurons **a** and **b**.

$$\begin{aligned} \tau_\theta \dot{\theta}_a &= {c_{a1}}^2 r_1 + 2c_{a1}c_{a2}s + {c_{a2}}^2 r_2 - \theta_a \\ \tau_w \dot{w}_{a1} &= {c_{a1}}^2 p_1 + 2c_{a1}c_{a2}q_1 + {c_{a2}}^2 q_2 - (c_{a1}r_1 + c_{a2}s)\theta_a \\ \tau_w \dot{w}_{a2} &= {c_{a2}}^2 p_2 + 2c_{a1}c_{a2}q_2 + {c_{a1}}^2 q_1 - (c_{a2}r_2 + c_{a1}s)\theta_a \\ \tau_\theta \dot{\theta}_b &= {c_{b1}}^2 r_1 + 2c_{b1}c_{b2}s + {c_{b2}}^2 r_2 - \theta_b \\ \tau_w \dot{w}_{b1} &= {c_{b1}}^2 p_1 + 2c_{b1}c_{b2}q_1 + {c_{b2}}^2 q_2 - (c_{b1}r_1 + c_{b2}s)\theta_b \\ \tau_w \dot{w}_{b2} &= {c_{b2}}^2 p_2 + 2c_{b1}c_{b2}q_2 + {c_{b1}}^2 q_1 - (c_{b2}r_2 + c_{b1}s)\theta_b \end{aligned} \tag{4.19}$$

where

$$\begin{aligned} r_1 &= \rho {x_{11}}^2 + (1-\rho){x_{21}}^2 \\ r_2 &= \rho {x_{12}}^2 + (1-\rho){x_{22}}^2 \\ s &= \rho x_{11}x_{12} + (1-\rho)x_{21}x_{22} \\ p_1 &= \rho {x_{11}}^3 + (1-\rho){x_{21}}^3 \\ p_2 &= \rho {x_{12}}^3 + (1-\rho){x_{22}}^3 \\ q_1 &= \rho {x_{11}}^2 x_{12} + (1-\rho){x_{21}}^2 x_{22} \\ q_1 &= \rho x_{11}{x_{12}}^2 + (1-\rho)x_{21}{x_{22}}^2 \end{aligned}$$

Now observe that in accordance with equation 4.17

$$\begin{aligned} \dot{v}_a &= \dot{c}_{a1}x_1 + \dot{c}_{a2}x_2 \\ &= \xi x_1 \dot{w}_{a1} + \eta x_1 \dot{w}_{b1} + \xi x_2 \dot{w}_{a2} + \eta x_2 \dot{w}_{b2} \\ &= \xi(x_1\dot{w}_{a1} + x_2\dot{w}_{a2}) + \eta(x_1\dot{w}_{b1} + x_2\dot{w}_{b2}) \end{aligned}$$

A similar expression exists for v_b. Thus, if $v_{a1} = \mathbf{w_a} \cdot x^{(1)}$, $v_{a2} = \mathbf{w_a} \cdot x^{(2)}$, $v_{b1} = \mathbf{w_b} \cdot x^{(1)}$, and $v_{b2} = \mathbf{w_b} \cdot x^{(2)}$, then in terms of the responses, the mean-field version of the BCM learning rule for two mutually inhibiting neurons **a** and **b** is derived as follows:

$$\begin{aligned} \tau_\theta \dot{\theta}_a &= \rho v_{a1}^2 + (1-\rho)v_{a2}^2 - \theta_a \\ \tau_w \dot{v}_{a1} &= \xi[\rho \mathbf{x^{(1)}} \cdot \mathbf{x^{(1)}} v_{a1}(v_{a1}-\theta_a) + (1-\rho)\mathbf{x^{(1)}} \cdot \mathbf{x^{(2)}} v_{a2}(v_{a2}-\theta_a)] \\ &+ \eta[\rho \mathbf{x^{(1)}} \cdot \mathbf{x^{(1)}} v_{b1}(v_{b1}-\theta_b) + (1-\rho)\mathbf{x^{(1)}} \cdot \mathbf{x^{(2)}} v_{b2}(v_{b2}-\theta_b)] \\ \tau_w \dot{v}_{a2} &= \xi[\rho \mathbf{x^{(2)}} \cdot \mathbf{x^{(1)}} v_{a1}(v_{a1}-\theta_a) + (1-\rho)\mathbf{x^{(2)}} \cdot \mathbf{x^{(2)}} v_{a2}(v_{a2}-\theta_a)] \\ &+ \eta[\rho \mathbf{x^{(2)}} \cdot \mathbf{x^{(1)}} v_{b1}(v_{b1}-\theta_b) + (1-\rho)\mathbf{x^{(2)}} \cdot \mathbf{x^{(2)}} v_{b2}(v_{b2}-\theta_b)] \\ \tau_\theta \dot{\theta}_b &= \rho v_{b1}^2 + (1-\rho)v_{b2}^2 - \theta_b \\ \tau_w \dot{v}_{b1} &= \xi[\rho \mathbf{x^{(1)}} \cdot \mathbf{x^{(1)}} v_{b1}(v_{b1}-\theta_b) + (1-\rho)\mathbf{x^{(1)}} \cdot \mathbf{x^{(2)}} v_{b2}(v_{b2}-\theta_b)] \\ &+ \eta[\rho \mathbf{x^{(1)}} \cdot \mathbf{x^{(1)}} v_{a1}(v_{a1}-\theta_a) + (1-\rho)\mathbf{x^{(1)}} \cdot \mathbf{x^{(2)}} v_{a2}(v_{a2}-\theta_a)] \\ \tau_w \dot{v}_{b2} &= \xi[\rho \mathbf{x^{(2)}} \cdot \mathbf{x^{(1)}} v_{b1}(v_{b1}-\theta_b) + (1-\rho)\mathbf{x^{(2)}} \cdot \mathbf{x^{(2)}} v_{b2}(v_{b2}-\theta_b)] \\ &+ \eta[\rho \mathbf{x^{(2)}} \cdot \mathbf{x^{(1)}} v_{a1}(v_{a1}-\theta_a) + (1-\rho)\mathbf{x^{(2)}} \cdot \mathbf{x^{(2)}} v_{a2}(v_{a2}-\theta_a)] \end{aligned} \tag{4.20}$$

Observing that each of ρ, $\mathbf{x}^{(1)}$, and $\mathbf{x}^{(2)}$ is non-zero, and setting the right hand side of equation 4.20 yields

$$\begin{aligned}
\rho v_{a1}^2 + (1-\rho)v_{a2}^2 - \theta_a &= 0 \\
\rho v_{b1}^2 + (1-\rho)v_{b2}^2 - \theta_b &= 0 \\
v_{a1}(v_{a1} - \theta_a) &= 0 \\
v_{a2}(v_{a2} - \theta_a) &= 0 \\
v_{b1}(v_{b1} - \theta_b) &= 0 \\
v_{b2}(v_{b2} - \theta_b) &= 0
\end{aligned}$$

which reduces to

$$\begin{aligned}
v_{a1}(v_{a1} - (\rho {v_{a1}}^2 + (1-\rho){v_{a2}}^2)) &= 0 \\
v_{a2}(v_{a2} - (\rho {v_{a1}}^2 + (1-\rho){v_{a2}}^2)) &= 0 \\
v_{b1}(v_{b1} - (\rho {v_{b1}}^2 + (1-\rho){v_{b2}}^2)) &= 0 \\
v_{b2}(v_{b2} - (\rho {v_{b1}}^2 + (1-\rho){v_{b2}}^2)) &= 0
\end{aligned} \tag{4.21}$$

Solving this system of equations which gives the fixed points

$$\begin{aligned}
(v_{a1}, v_{a2}, \theta_a, v_{b1}, v_{b2}, \theta_b) = \{&(0,0,0,0,0,0), \\
&\left(\tfrac{1}{\rho}, 0, \tfrac{1}{\rho}, \tfrac{1}{\rho}, 0, \tfrac{1}{\rho}\right), \\
&\left(0, \tfrac{1}{1-\rho}, \tfrac{1}{1-\rho}, 0, \tfrac{1}{1-\rho}, \tfrac{1}{1-\rho}\right), \\
&\left(\tfrac{1}{\rho}, 0, \tfrac{1}{\rho}, 0, \tfrac{1}{1-\rho}, \tfrac{1}{1-\rho}\right), \\
&\left(0, \tfrac{1}{1-\rho}, \tfrac{1}{1-\rho}, \tfrac{1}{\rho}, 0, \tfrac{1}{\rho}\right), \\
&(1,1,1,1,1,1)\}
\end{aligned} \tag{4.22}$$

Castellani et al [10] and Intrator and Cooper [33] give a detailed analysis on the stability of these fixed points. They showed that apart from $(0,0,0,0,0,0)$ and $(1,1,1,1,1,1)$ which are neither stable nor selective, all the fixed points are stable and selective.

If the neurons now receive the stimulus pattern $\mathbf{x}$ from $\mathring{A}$ (described in section 3.2.2) such that $Pr[\mathbf{x}(t) = \mathbf{x}^{(1)}] = Pr[\mathbf{x}(t) = \mathbf{x}^{(2)}] = \frac{1}{2}$, then equation 4.19 becomes

$$\begin{aligned}
\tau_\theta \dot{\theta}_a &= {c_{a1}}^2 r + 2c_{a1}c_{a2}s + {c_{a2}}^2 r - \theta_a \\
\tau_w \dot{w}_{a1} &= {c_{a1}}^2 p + 2c_{a1}c_{a2}q + {c_{a2}}^2 q - (c_{a1}r + c_{a2}s)\theta_a \\
\tau_w \dot{w}_{a2} &= {c_{a2}}^2 p + 2c_{a1}c_{a2}q + {c_{a1}}^2 q - (c_{a2}r + c_{a1}s)\theta_a \\
\tau_\theta \dot{\theta}_b &= {c_{b1}}^2 r + 2c_{b1}c_{b2}s + {c_{b2}}^2 r - \theta_b \\
\tau_w \dot{w}_{b1} &= {c_{b1}}^2 p + 2c_{b1}c_{b2}q + {c_{b2}}^2 q - (c_{b1}r + c_{b2}s)\theta_b \\
\tau_w \dot{w}_{b2} &= {c_{b2}}^2 p + 2c_{b1}c_{b2}q + {c_{b1}}^2 q - (c_{b2}r + c_{b1}s)\theta_b
\end{aligned} \tag{4.23}$$

where

$$\begin{aligned}
r = r_1 = r_2 &= \tfrac{1}{2} \\
s &= \sin\alpha\cos\alpha \\
p = p_1 = p_2 &= \tfrac{1}{2}(\cos^3\alpha + \sin^3\alpha) \\
q = q_1 = q_2 &= \tfrac{1}{2}(\sin\alpha\cos\alpha)(\sin\alpha + \cos\alpha)
\end{aligned}$$

and equation 4.20 becomes

$$\begin{aligned}
\tau_\theta \dot{\theta}_a &= \tfrac{1}{2}(v_{a1}^2 + v_{a2}^2) - \theta_a \\
\tau_w \dot{v}_{a1} &= \tfrac{\xi}{2}[v_{a1}(v_{a1} - \theta_a) + \cos\beta\, v_{a2}(v_{a2} - \theta_a)] \\
&+ \tfrac{\eta}{2}[v_{b1}(v_{b1} - \theta_b) + \cos\beta\, v_{b2}(v_{b2} - \theta_b)] \\
\tau_w \dot{v}_{a2} &= \tfrac{\xi}{2}[\cos\beta\, v_{a1}(v_{a1} - \theta_a) + v_{a2}(v_{a2} - \theta_a)] \\
&+ \tfrac{\eta}{2}[\cos\beta\, v_{b1}(v_{b1} - \theta_b) + v_{b2}(v_{b2} - \theta_b)] \\
\tau_\theta \dot{\theta}_b &= \tfrac{1}{2}(v_{b1}^2 + v_{b2}^2) - \theta_b \\
\tau_w \dot{v}_{b1} &= \tfrac{\xi}{2}[v_{b1}(v_{b1} - \theta_b) + \cos\beta\, v_{b2}(v_{b2} - \theta_b)] \\
&+ \tfrac{\eta}{2}[v_{a1}(v_{a1} - \theta_a) + \cos\beta\, v_{a2}(v_{a2} - \theta_a)] \\
\tau_w \dot{v}_{b2} &= \tfrac{\xi}{2}[\cos\beta\, v_{b1}(v_{b1} - \theta_b) + v_{b2}(v_{b2} - \theta_b)] \\
&+ \tfrac{\eta}{2}[\cos\beta\, v_{a1}(v_{a1} - \theta_a) + v_{a2}(v_{a2} - \theta_a)]
\end{aligned} \tag{4.24}$$

The stable fixed points of equation 4.24 are

$$(v_{a1}, v_{a2}, \theta_a, v_{b1}, v_{b2}, \theta_b) = \{(2,0,2,2,0,2),(0,2,2,0,2,2),(2,0,2,0,2,2),(0,2,2,2,0,2)\}$$

In terms of the synaptic weights,

1. the fixed points $(2,0,2,2,0,2)$ and $(0,2,2,0,2,2)$ are symmetric with respect to the synaptic weights of the neurons, that is $w_{a1} = w_{b1} \neq w_{a2} = w_{b2}$. At these fixed point, both neurons are selective and both neurons choose the same stimulus pattern.
2. the fixed points $(2,0,2,0,2,2)$ and $(0,2,2,2,0,2)$ are asymmetric with respect to the synaptic weights of the neurons, that is $w_{a1} = w_{b2} \neq w_{a2} = w_{b1}$. At this fixed point, both neurons are selective, each chooses a different stimulus pattern.

It must be noted that the observed synaptic weight symmetries are specific to the stimulus class $\mathring{A} = \{(\cos\alpha, \sin\alpha),(\sin\alpha, \cos\alpha)\}$.

4.2 OSCILLATORY, TOROIDAL, AND CHAOTIC PROPERTIES

For two mutually inhibiting neurons, the BCM dynamics exhibits interesting behaviors that are better captured in terms of the synaptic weights. As seen in section 4.1.4, the mean-field model has two types of stable fixed points:

1. stable fixed points that are symmetric with respect to the synaptic weights of the neurons, that is $w_{a1} = w_{b1} \neq w_{a2} = w_{b2}$. Call these fixed points $p1$
2. stable fixed point that are asymmetric with respect to the synaptic weights of the neurons, that is $w_{a1} = w_{b2} \neq w_{a2} = w_{b1}$. Call these fixed point $p2$

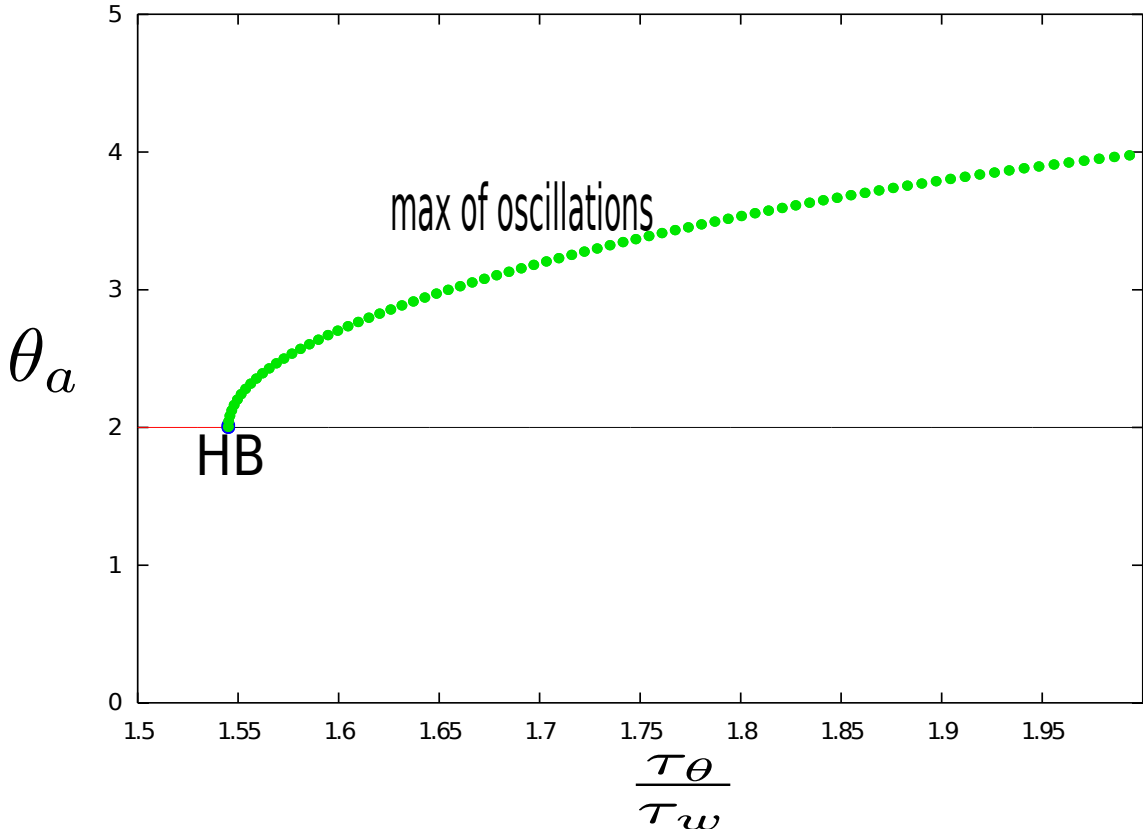

Figure 4.5: Bifurcation Diagram when starting from the symmetric fixed point. $\alpha = 0.4$, $\gamma = 0.25$

The numerical results presented in this section are specific to the stimulus class $\mathring{A} = \{(\cos\alpha, \sin\alpha), (\sin\alpha, \cos\alpha)\}$.

An instance of p_1 is $(\theta_a, \theta_b, w_{a1}, w_{a2}, w_{b1}, w_{b2}) = (2, 2, -1.4, -1.4, 3.3, 3.3)$ achieved for $\alpha = 0.4$, $\gamma = 0.25$, and $\tau_\theta/\tau_w = 0.1$ with an initial condition of $(0, 0, 0.1, 0.11, 0.09, 0.087)$. Continuously increasing τ_θ/τ_w eventually results to a Hopf

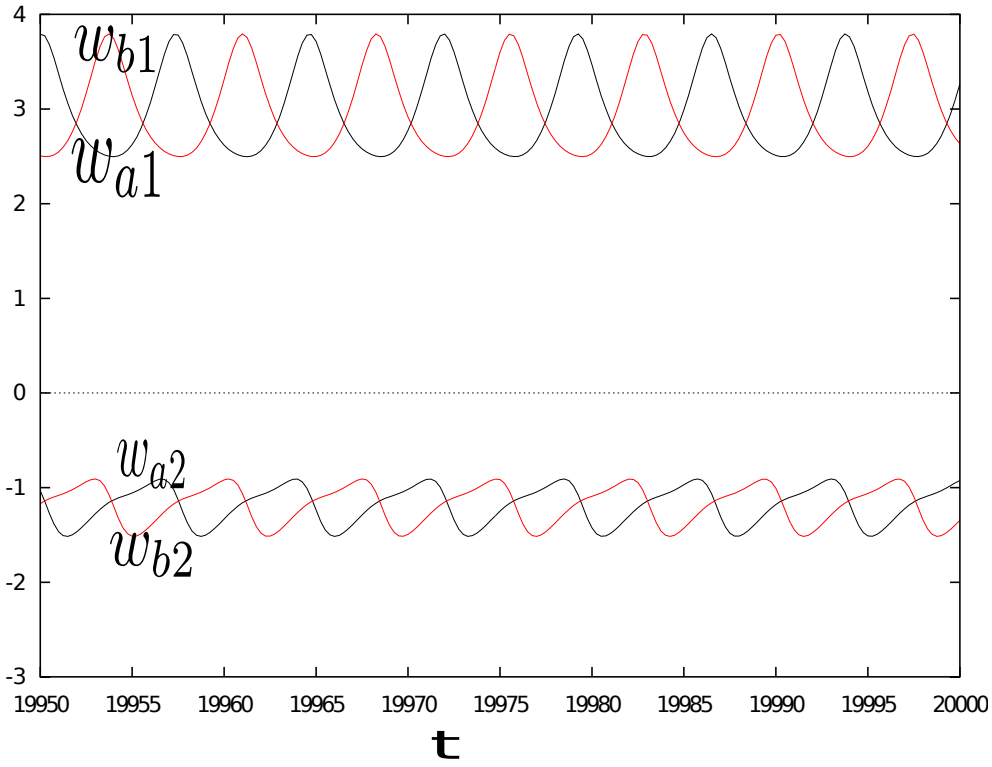

Figure 4.6: symmetric fixed point bifurcates to phase shifted oscillations. $\tau_\theta/\tau_w = 1.64$, $\alpha = 0.4$, $\gamma = 0.25$

bifurcation (HB in figure 4.5) at $\tau_\theta/\tau_w = 1.55$. Thus, the system has a stable steady state in the range $0 < \tau_\theta/\tau_w < 1.55$ and an oscillatory steady state when $\tau_\theta/\tau_w > 1.55$. The green curve in figure 4.5 are the maximum values of the oscillation for each value of τ_θ/τ_w. Figure 4.6 shows a non-synchronous oscillation of the weights when $\tau_\theta/\tau_w = 1.64$. Notice that w_{a1} and w_{b1} share the same range of oscillation and so do w_{a2} and w_{b2}. A similar relationship exists between θ_a and θ_b

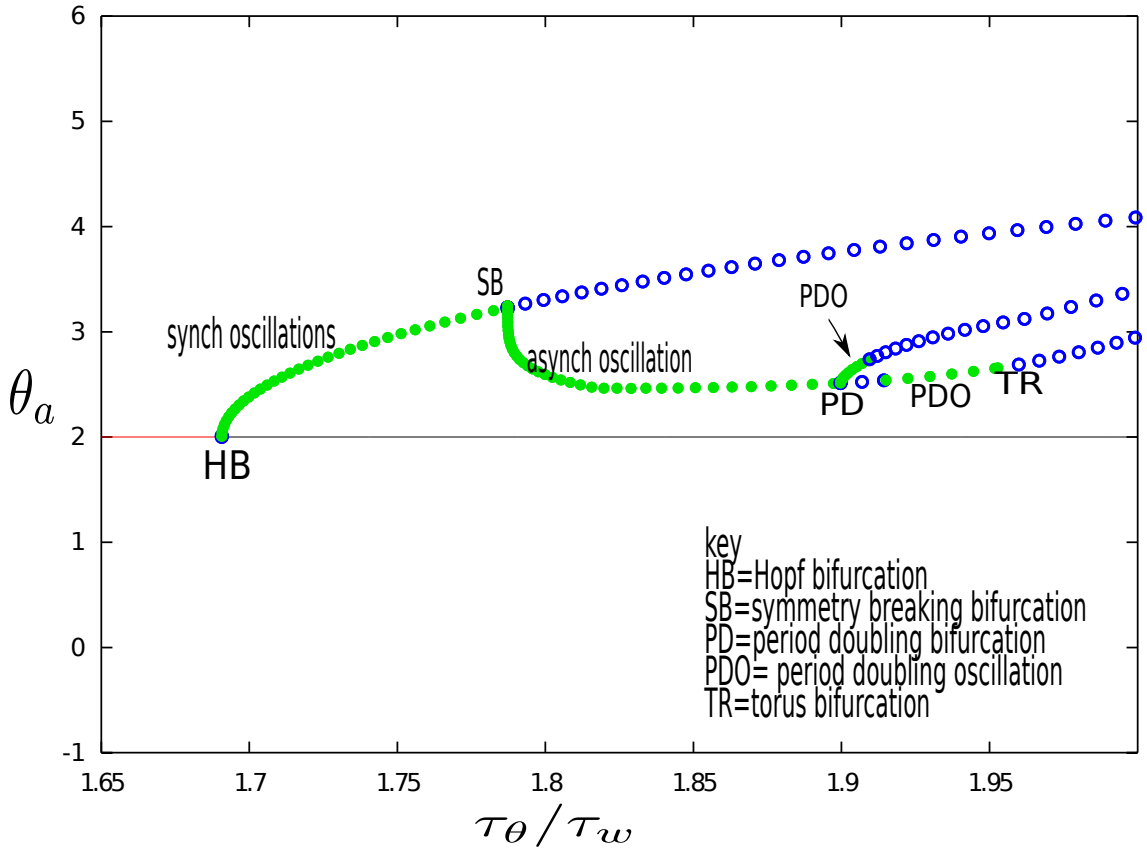

Figure 4.7: Bifurcation Diagram when starting from the asymmetric fixed point. $\alpha = 0.4$, $\gamma = 0.25$

The stability of the p_2 persists for small enough values of τ_θ/τ_w, however, as τ_θ/τ_w increases, the fixed point also bifurcates and loses stability. For $\alpha = 0.4$, $\gamma = 0.25$, with an initial condition of $(\theta_a, \theta_b, w_{a1}, w_{a2}, w_{b1}, w_{b2}) = (0, 0, 0.1, 0.091, 0.086, 0.11)$, the system converges to the fixed point $(2, 2, 2.36. - 0.46, -0.46, 2.36)$ when $\tau_\theta/\tau_w = 0.1$. Stability persists as τ_θ/τ_w increases until $\tau_\theta/\tau_w = 1.69$ where a Hopf Bifurcation occurs and the

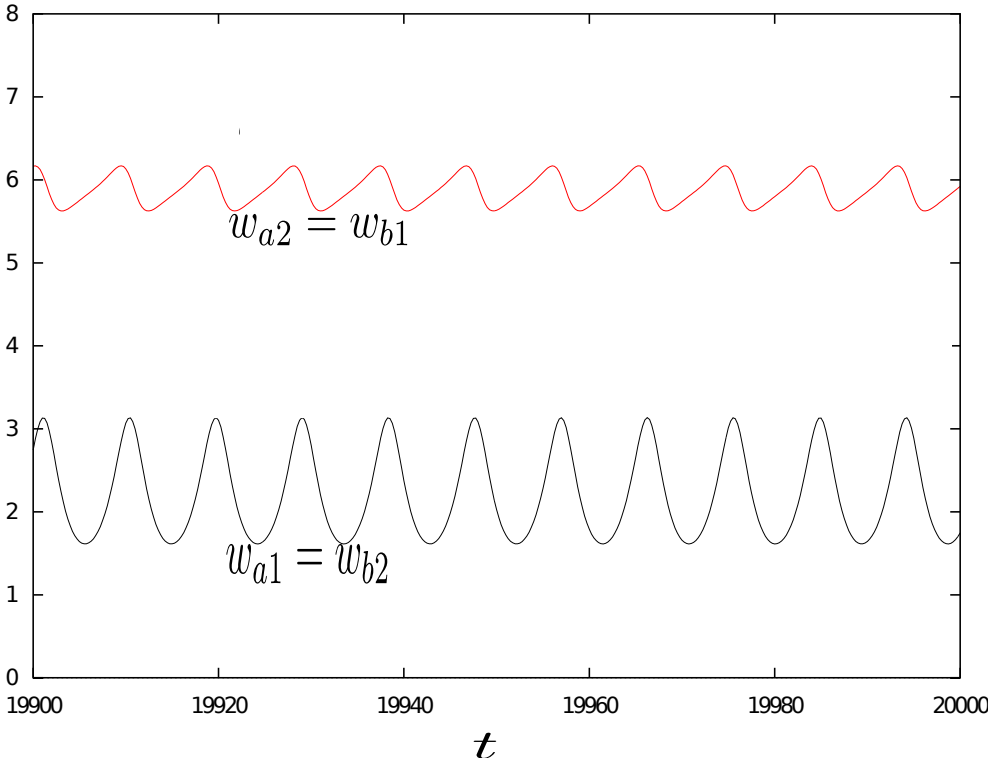

Figure 4.8: Synchronous oscillations when $\tau_\theta/\tau_w = 1.742$, $\alpha = 0.4$, $\gamma = 0.25$

system assumes an oscillatory behavior. Between $\tau_\theta/\tau_w = 1.69$ and $\tau_\theta/\tau_w = 2$, the system exhibits several interesting dynamical properties as τ_θ/τ_w increases. These properties are summarized in figure 4.7, a bifurcation diagram of $\theta_a - vs - \tau_\theta/\tau_w$.

For $1.69 < \tau_\theta/\tau_w < 1.787$, the system exhibits a synchronous oscillatory steady with $w_{a1} = w_{b2}$, $w_{a2} = w_{b1}$, and $\theta_a = \theta_b$. The green points are the maximum values of the oscillation for each value of τ_θ/τ_w. Figure 4.8 shows this oscillatory steady state for $\tau_\theta/\tau_w = 1.742$ with the same parametric values and initial conditions stated above.

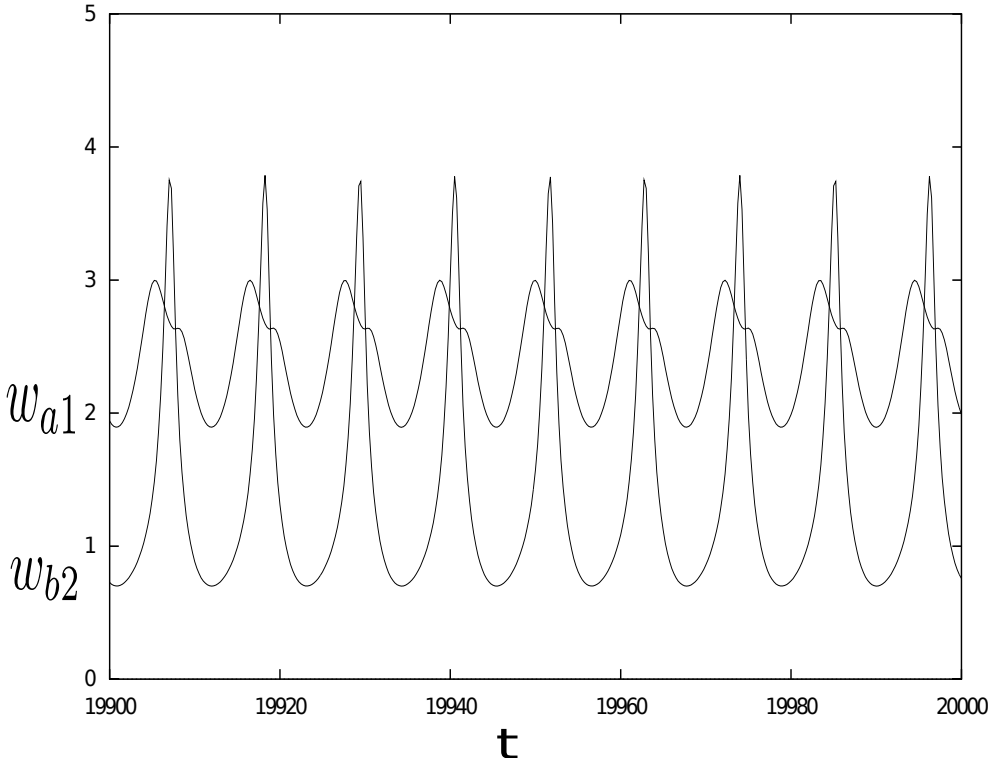

Figure 4.9: Asynchronous oscillations when $\tau_\theta/\tau_w = 1.84$, $\alpha = 0.4$, $\gamma = 0.25$

At $\tau_\theta/\tau_w = 1.787$ the system experiences a qualitative change through a symmetry breaking bifurcation. This leads to the annihilation of the synchronous oscillation previously observed, leading to an asynchronous oscillation which persists in the interval $1.787 < \tau_\theta/\tau_w < 1.9$. Referring back to figure 4.7, the green curve are the minimum values of the oscillation while the blue points are the θ_a values of the center of the associated periodic orbit. Figure 4.9 shows an instance of this behavior when $\tau_\theta/\tau_w = 1.84$ where w_{a1} and w_{a2} separates from one anther. Notice that there is now a slight increase in the period of the oscillation.

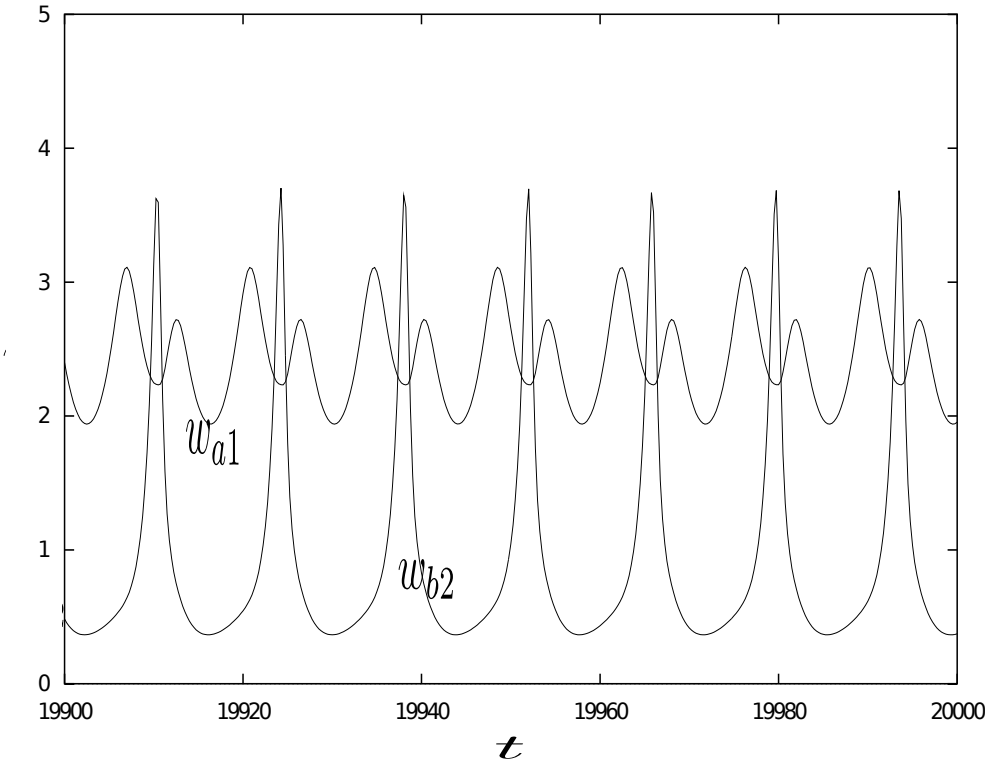

Figure 4.10: Period of oscillation doubles when $\tau_\theta/\tau_w = 1.95$, $\alpha = 0.4$, $\gamma = 0.25$

At $\tau_\theta/\tau_w = 1.9$ the system experiences another qualitative change through a period doubling bifurcation. The oscillatory behavior is still observed, however, the period of oscillation is now double the period of the initial synchronous oscillation. See figure 4.10 for an example of this behavior when $\tau_\theta/\tau_w = 1.93$. This period doubling oscillation is seen in the ininterval $1.9 < \tau_\theta/\tau_w < 1.95$. Again, Refer back to figure 4.7. Notice that in this interval, the green curve started out being on top of the blue curved (in which case, it is the maximum values of the oscillations) and then switches and goes under the blue curve (in which case, it is the minimum values of the oscillations). The reason for this

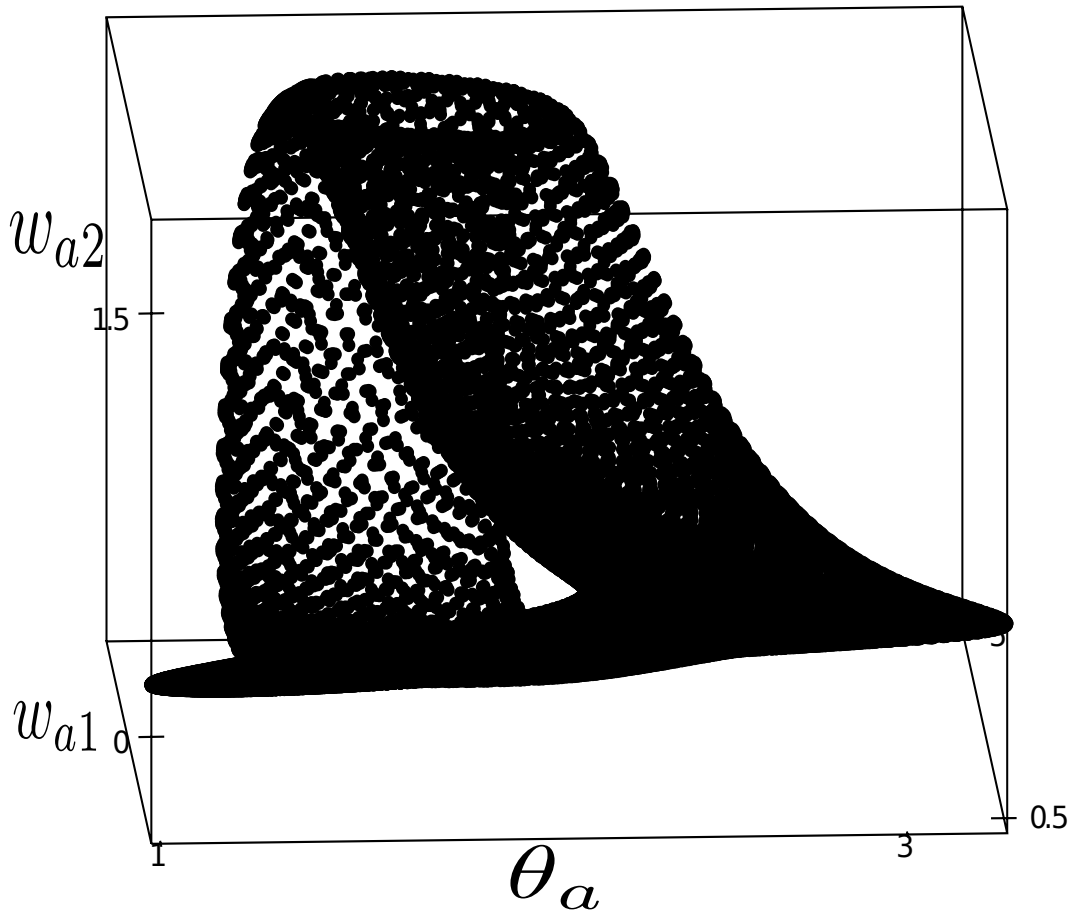

Figure 4.11: Torus when $\tau_\theta/\tau_w = 1.965$, $\alpha = 0.4$, $\gamma = 0.25$

shift is not clear. In both cases the blue curve is the θ_a values of the center (mean of the maximum and minimum of oscillation) of the associated periodic orbit.

At $\tau_\theta/\tau_w = 1.953$, the system bifurcates to a torus dynamic. An instance of such a torus is shown in figure 4.11 when $\tau_\theta/\tau_w = 1.965$. Figure 4.12 is a Poincare map detailing the toroidal behavior for the $w_{a1} = 1$ poincare section. This toroidal behavior persists until

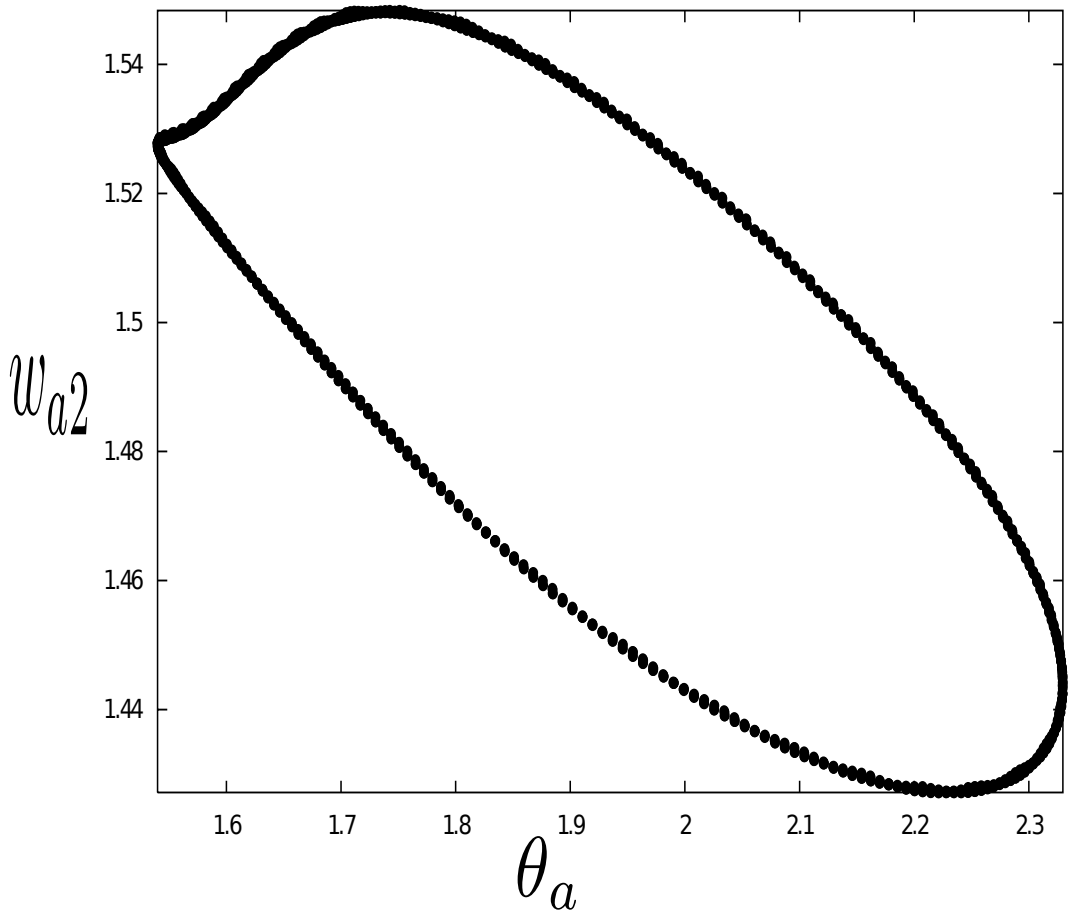

Figure 4.12: Torus poincare map when $\tau_\theta/\tau_w = 1.965$ ($w_{a1} = 1$ section) , $\alpha = 0.4$, $\gamma = 0.25$

$\tau_\theta/\tau_w = 2$ where the system becomes chaotic. Figure 4.13 shows a $w_{a1} = 1$ section of such a scenario with a Lyaopunov exponent of 0.0137. Another way of looking at it is that the previously shown poincare map looses its roundness.

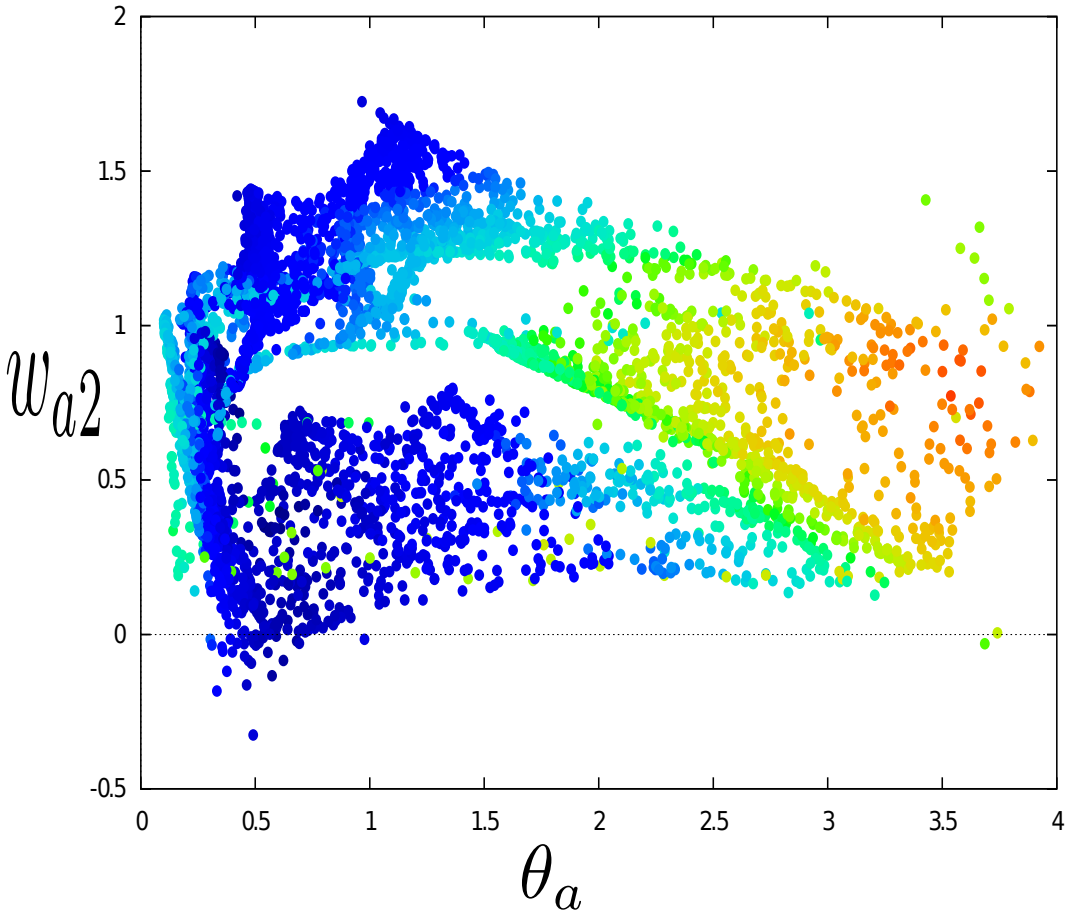

Figure 4.13: Chaotic behavior when $\tau_\theta/\tau_w = 2$ ($w_{a1} = 1$ section), $\alpha = 0.4$, $\gamma = 0.25$

4.3 SUMMARY

In the present chapter, it has been shown that, for two mutually inhibiting BCM neurons, slowing down homeostasis past a certain parametric value reveals a few interesting dynamical properties. In particular, the system undergoes several bifurcations as τ_θ/τ_w (ratio of

time scale factor of homeostasis to that of synaptic weights) gets closer to 2. As learned in section 3.2.5, These bifurcations negatively affect the selectivity of the neurons. As τ_θ/τ_w approaches 2, the steady state of the system becomes oscillatory, then toroidal, and finally chaotic (when $\tau_\theta/\tau_w = 2$) .

5.0 CLUSTERING PROPERTY OF BCM NEURON

Since a BCM neuron is selective, it makes sense to imagine that, within a data set, it will become very responsive to a cluster and not to others. The present chapter explores this suggested clustering property, while adhering to the time-scale conditions established in chapters 3 and 4. Section 5.1 is a preliminary analysis that investigates how the clustering power of the BCM neuron varies with the radius of the clusters and how far they are from one another. Section 5.2 proposes a clustering algorithm that can be applied to an arbitrary data set in which each sample has the exact same number of attributes. In section 5.3 the performance of this clustering algorithm is compared to those of a few other well known clustering algorithms. Except where noted, all the numerical simulations in this chapter were prepared using Matlab [31],

5.1 PRELIMINARY ANALYSIS

For $0 \leq b < 1$, consider the linearly independent vectors $(b,1,1)$, $(1,b,1)$, and $(1,1,b)$. These vectors are of equal magnitude, mutually equidistant, and are farthest apart from one another when $b = 0$ (in which case they lie on the yz plane, xz plane, and xy plane respectively). They get closer to one another as b increases, eventually becoming identical

when $b = 1$. Let $0 < \varepsilon << 1$ and $\{r_i\}_1^{3N}$ be a set of $3N$ uniformly distributed real numbers between -1 and 1. Define the groups of points, C_1, C_2, and C_3 built around $(b,1,1)$, $(1,b,1)$, and $(1,1,b)$, as follows:

$$C_1 = \{x^{(i)} | (b,1,1) + \varepsilon r_i (1,1,1), i = 1 \ldots N\}$$
$$C_2 = \{x^{(i)} | (1,b,1) + \varepsilon r_i (1,1,1), i = N+1 \ldots 2N\}$$
$$C_3 = \{x^{(i)} | (1,1,b) + \varepsilon r_i (1,1,1), i = 2N+1 \ldots 3N\}$$

Thus the groups have the centers $(b,1,1)$, $(1,b,1)$, and $(1,1,b)$, and each group can described as a set noisy instances of its center. See figure 5.1 for a visualization of such a set when $N = 30$, $\varepsilon = 0.3$ for $b = 0.2$ and $b = 0.4$.

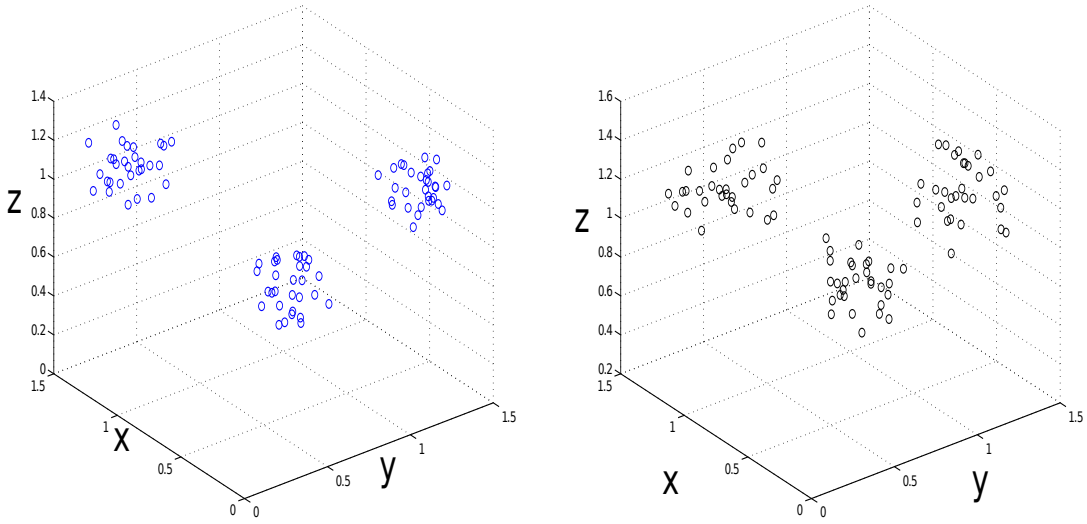

(a) (b)

Figure 5.1: C_1, C_2, and C_3 for (a) $b = 0.2$ (b) $b = 0.4$ and $\varepsilon = 0.3$

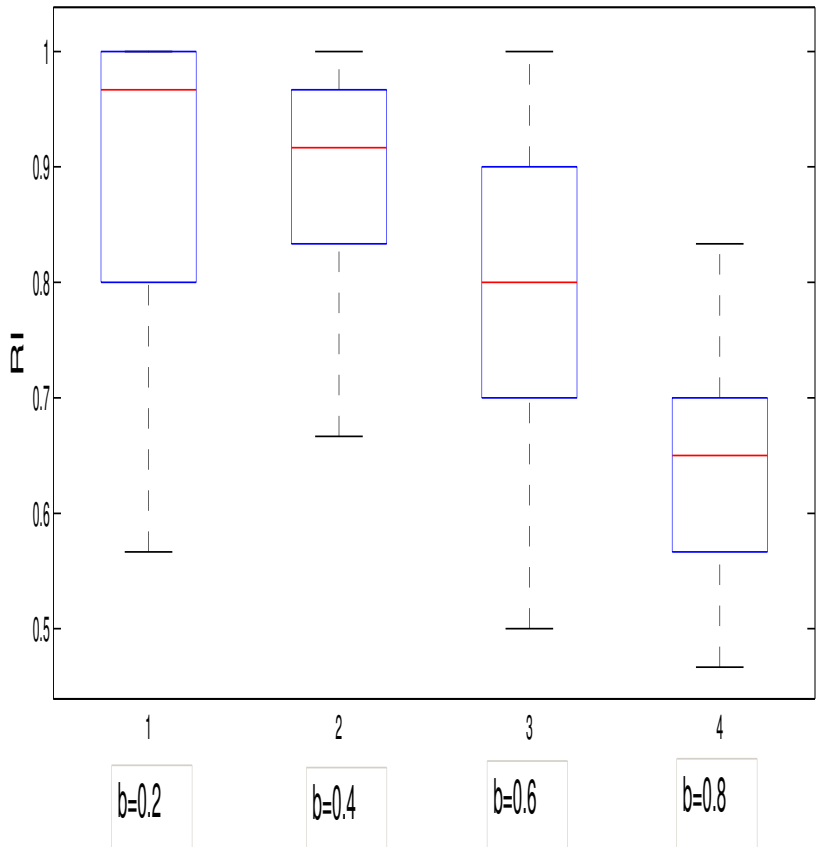

Figure 5.2: Distributions of rand indices for 100 simulations of each value of b. In each case $\varepsilon = 0.3$

The goal in this section is to measure how selective a BCM neuron is among clusters. In the case described above, the groups of points have linearly independent centers. The setup is to train the neuron using the BCM learning rule by running a few thousand iteration of the system of equations: $\tau_w \frac{d\mathbf{w}}{dt} = v\mathbf{x}(v-\theta)$ and $\tau_\theta \frac{d\theta}{dt} = v^2 - \theta$. The vector $\mathbf{w}$ is

initialized with values in the interval $(0, 0.3)$ while $\tau_\theta = 1$ and $\tau_w = 10$. At each iteration, $\mathbf{x}$ is randomly chosen from $C_1 \cup C_2 \cup C_3$. Recall that $v = \mathbf{w} \cdot \mathbf{x}$ is the response to $\mathbf{x}$ where $\mathbf{w}$ is the synaptic weight vector. After training, let the responses to the neurons, in ascending order be

$$v_1 \leq v_2 \leq \ldots v_M$$

where $M \leq 3N$. Simulations have shown that there is a cut-off index k such that $\forall j$, $v_k - v_{k-1} >> v_j - v_{j-1}$. Define a high-response point as a point that yields one of the responses in $\{v_k, v_{k+1}, \ldots, v_M\}$, and a low-response point as a point that yields one of the responses in $\{v_1, v_2, \ldots, v_{k-1}\}$. It is expected that a cluster, say C_k, will contain all the high-response points. If this happens, then it can be concluded that the neuron has designated C_k as a cluster in the data set. However, it is quite possible that some high-response points are outside C_k, and it is also possible that some low-response points are in C_k. The Rand index (RI) is defined as the ratio of correctly classified samples to the total number of samples in the data set [57], [29]. This means the value of the Rand index ranges between 0 and 1. The higher the Rand index, the better the clustering result. This index can be used to measure how well the neuron perform the clustering task, and in this particular case is defined as

$$RI = \frac{A + B}{A + B + C + D}$$

where

$A =$ number of high-response points in C_k

$C =$ number of high-response points outside of C_k

$B =$ number of low-response points outside of C_k

$D =$ number of low-response points in C_k

For $N = 30$, figures 5.2 shows the box plot for several values of b. Each box plot contains the distribution of the Rand indices for 100 simulations of the described setup. In each

cease $\varepsilon = 0.3$, and the elements of $\mathbf{w}$ are initialized to values in the interval $(0, 0.3)$. As can be observed, the mean Rand index for decreases as b increases. This is as expected since the clusters are closer to one another as b increases.

5.2 METHODS

This section discusses a clustering algorithm that is based on the selectivity of the BCM neuron.

5.2.1 Variables

The algorithm for this task will involve the variables X, n d, v, $\mathbf{w}$, θ, τ_w, τ_θ, R, κ, and δ. These variable are characterized as follows:

1. X is an $n \times d$ matrix containing the data set.
2. n is the number of data points in the data set.
3. d is the number of attributes of each data point.
4. v is the activity of the neuron.
5. $\mathbf{w}$ is a $d-$dimensional vector of the synaptic weights of the neuron. To avoid convergence to a degenerate fixed point, $\mathbf{w}$ should not be initialized with the zero vector.
6. θ is the activity threshold of the neuron.
7. R is an $n-$dimensional vector. The element R_i corresponds to the response of the neuron to the ith data point of X.
8. τ_w is the time-scale factor for $\mathbf{w}$.
9. τ_θ is the time-scale factor for θ. As has been shown in chapters 3 and 4, steady state stability is guaranteed if $\tau_\theta / \tau_w << 1$.

10. *numItr* is the number of iterations needed for the synaptic weights to convergence.
11. κ and δ are cluster detection cutoff factors. δ is an expected average difference in the neuronal responses between two data points in the same cluster. This is usually very small (say, in the order of 0.1). $\kappa\delta$ is the expected minimum difference in the neuronal responses between two data points in two different clusters, implying that κ should be chosen in a such a way that $\kappa\delta$ is large enough to reflect the this. However, as can be deduced in the algorithms that follow, if κ is too large, points belonging to different clusters may be grouped together. Other than by experimentation, there is currently no hard rule in determining the value of κ and δ.

The mechanism of BCM clustering algorithm (algorithm 2) can be described as "detect and eliminate". It trains the BCM neuron with the data set, detects the high-response data points, designate them as cluster, and eliminate them from the data set. It then repeats this procedure until the data set is empty.

5.2.2 Algorithm pseudocode

1 Initialize $v = 0$, $\theta = 0$, $\mathbf{w}$ = a non-zero vector ;
2 **for** $itr = 1$ *to* *numItr* **do**
3 $\quad x$ = a random row of X ;
4 $\quad v = x\mathbf{w}^{\mathbf{T}}$;
5 $\quad \mathbf{w} = w + \frac{1}{\tau_w} v(v-\theta)x$;
6 $\quad \theta = \theta + \frac{1}{\tau_\theta}(v^2 - \theta)$;
7 **end**
8 $R = X\mathbf{w}^{\mathbf{T}}$;

Algorithm 1: Using the data set X to train a BCM neuron

while X *is not empty* **do**
    Train neuron by running algorithm 1 and computing R ;
    $S = sort(R)$ in descending order ;
    Assign $\delta =$ very small positive number (say $\delta = 0.1$) ;
    Assign $\kappa =$ positive number greater than 1 (say $\kappa = 10$) ;
    if $lengthOfS == 1$ **then**
        X contains just one row (i.e one data point);
        Designate this row as a cluster, and eliminate it from X ;
    else if $lengthOfS == 2$ **then**
        X contains just two rows (i.e two data points);
        if $S_1 - S_2 > \kappa\delta$ **then**
            Designate row 1 as a cluster and row 2 as another clusters, and eliminate both rows from X ;
        else
            Designate the two rows as a cluster, and eliminate both rows from X ;
        end
    else
        $j < lengthOfS$ is the minimum integer such that $S_j - S_{j+1} \geq \kappa(S_{j+1} - S_{j+2})$. If no such j exists, then assign $j = lengthOfS$;
        Assign $C =$ a subset $\{x_i\}$ of the rows of X whose responses $\{R_i\}$ are such that each $R_i \geq S_j$;
        Designate C as a cluster, and eliminate the rows in C from X
    end
end

Algorithm 2: BCM clustering algorithm

The BCM clustering algorithm uses Euler's method to solve the system of ordinary differential equations in the BCM learning rule. The convergence rate of Euler's method can be analytically determined for Lipschitz continuous functions, and pretty difficult to determine for functions that are not Lipschitz continuous, especially when stochasticity is involved, like in algorithm 2. Even though the BCM learning rule is not Lipschitz continuous, experimental simulations show that as long as $\tau_\theta/\tau_w << 1$, the algorithm converges in a reasonable amount of time.

To get an idea of how many iterations is needed for convergence of the BCM clustering algorithm, consider the case where the data set X contains only two linearly independent vectors of equal magnitudes (or two tight clusters with linearly independent centers equidistant from the origin). Experimental simulations show that in this case, the number of iterations it takes to converge depends on the angle between the vectors: the closer the vectors are to being linearly independent, the longer it takes to converge. With $\tau_w = 100$, $\tau_\theta = 10$, table 5.1 shows the number of iterations needed for convergence, as a function of β, the angle between the two stimulus vectors. Here, the definition of convergence is as follows:

Definition 5.1. *Given a small ε, the BCM clustering algorithm is said to converge after T iterations if for any $t > T$,*

$$||\mathbf{w}_t - \mathbf{w}_T|| < \varepsilon$$

where $\mathbf{w}_s$ is the synaptic weight vector at iteration s, and $||\ ||$ can be computed using the Euclidean distance.

In the simulations presented in subsequent sections, the number of iterations in set to $numItr = 10000$. The number is larger than the worst case shown in table 5.1 and has proven to be very sufficient for convergence.

Table 5.1: Average number of iterations needed for convergence (over 10 runs), as a function of the angle between two stimulus vectors. $\tau_w = 100$, $\tau_\theta = 10$

β	number of iterations
$\pi/12$	8936
$\pi/8$	3575
$\pi/6$	2682
$\pi/4$	1491
$\pi/3$	895
$\pi/2$	796

5.2.3 Algorithm complexity

5.2.3.1 Algorithm 1 The parts of this algorithm that contribute in determining its computational complexity are the for-loop that starts on line 3, and the matrix-vector multiplication in line 9. The for-loop runs a constant number of times ($numItr$) which does not depend on the size of the data. Line 5 is the dot product of two d-dimensional vectors, and has a complexity of $O(d)$. Each of lines 6 and 7 has a complexity of $O(1)$ since the dominant operation in each of them is the multiplication of a vector by a constant. Thus the complexity of lines 3 to 8 of the algorithm is $O(d)$. Line 9 is the multiplication of an $n \times d$ matrix by a $d-$dimensional vector, which has a complexity of $O(nd)$. Therefore the overall complexity algorithm 1 is $O(nd)$.

5.2.3.2 The BCM clustering algorithm (Algorithm 2)

In terms of computational complexity, the major parts of the BCM clustering algorithm are line 2, line 3, and the if-else block (lines 6-20). The contributions of these major parts, in computing the complexity of the BCM clustering algorithm, can be enumerated as follows:

1. As explained in section 5.2.3.1, Line 2 has a complexity of $O(nd)$.
2. Line 3 can be done with a merge sort, which has a complexity of $O(n \log n)$.
3. The most computationally complex part of the if-else block is lines 17–20. Line 17 is a sequential comparison of consecutive elements of an $n-dimensional$ vector, and has a complexity of $O(n)$. Line 18 also has a complexity of $O(n)$ since it is the sequential comparison of the elements of an $n-dimensional$ vector to a threshold. Line 19 is the deletion or flagging of at most n rows in a matrix, and has a complexity of $O(n)$.

If m is the number of clusters detected, the while loop that starts at line 1 and ends at line 21 runs exactly m times . In the worst case scenario, which is very unlikely, $m = n$. Otherwise $m < n$. Thus the overall complexity of the BCM clustering algorithm is $O(m(n \log n + nd))$ where m is the number of clusters, d is the number of attributes of each data point, and n is the number of points in the data set.

5.3 PERFORMANCE

5.3.1 Performance on data sets

To test the performance of the BCM clustering algorithm, it is applied to the following data sets.

1. **Linearly separable data sets** : A data set is said to be linearly separable if for each

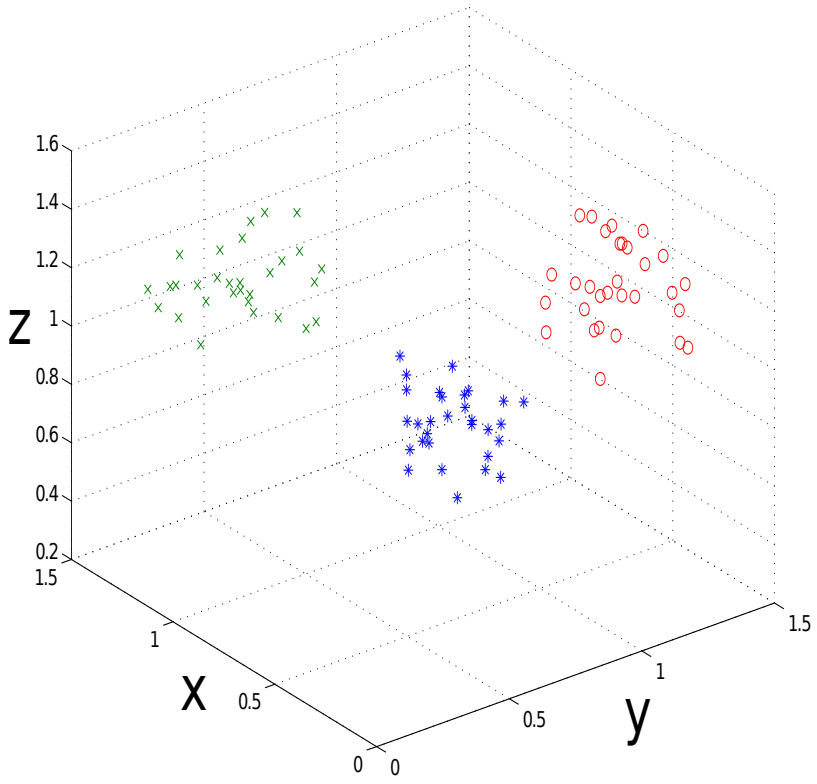

Figure 5.3: High RI performance of BCM clustering algorithm on a data set with three linearly separable clusters

cluster in the data set, there exists a plane that can be used to separate the cluster from the remainder of the data set. Figure 5.3 and figure 5.4 show the best performances of the BCM clustering algorithm on two linearly separable data sets. in order of detection, the clusters are blue asterisk, red circle, green cross, and black plus sign (only in figure

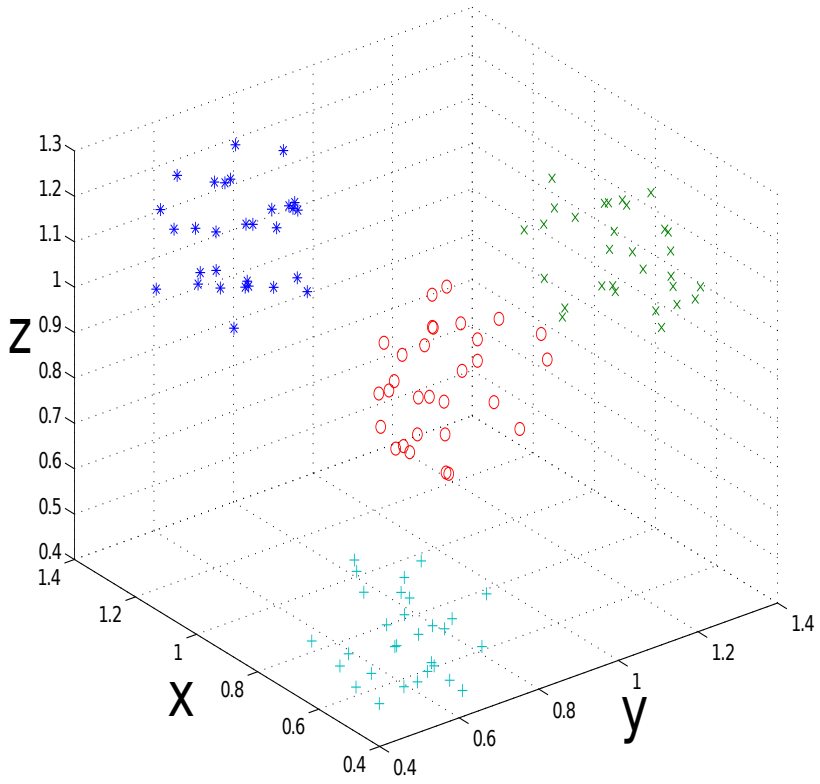

Figure 5.4: High RI performance of BCM clustering algorithm on a data set with four linearly separable clusters

5.4). Simulations are done with $\tau_w = 10$, $\tau_\theta = 1$, $numItr = 10000$, $\kappa = 10$, $\delta = 0.05$, and $\mathbf{w}$ is initialized with numbers in the interval $(0, 0.3)$.

2. **Linearly inseparable data set**: Figure 5.5 shows the performance of the algorithm on a data set that is not linearly separable. In order of detection, the clusters are blue

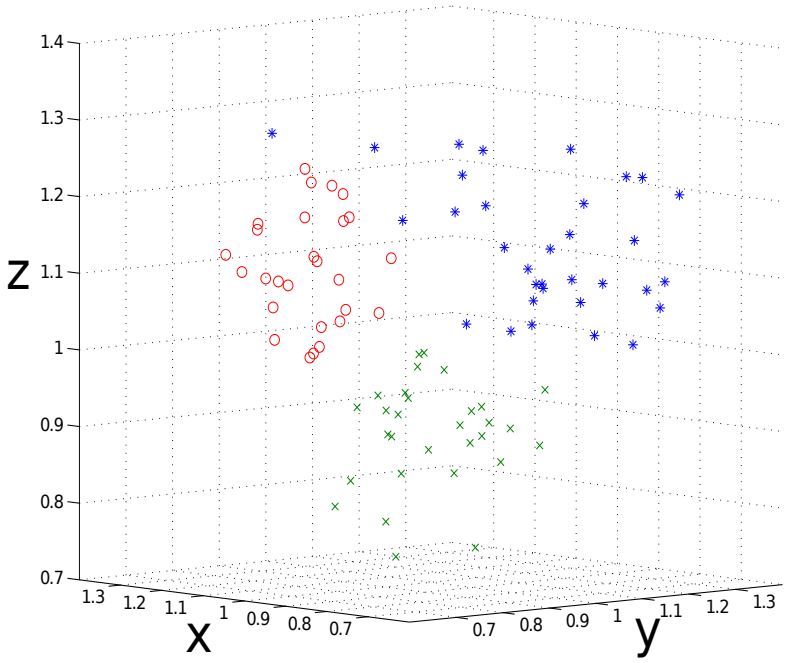

Figure 5.5: A typical performance of BCM clustering algorithm on a data set with linearly non-separable clusters

asterisk, red circle, and green cross. Simulations are done with $\tau_w = 10$, $\tau_\theta = 1$, $numItr = 10000$, $\kappa = 10$, $\delta = 0.05$, and $\mathbf{w}$ is initialized with numbers in the interval $(0, 0.3)$.

3. **Iris data set**: This data set was introduced by Sir Ronald Fisher in 1936 [20] and can be found on the UCI machine learning repository [2]. The set contains 150 data points on three species of the Iris flower comprising 50 samples from the Iris setosa species, 50 from Iris virginica, and 50 from Iris versicolor. It measures (in cm) the

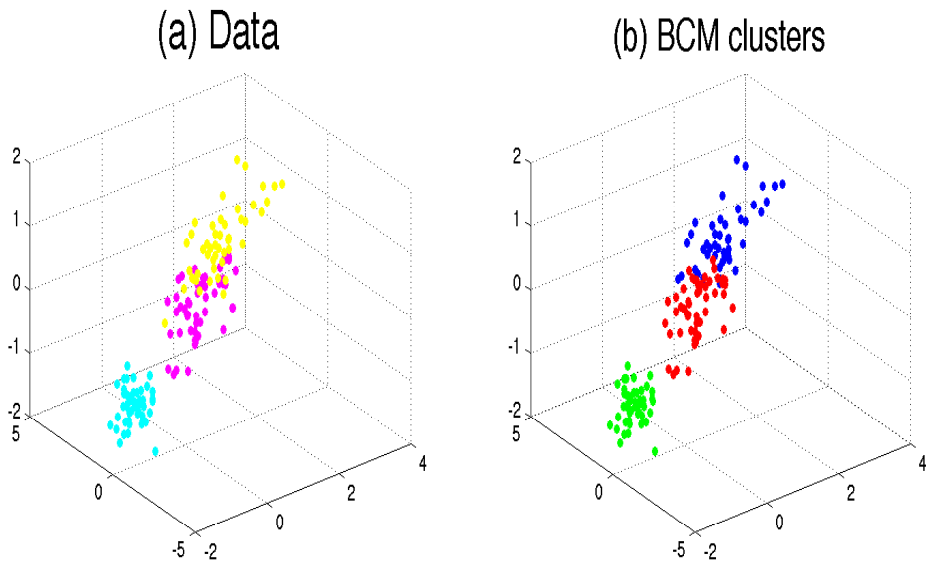

Figure 5.6: (a) Iris data set (b) Iris data set clustered using the BCM clustering algorithm.

following four attributes for each sample: length of the sepal, the width of the sepal, the length of the petal, and the width of the petals. This data set is hardly analyzed by clustering since there are only two obvious clusters (within three groups): one of the clusters contains Iris setosa, while the other cluster contains both Iris virginica and Iris versicolor and is not separable without the species information Fisher used. Figure 5.6(a) shows a 3-d projection of the iris data points. The cyan points are samples of iris setosa, the purple points are samples of iris virginica, and the yellow points are samples of iris versicolor. Figure 5.6(b) shows a typical clustering result of this data using the BCM clustering algorithm. In this figure, The blue cluster was detected first, the red one second, and the green one third. Simulations are done with $\tau_w = 10$, $\tau_\theta = 1$, $numItr = 10000$, $\kappa = 10$, $\delta = 0.1$, and $\mathbf{w}$ is initialized with numbers in the

interval $(0, 0.3)$.

4. **Cardiotocography data set** : This data set consists of measurements of fetal heart rate (FHR) and uterine contraction (UC) features on cardiotocograms classified by expert obstetricians. This data set can be found on the UCI machine learning repository [2]. The data set consists of 2126 samples and each sample has 23 attributes. With respect to morphological patterns, each sample in the data set can be placed into one of ten groups $A, B, C, D, \ldots J$. Each of the samples is already pre-classified to be in one of these groups. The task here is to determine how similar to the grouping $A, B, C, D, \ldots J$, the clustering detected by the BCM clustering algorithm is. In addition to this task, the within-cluster similarity is also measured. Simulations are done with $\tau_w = 10$, $\tau_\theta = 1$, $numItr = 10000$, $\kappa = 7$, $\delta = 0.04$, and $\mathbf{w}$ is initialized with numbers in the interval $(0, 0.3)$.

The performance of the BCM clustering algorithm, on these data sets, in comparison to a few other clustering algorithms, are discussed in section 5.3.2

5.3.2 Performance comparison

The Rand index can be used to measure clustering accuracy. This applies especially to the linearly separable data sets in figures 5.3 and 5.4, along with the Iris flower data set, because the visualizable clusters of data sets can serve as benchmark. In the case if the Iris flower data, the grouping of the flower samples can serve as benchmark. The Rand index can also be used to measure clustering accuracy in the case of the cardiotocography data set since the classifications $A, B, C \ldots, J$ of the data can be used as a benchmark. Recall the definition of the Rand index (RI)

$$RI = \frac{TP + TN}{TP + TN + FP + FN}$$

where

TP = sum of the true positives in all the clusters

FP = sum of the false positives in all the clusters

TN = sum of the true negatives in all the clusters

FN = sum of the false negatives in all the clusters

and

- a true positive is a point that belongs to the same group in both the clustering result and the benchmark
- a false positive is a point that belongs to a group in the clustering result, but belongs to another group in the benchmark
- a true negative is a point that does not belongs to a group in the clustering result, and also does not belongs to that group in the benchmark
- a false negative is a point that does not belongs to a group in the clustering result, but belongs to that group in the benchmark

To get a better understanding of the performance of the BCM clustering algorithm, three other clustering algorithms are employed to perform the clustering tasks discussed in section 5.3.1.

The first is k-means, a centriod based clustering algorithm where each cluster is represented by a central mean vector (center) – which may not necessarily be one of the points of the cluster [65]. The algorithm is an iterative optimization process which at each iteration finds an new centers and assigns each data point to the cluster center nearest to it [43]. The algorithm terminates when the squared distances of the points from the centers are minimized.

The second is the expectation-maximization (EM) algorithm. This clustering algorithm is distribution based in that it assumes a number of Gaussian distributions– corre-

sponding to the desired number of clusters. The parameters of these distributions along with the likelihood (probability) of each point belonging to any of the distributions are initialized randomly, and updated iteratively. At convergence, each point it assigned to the distribution for which it has the most likelihood. [8]

The third is hierarchical clustering. Hierarchical clustering can be either agglomerative or divisive, however the focus here will be on agglomerative clustering. At the start of an agglomerative clustering process, each data point is initialized as a cluster, and at each iteration, two clusters are combined based on how close to each other they are. This continues until the whole data set becomes one cluster. At the end, to determine the number of clusters in the data, a threshold distance is set for which, if any two clusters are of that distance apart, they then cannot belong together. The comparison in this section will be done with the complete linkage (CLINK) [61] agglomerative clustering where, in each iteration, the distance between two clusters is determined with the distance between the two elements in (one in each cluster) that are farthest apart.

Table 5.2 shows the results of applying the different clustering algorithms to the discussed data sets. Each number is the mean Rand index over 100 runs of each algorithm.

As can be seen, the performance of the BCM clustering algorithm compares well with those of the other clustering algorithms. For instance, on the cardiotocography data set, the algorithm has the second best Rand index of 0.7815. This is second to, and not too far from, that of k-means (0.7923).

The Rand index is only suitable for measuring accuracy when there is a benchmark to which the result can be compared. A good clustering algorithm should produce clusters with high similarity within a cluster and high dissimilarity between clusters. Therefore when there is no such benchmark, the next appropriate approach is to take into consideration a combination the similarity of points within the clusters and the dissimilarity between the clusters. The Davies - Bouldin (DB) index [15] does this , and can be calculated in the

Table 5.2: Mean Rand indices (over 100 runs) for different clustering algorithms

Data set	BCM (algorithm 2)	k-means	EM	CLINK
figure 5.3 data set	0.9332	0.9467	0.9232	0.9429
figure 5.4 data set	0.9432	0.9267	0.9032	0.9543
Iris data set	0.8513	0.8100	0.7711	0.7364
Cardiotocography data set	0.7815	0.7923	0.7713	0.7583

following way :

$$DB = \frac{1}{n}\sum_{i=1}^{n} \max_{i \neq j} \left(\frac{\sigma_i + \sigma_j}{d(c_i, c_j)} \right)$$

where

n is the number of clusters.

c_x is the centroid of cluster x.

σ_x is the average distance of all elements in cluster x to centroid c_x.

$d(c_i, c_j)$ is the distance between centroids c_i and c_j.

In a clustering result with high intra-cluster similarity and low inter cluster similarity, the numerator of the inside of each term of the summation above should be less than the denominator. Thus, a reasonable DB index should be less than one. In addition, the algorithm that yields the best clustering result should have the lowest DB index. Table 5.3 shows the DB indices for different algorithms on the linearly non-separable data sets. Each algorithm is adjusted to yield three clusters, and each number is the mean of DB index over 100 runs.

Table 5.3: Mean DB indices (over 100 runs) for different clustering algorithms

Data set	BCM (algorithm 2)	k-means	EM	CLINK
figure 5.5 data set	0.3611	0.291	0. 3991	0.3010
Iris data set	0.3310	0.3012	0. 4021	0.3211
Cardiotocography data set	0.2411	0.2210	0. 4021	0.2437

Again, the performance of the BCM clustering algorithm compares well with those of the other clustering algorithms. On the cardiotocography data set for instance, the algorithm has the second best DB index of 0.2411. This is second to, and not too far from, that of k-means (0.2210).

The results on tables 5.2 and 5.3 show that in general the BCM clustering algorithm performs well when the data set is linearly separable. When the data is not linearly separable, the performance is comparable to that of k-means, EM, and CLINK. Table 5.3 shows, however, that is k-means a better algorithm in terms of internal evaluation, that is if the combination of intra-cluster similarity and inter-cluster dissimilarity is a the main criterion for measurement.

5.3.3 Computational complexity and run time comparison

As already derived, the complexity of the BCM clustering algorithm is $O(m(n\log n + nd))$ where m is the number of clusters, d is the number of attributes of each data point, and n is the number of points in the data set. The is generally better than the complexity of

Table 5.4: Mean CPU time, in seconds, (over 100 runs) for different clustering algorithms

Data set	BCM (algorithm 2)	k-means	EM	CLINK
figure 5.3 data set	0.2108	0.3004	0.3891	0.4021
figure 5.4 data set	0.2601	0.3876	0.4001	0.4210
Iris data set	0.2513	0.3100	0.4711	0. 4364
Cardiotocography data set	5.8753	7.2953	7.7613	7. 8553

the other three algorithms. Each of EM and k-means clustering algorithms has a best case complexity of $O(n^{md+2}\log n)$ [30], and the complete linkage hierarchical clustering algorithm has a complexity of $O(n^3)$ [8].

Table 5.4 show the mean CPU time, in seconds, (over 100 runs) of each clustering algorithm on the data sets already discussed. As can be seen, the BCM clustering algorithm is faster than the other algorithms. On the cardiotocography data set for instance, the algorithm took only about 80% of the CPU time of k-means.

5.4 SUMMARY

In this chapter, it has been shown that the BCM neuron has the ability to detect data clusters when trained under the right conditions. Based on this fact, a clustering algorithm has been proposed. For linearly separable data sets, the algorithm has an excellent performance. For

data sets that are not linearly separable, the performance of the algorithm is comparable to those of k-mean, EM, and hierarchical clustering algorithms.

6.0 DISCUSSION

This dissertation explores the BCM learning rule as a dynamical system, uncovering several stability and instability properties. In addition, it investigates the clustering property of the BCM neuron.

6.1 CONTRIBUTIONS OF DISSERTATION

The main contributions of this dissertation can be enumerated in the following way:

1. Mean-field models of the BCM learning rule are usually written as a rate of change of the synaptic weights with time. With this approach to the mean-field, it is difficult to arrive at the fact that the fixed points – not their stability – of the learning rule depend only on the probabilities with which each stimulus vector is presented. This dissertation gives a derivation of the mean-field model of the BCM learning rule as a rate of change of the activity response v, with time. The derived model considers a general situation where two stimuli of any magnitude and orientation are presented with probabilities ρ and $\rho - 1$. The appeal of this derivation is that it easily highlights the fact that the fixed points depend on these probabilities. Additionally, the derivation is important because the dynamics of BCM learning rule are driven by the activity

response (not the synaptic weights), and many analyses in the literature rely on this fact.

2. This dissertation presents and proves analytical results that express the stability conditions of the BCM learning rule in terms of the angle between the stimuli and the time-scale of the homeostasis variable. This is important because it helps a user of the learning rule determine the parametric regime that ensures stability.
3. This dissertation presents numerical results of an exhaustive exploration of the different dynamical behaviors of the BCM learning rule for single neuron and two mutually inhibiting neurons. This is important because it helps a user of the learning rule know what to expect in different parametric regimes.
4. This dissertation demonstrates that homeostasis time-scale actually matters to the stability of synaptic plasticity. More importantly it corroborates the work of Zenke et al [67] who claim that homeostasis needs to to have a faster rate of change for spike-timing-dependent plasticity to achieve stability. The assertion here can be backed up by the fact the Izhikevich and Desia [36] who showed that the BCM learning rule follows directly from STDP under certain conditions.
5. This dissertation presents a thorough analysis of the data clustering property of the BCM neuron. Performance analysis shows that in linearly separable data sets, the BCM neuron can detect clusters with high accuracy.
6. This dissertation presents a clustering algorithm based on the BCM learning rule. The proposed algorithm has a computational complexity of $O(m(n\log n + nd))$, where m is the number of clusters, and n is the number of data points. This is better than that of k-means Expectation-maximization (EM) clustering algorithms. For instance k-means has a best case complexity of $O(n^{md+2}\log n)$ [30] where d is the dimension of the data. Furthermore, the algorithm does not require a specification of the desired number of clusters (though if there is need to to this, it can easily be achieved by

simply replacing the 'while' loop with a 'for' loop). In these regards, the algorithm is more appealing than algorithms like k-means and EM clustering algorithms which are computationally more complex, and do require the user to specify the number of clusters before hand. Performance comparison shows that for linearly separable example data sets, the algorithm performs excellently, and for non-linearly separable examples, the algorithm is comparable to k-means, EM, and agglomerative clustering algorithms.

6.2 FUTURE WORK

A possible direction of future work relating to this dissertation is to perform an analysis of a large network of BCM neurons, by observing what happens to the network dynamics at different time-scale parametric regimes. A good starting point is to explore the dynamic for a fully connected network with equal inhibition, that is, each neuron is coupled with every other neuron in the network and inhibits each of them equally. The next step would be to let the amount of inhibition vary according to how far away the inhibiting neuron is.

At this time, the clustering algorithm proposed only deals with data with numerical values and it does not handle missing attributes. Thus, a future work should gear towards improving the algorithm in such a way that it deals with data points with missing attributes, and at the same time handle data sets with nonnumeric values.

7.0 BIBLIOGRAPHY

[1] S. Albayrak. Unsupervised clustering methods for medical data: An application to thyroid gland data. *Artificial Neural Networks and Neural Information Processing ICANN/ICONIP 2003*, Vol. 2714, pp. 695-701, 2003.

[2] K. Bache and M. Lichman. UCI machine learning repository, 2013.

[3] C. M. Bachman, S.A. Musman, D. Luong, and A. Schultz. Unsupervised bcm projection pursuit algorithms for classification of simulated radar presentations. *Neural Networks*, Vol. 7, pp. 709-728, 1994.

[4] L. Benuskova, Diamond M. E., and F. F. Ebner. Dynamic synaptic modification threshold: computational model of experience-dependent plasticity in adult rat barrel cortex. *Proc. Natl. Acad Sci.*, Vol. 91, pp. 4791-4795, 1994.

[5] G. Q. Bi and M. M. Poo. Synaptic modications in cultured hippocampal neurons: Dependence on spike timing, synaptic strength, and postsynaptic cell type. *J. Neurosci.*, vol. 18, pp. 10464 - 10472, 1998.

[6] E. Bienenstock. *A Theory of development of neuronal selectivity*. Brown University doctoral thesis, 1980.

[7] E. L. Bienstock, L.N. Cooper, and P.W. Munro. Theory for the development of neuron selectivity: orientation specificity and binocular interaction in visual cortex. *Journal of Neuroscience*, Vol.2, pp. 32-48, 1982.

[8] C Bishop. *Pattern recognition and Machine Learning*. Springer, 2006.

[9] D. V. Buonomano and M. M. Merzennich. Cortical plasticity: From synapses to maps. *Annual Review of Neuroscience*, Vol. 21, pp. 149-186, 1998.

[10] G. C. Castellani, N. Intrator, H. Shouval, and L.N. Cooper. Solutions of the bcm learning rule in a network of lateral interacting nonlinear neurons. *Computational Neural System*, Vol. 10, 1999.

[11] K. Cheng, T. Hasegawa, K.S. Saleem, and Tanaka K. Comparison of neuronal selectivity for stimulus speed, length, and contrast in the prestriate visual cortical areas v4 and mt of the macaque monkey. *J. Neurophysiology*, Vol. 71(6), pp. 2269-80, 1994.

[12] L. N. Cooper and M. F. Bear. The bcm theory of synapse modification at 30: interaction of theory with experiment. *Nature*, Vol. 13, 798, 2012.

[13] L. N. Cooper, F. Liberman, and E. Oja. A theory for the acquisition and loss of neuron specificity in the visual cortex. *Biological Cybernetics*, Vol. 33, pp. 9-28, 1979.

[14] T. Czuba, L. Cormack, A. Huk, and A. Kohn. Neuronal selectivity for directions of 3d motion in area mt. *Journal of Vision*, Vol. 13(9), art. 608, 2013.

[15] D. L. Davies and D. W. Bouldin. A cluster separation measure. *IEEE Transactions on Pattern Analysis and Machine Intelligence*, Vol. 1, pp. 224-227, 1979.

[16] Y. Dotan and N. Intrator. Multimodality exploration by an unsupervised projection pursuit neural network. *IEEE Trans. Neural Net.*, Vol. 9, pp. 464-472, 1998.

[17] Bard Ermentrout. Xppaut 7.0 dec 2012. http://www.math.pitt.edu/~bard/xpp/xpp.html, 2012.

[18] G. B. Ermentrout and D. H. Terman. *Mathematical Foundations of Neuroscience*. Springer, 2010.

[19] G.D. Field and E.J. Chichilnisky. Information processing in the primate retina: Circuitry and coding. *Annu Rev Neurosci.*, Vol. 30, pp. 1-30., 2007.

[20] R. A. Fisher. The use of multiple measurements in taxonomic problems. *Annals of Eugenics*, Vol. 7, pp. 179 - 188, 1936.

[21] F. R. Gantmacher. *Applications of the Theory of Matrices*. Wiley, New York, 1959.

[22] P. Haider, L. Chiarandini, and U. Brefeld. Disriminative clustering for market segmentation. *ACM journal*, 978, 2012.

[23] M. Hamada, Y. Terao, R. Hanajima, Y. Shirota, S. Nakatani-Enomoto, T. Furubayashi, H. Matsumoto, and Y. Ugawa. Bidirectional long-term motor cortical plasticity and metaplasticity induced by quadripulse transcranial magnetic stimulation. *J Physiol*, Vol. 586(16), pp. 3927 - 47, 2008.

[24] D Hebb. *The organization of behavior*. J. Wiley and Sons, 1949.

[25] J. Hertz, Krogh A., and R. Palmer. *Introduction to the theory of neural computation*. Addison-Wesley, 1991.

[26] D. H. Hubel and T. N Wiesel. The period of susceptibility to the physiological effects of unilateral eye closure in kittens. *J Physiol*, Vol. 206(2), pp. 419436, 1970.

[27] D. H. Hubel and T.N. Wiesel. Receptive fields of single neurones in the cat's striate cortex. *Journal of Physiology*, Vol.148, pp. 574 - 591, 1959.

[28] D. H. Hubel and T.N. Wiesel. Receptive fields, binocular interaction and functional architecture in the cat's visual cortex. *Journal of Physiology*, Vol. 160, pp. 106154, 1962.

[29] L. Hubert and P. Arabie. Comparing partitions. *Journal of Classification*, vol. 2 (1), pp. 193-218, 1985.

[30] M. Inaba, N. Katoh, and H. Imai. Applications of weighted voronoi diagrams and randomization to variance-based k-clustering. *Proceedings of 10th ACM Symposium on Computational Geometry*, pp. 332 - 339, 1994.

[31] The MathWorks Inc. Matlab and statistics toolbox release 2012b. http://www.mathworks.com/, 2012.

[32] N. Intrator. Feature extraction using unsupervised neural network. *Neural Computation*, Vol. 4, pp. 98-107, 1992.

[33] N. Intrator and L.N. Cooper. Objective function formulation of the bcm theory for visual cortical plasticity: statistical conections, stability conditions. *Neural Networks*, Vol. 5, pp. 3-17, 1992.

[34] N. Intrator and J. I. Gold. Three-dimension object recognition of gray level images: the usefulness of distinguishing features. *Neural Computation*, Vol. 5, pp. 61-74, 1993.

[35] N. Intrator, J. I. Gold, H. H. Blthoff, and S. Edelman. Three-dimensional object recognition using an unsupervised neural network: Understanding the distinguishing features. *Proceedings of the 8th Israeli Conference on AICV*, 1991.

[36] E. M. Izhikevich and N.S. Desia. Relating stdp to bcm. *Neural Computation*, Vol. 15, pp. 15111523, 2003.

[37] R.S. Johansson and A. B. Vallbo. Tactile sensory coding in the glabrous skin of the human hand. *TINS*, 1983.

[38] P. Kalyani. Approaches to partition medical data using clustering algorithms. international. *Journal of Computer Applications*, Vol. 49 (23), pp. 7-10, 2012.

[39] E. R. Kandel, J. H. Schwartz, and T. M. Jessell. *Principles of neural science, 4th ed.* McGraw-Hill, 2000.

[40] S. M. Kirkwood, A.and Dudek, J. T. Gold, C. D. Aizenman, and M. F. Bear. Common forms of synaptic plasticity in the hippocampus and neocortex in vitro. *Science*, Vol. 260, pp. 1518- 1521, 1993.

[41] C. C. Law and L. N. Cooper. A bcm neuron trained with natural images. *Proceedings of World Congress on Neural Networks*, Vol. 1, 1993.

[42] W. Liu. Criterion of hopf bifurcations without using eigenvalues. *Journal of Mathematical Analysis and Applications*, Vol. 182, pp. 250-256, 1994.

[43] S. Lloyd. Least squares quantization in pcm. *IEEE Transactions on Information Theory*, Vol. IT-28, NO. 2, 1982.

[44] G. W. Milligan and S. C. Hirtle. Clustering and classification methods. In I. B. Weiner, editor, *Handbook of Psychology*. John Wiley and Sons, Inc, 2013.

[45] E. Munro. *Neural Plasticity:Single Neuron Models for Discrimination and Generalization and an Experimental Ensemble Approach*. Brown University doctoral thesis, 1983.

[46] P. W. Munro. A model for generalization and specification by a single neuron. *Biol. Cybern*, Vol. 51, pp. 169-179, 1984.

[47] J.F. Mller, Y. Orekhov, Y. Liu, and U. Ziemann. Homeostatic plasticity in human motor cortex demonstrated by two consecutive sessions of paired associative stimulation. *Eur J Neurosci.*, Vol. 25(11), pp. 3461 - 3468, 2007.

[48] M. N. Nass and L.N. Cooper. A theory for the development of feature detecting cells in the visual cortex. *Biological Cybernetics*, Vol. 19, pp. 1-18, 1975.

[49] I. Nauhaus, A. Benucci, M. Carandini, and D. L. Ringach. Neuronal selectivity and local map structure in visual cortex. *Neuron*, Vol. 57, pp. 673-679, 2008.

[50] C. Pantev, H. Okamoto, B. Ross, W. Stoll, E. Ciurlia-Guy, R. Kakigi, and T. Kubo. Lateral inhibition and habituation of the human auditory cortex. *Eur J Neurosci.*, Vol. 19(8), pp. 2337-44., 2004.

[51] A. Pascal-Leone, C. Freitas, L. Oberman, J. C. Horvath, M. Halko, M. Eldaief, S. Bashir, and M. Vernet. Characterizing brain cortical plasticity and network dynamics across the age-span in health and disease with tms-eeg and tms-fmri. *Brain Topogr*, Vol. 24, pp. 302 - 315, 2011.

[52] A. Pascual-Leone, A. Amedi, F. Fregni, and L. B. Merabet. The plastic human brain cortex. *Annual Review of Neuroscience*, Vol. 28, pp. 377-401, 2005.

[53] L. Perko. *Differential equations and dynamical systems*. Springer-Verlag, 2001.

[54] A. Poljovka and L. Benuskova. Pattern classification with the bcm neural network. *Unpublished*.

[55] M. I. Posner and S. W. Keele. On the genesis of abstract ideas. *J. Exp. Psych*, Vol. 77, pp. 353-363, 1968.

[56] M. I. Posner and S. W. Keele. Retention of abstract ideas. *J. Exp. Psych*, Vol. 83, pp. 353-363, 1970.

[57] W. M. Rand. Objective criteria for the evaluation of clustering methods. *Journal of the American Statistical Association*, Vol. 66, No. 336, 1971.

[58] J. P. Rauschecker and W. Singer. The effects of early visual experience on the cat's visual cortex and their possible explanation by hebb synapses. *J. Physiology*, Vol. 310, pp. 215-239, 1981.

[59] C. Sherrington. *The integrative action of the nervous sytem*. Charles Scribner's Sons, 1906. Reprinted by Cambridge University Press in 1948, 1906.

[60] H. Shouval, N. Intrator, and L.N. Cooper. Bcm network develops orientation selectivity and ocular dominance in natural scene environment. *Elsevier Science*, Vol. 37 (23), pp. 3339-3342, 1997.

[61] R. Sibson. Slink: an optimally efficient algorithm for the single-link cluster method. *The Computer Journal*, 1973.

[62] B. F. Skinner. *The Behavior of Organisms*. Appleton-Century-Crofts, Inc. New York, 1938.

[63] M. Wedel and W. Kamakura. *Market segmentation: conceptual and methodological foundations*. Springer, 2000.

[64] E. W. Weisstein. Routh-hurwitz theorem. http://mathworld.wolfram.com/Routh-HurwitzTheorem.html, January 2014.

[65] I. H. Witten, E. Frank, and M. A. Hall. *Data Mining*. Morgan Kaufmann, 2011.

[66] S. Yantis. *Sensation and Perception*. Worth Publishers, 2013.

[67] F. Zenke, G. Hennequin, and W. Gerstner. Synaptic plasticity in neural networks needs homeostasis with a fast rate detector. *Computational Biology*, Vol. 9, issue 11, e1003330, 2013.